AN ABSTRACT OF THE THESIS OF

<u>DEAN GOODMAN</u> for the degree of <u>MASTER OF SCIENCE</u>

in <u>GEOPHYSICS</u> presented on <u>April 15, 1983</u>

Title: <u>SEISMIC REFRACTION SURVEY OF CRUSTAL AND UPPER MANTLE</u>

<u>STRUCTURES IN THE WEST PHILIPPINE BASIN</u>

Abstract approved: <u>_Redacted for Privacy_____</u>
L. Dale Bibee

Crustal and upper mantle structures in the West Philippine Basin, along 17-18°N, have been determined using explosions as sources and ocean bottom seismometers to measure refracted compressional waves. Seismic refraction profiles out to nearly 500 km were completed. Shallow structure was measured using small shots, 1 - 240 lbs., and the deeper structure was probed with large explosions, 0.9-1.8 tons.

A velocity-depth inversion using short range data shows the upper crust to have strong velocity gradients which gradually decrease with depth. The lower crust is characterized by a nearly constant velocity gradient of $0.24 \sec^{-1}$. Standard delay-time functions and a modified function accounting for lateral velocity gradients were also used in travel time inversion. Results from the two methods are comparable and yield ~ 1.5 km transitional zone thicknesses in the basin. Although they vary slightly in magnitude between methods, West Philippine Basin oceanic layer thicknesses are abnormally thin, by about 2 km, when compared to average crust. Total crustal thicknesses are shown to be thinner in the eastern part of the basin, approaching only 3 km. Crustal thinning toward the east is consistent

with the Palau-Kyushu Ridge being a remnant transform fault connecting Philippine and Kula-Pacific ridges in the past.

Predicted water depths in the basin are about 300 meters shallower than observed depths when compensated to average mantle depths found for the Western North Pacific. The depth anomaly cannot be fully reconciled by thin crust, and requires a deeper-seated anomaly to be present in the West Philippine Basin.

Temperature and pressure modeling using experimental measurements from proposed mantle constituents indicate high seismic gradients in the upper mantle and may suggest that a multi-component or graded mantle exists beneath the marginal sea.

Seismic Refraction Survey of Crustal and Upper Mantle
Structures in the West Philippine Basin

by

Dean Goodman

A THESIS

submitted to

Oregon State University

in partial fulfillment of
the requirements for the
degree of

Master of Science

Commencement June 1983

APPROVED:

Redacted for Privacy

Assistant Professor of Geophysics
in charge of major

Redacted for Privacy

Dean of School of Oceanography

Redacted for Privacy

Dean of Graduate School

Date thesis is presented __April 15, 1983__

Typed by Donna Moore for __Dean Goodman__

ACKNOWLEDGEMENTS

Joanne Huppunen for being there.

Eric Brandt for making me realize my problems were
minuscule in comparison.

Bruce Dubendorff for boasting fathomlessly . . . I hope
no one has told him Florida is in L.A. county.

Mike Fehler for giving me a chance to strut my stuff.

Donna Moore who has my deepest sympathy for typing this
'aboundness'.

Gunnar Bodvarsson for showing me that some scientists can
also exhibit a great deal of humanity.

Fa Dwan, Dennis Schultz, Karin Schultz, Bob Karlin, Shaul
Levi, Randy Jacobson, Bill Menke, Oswaldo Sanchez, and
the rest of the geophysics clan for making my temporal
event here an eternal one.

My parents, Rachel and Lazarus, I present this work to, since
without their togetherness some years back none of this could have
happened. Because I'm kindhearted, I forgive them.

TABLE OF CONTENTS

LIST OF FIGURES

LIST OF TABLES

SEISMIC REFRACTION SURVEY OF CRUSTAL
AND UPPER MANTLE STRUCTURES IN
THE WEST PHILIPPINE BASIN

INTRODUCTION

Isolated ocean basins found at the margins between continents and major ocean basins have been termed 'marginal' seas. It has for long been the desire of oceanographers to understand the genesis of these basins, most of which are geographically concentrated in the Western Pacific Ocean (Figure 1). The earliest models suggested marginal basins were a result of continental subsidence (Lawson, 1932), however, this origin was eventually disproven as numerous seismic refraction samplings revealed crustal velocities and mantle depths similar to that of the major oceans (Gaskell, 1959). From latest efforts, two theories have been developed. One theory suggests that marginal basins represent older oceanic crust trapped as a result of the initiation of intraplate subduction or from the relative motion of trench boundaries (Uyeda and Ben-Avraham, 1972). An alternate model for explaining the structural history of marginal sea basins proposes they are formed by extension behind a developing island arc (Karig, 1971a).

The Philippine Sea located in the Western Pacific is a trench delineated plate juxtaposed between the Asian continent and the Pacific Ocean. It is composed of several distinctly defined basins, the largest of which is the West Philippine Basin (Figure 2). Although the Philippine basins are of an oceanic character, they are still very anomalous structurally when compared to normal oceans. Surface wave investigations have found the base of the lithosphere,
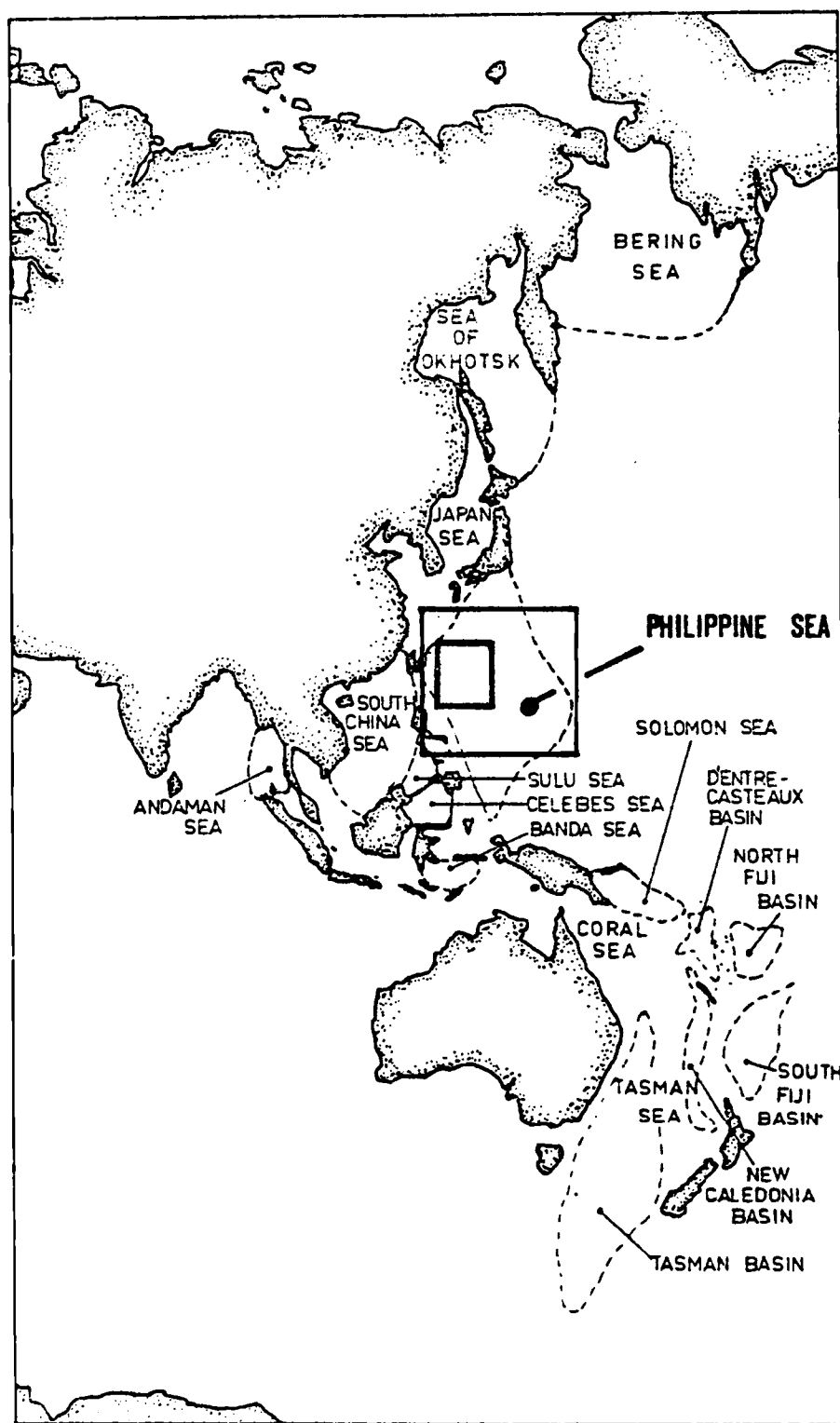
Figure 1. Map of marginal seas in the Western Pacific Ocean (after Packham and Falvey, 1971). Blocked areas show locations of bathymetric charts of the Philippine Sea (Figure 2; large block) and the West Philippine Sea (Figure 5; small block).

as indicated by a decrease in shear wave velocity lies at depths of only 30 km in the Philippine Sea, nearly half that found in oceanic regions of a similar age. Attenuation studies have found there to be a decrease in seismic energy absorption at 90 km depths and may signify a rather shallow base for the asthenosphere. Crustal thicknesses in the Philippine Sea have been found to be thin, especially so in the West Philippine Basin. In comparison to ocean floor of a similar age (Eocene), this basin is anomalously deep - by as much as 1 km. This may in part be an isostatic response to crustal and/or upper mantle anomalies.

During February-March of 1981, in cooperation with Scripps Institution of Oceanography, an experiment was conducted to determine compressional and shear wave velocities as well as attenuation at depth in the Philippine Sea. To accomplish this goal, a long refraction line extending to nearly 500 km was shot using large explosions. To determine shallow crustal variations along the shot line, smaller explosive sources were used. The locale chosen in the Philippine Sea was the West Philippine Basin. The advantages to a study in this region, from a logistic standpoint were:

1. The West Philippine Basin could accomodate travel paths exceeding 600 km in length which do not cross structural features.

2. Bathymetry in the northeast section of the basin is rather uniform, suggesting that the subsurface structure is fairly uniform as well. Inversion techniques requiring lateral homogeneity could therefore be implemented to successfully model the data.

3. Previous refraction experiments have shown the West Philippine Basin to propagate acoustic energy efficiently, out to large ranges. Thus, good signal to noise ratios can be achieved with shot sizes no bigger than 5 tons at extended ranges, and less than 120 lbs at small ranges out to 60 km.

4. Earthquakes from active subduction at the Ryukyu and Philippine trenches could provide for an extension of the refraction solution and also relay information regarding oceanic P_n and S_n phases.

A detailed knowledge of the seismic structure in the basin will allow us to measure the contributions of the crustal and mantle structures to the observed depth anomaly. The presence of the lithosphere-asthenosphere boundary at such a shallow depth could provide us with a rare opportunity to map changes that take place in the compressional wave velocities corresponding to the anomalous shear velocities measured from surface wave studies. The outcome of this investigation could also be of great importance in evaluating the geologic nature of the lithosphere asthenosphere transition which has become so important in plate tectonic theory, and possibly, shed some light on the origin of one of the biggest enigmas in the world's oceans, the West Philippine Sea.

REGIONAL TECTONICS

General Physiography

The West Philippine Basin is the largest marginal basin in the world and is by far the deepest, exhibiting mean water depths approaching 6000 meters (Sclater et al., 1976). A series of trenches and submarine ridges structurally define the borders and interior of this basin and the rest of the Philippine Sea (Figure 2). The Central Basin Fault (also known as the Philippine Ridge or Central Basin Ridge) divides the basin into northwest and southwest sections. The western boundaries, also delineating the western extent of the Philippine Sea Plate, are the Mindano (Philippine) and Ryukyu trenches. On the eastern border of the basin is the north-south trending Palau-Kyushu Ridge. This ridge separates the West Philippine Basin from the Parece Vela and, to the north the Shikoku marginal seas. Further east are increasingly arcuate structures (Karig, 1978): the South Honshu Ridge, defining the eastern flank of the Parece Vela Basin; the Mariana Trough, a young marginal basin behind the Mariana Islands; and the Mariana trench. The Mariana trench along with the Izu-Bonin trench to the north describe the eastern Philippine plate boundary. To the south of the Mariana trench the discontinous Yap and Palau trenches delineate the southern plate boundary.

Seismicity

Regional seismicity is predominantly confined to the major trench systems defining the Philippine Sea plate (Barazangi and
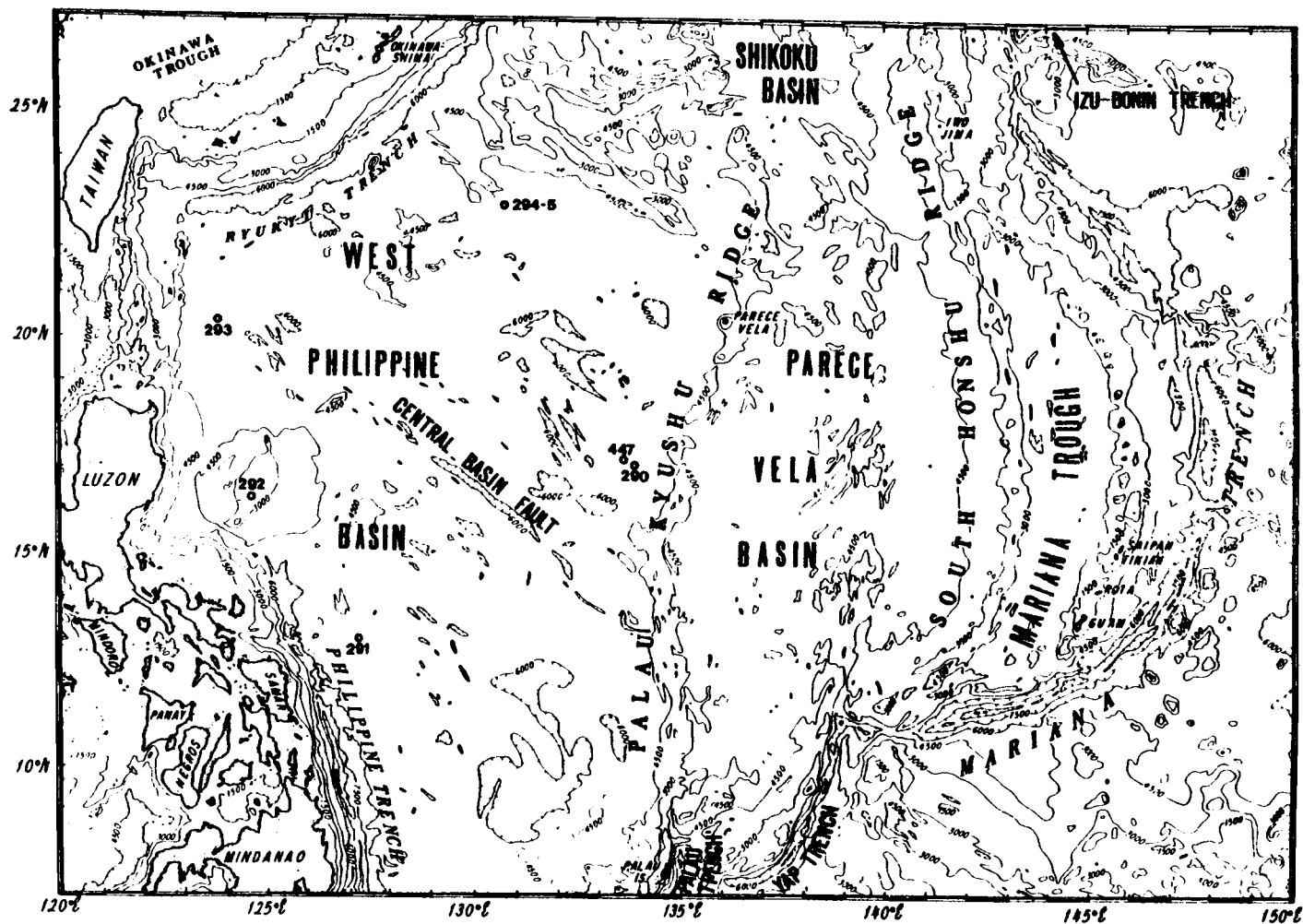
Figure 2. General bathymetry and physiographic features of the Philippine Sea. Leg 31 and 59 DSDP sites in the West Philippine (290-294(-5), 447a) are provided.

Dorman, 1969; Katsumata and Sykes, 1969) with little or no activity occurring within the interiors of the plate (Shimamura et al., 1975).

Earthquakes originating at shallow depths are found along most of the western edge of the plate, but with some small gaps in the seismicity (Katsumata and Sykes, 1969). Shallow earthquakes on the eastern plate boundary occur in a continuous belt from the Izu-Bonin to the southern end of the Marianas trench system, where activity abruptly decreases. Barazangi and Dorman (1969) report a gap in the seismicity beginning at the southern tip of the Marianas, extending through the Yap and Palau arc systems and onward to the Indian-Pacific-Philippine Sea plate triple junction.

Earthquakes of an intermediate depth, $\sim$70-300 km, occur on the western boundary with some clustering of locations at the Philippine trench and in the Ryukyu-Taiwan regions. Intermediate earthquakes located along the Izu-Bonin-Mariana trench system show an intense region of activity between 17° and 20°N (Katasumata and Sykes, 1969).

Deeper seismic events, greater than 300 km are mostly confined to the eastern plate boundary, and are more frequent in the northern Izu-Bonin trench system than in the Mariana's. A few deep earthquakes west of the southern Philippine island of Mindanao have been reported (Barazangi and Dorman, 1969).

Source mechanism studies from earthquakes reveal the Pacific plate is presently underthrusting the Philippine Sea plate, about a pole of rotation near 7°N, 142°E in a westerly direction (Katsumata and Sykes, 1969). This low latitude pole of rotation, also verified by other studies (Morgan in Le Pichon et al., 1973; Solomon and Sleep, 1974) is used to explain the seismic gap along the southeastern plate

boundary as well as the decrease in hypocentral depths southward from the Izu-Bonin arc system (Katsumata and Sykes, 1969). Relative motion between the China and Philippine Sea plates in the Ryukyu-Taiwan region is in a northerly direction (Katsumata and Sykes, 1969). South of this area overthrusting of the Philippine Sea plate onto the China plate, or as yet some unmapped intermediate platelet occurs (Fitch, 1970; LePichon et al., 1973).

Tectonic History

The tectonic history and relationships of the plate interior is fairly well known for the eastern marginal basins and only poorly understood in the western part of the Philippine Sea.

From the east the marginal basins get progressively older westward. The Mariana Trough, the youngest, is an active back-arc basin behind the Mariana Islands (Ambos and Hussong, 1982; Bibee et al., 1980; Karig, 1978). The oldest sediments overlying basement are less than 5.6 m.y. in age and relate to an opening of this inter-arc basin beginning in the Miocene (uyeda and Hussong, 1978). Spreading rates are estimated to be 1.5 cm/yr half rate, at the widest sections of the trough (Bibee et al., 1980), grading to zero in the northern and southern ends (Ambos and Hussong, 1982; Karig, 1978).

The Parece Vela basin is much older than the Mariana Trough, dating back to Oligocene time (Kroenke, 1978a). The western flank of the basin, the Palau-Kyushu ridge, began volcanic activity about 40 m.y. ago and continued to 32 m.y. after which the ridge split with an active eastern segment, the South Honshu ridge, and became a quiescent remnant arc (Kroenke, 1978b; Mrozowski and Hayes, 1979).

The active South Honshu ridge then began migrating eastward at 5 cm/yr (full rate) (Kroenke and Scott, 1978b), creating the Parece Vela Basin. The spreading continued into the mid-Miocene, ~15 m.y., and then ceased. Volcanism continued on the South Honshu ridge for an additional 4 m.y. (Kroenke and Scott, 1978b). Subsequently, the ridge became a dormant, remanent arc when the now active, Mariana Island arc split to form the Mariana Trough.

Results from DSDP holes 296 and 297 show the Shikoku Basin to have had similar periods of extension with that of the Parece Vela Basin to the south (Karig, 1975), with minor variations (Mrozowski and Hayes, 1979). For this reason it is thought to be a northerly extension of the Parece Vela Basin; the two of which form a single marginal sea basin (Karig, 1975; Karig, 1971b).

The structural history of the West Philippine Basin is not well known. Several models have been developed for explaining the origin of this basin and it's relationship to the rest of the Philippine Sea. These theories can be divided into two rather distinct groups. One suggests the West Philippine Basin represents trapped oceanic crust, the other proposes that the basin resulted from inter-arc spreading.

Among the proponents for a trapped oceanic floor origin are Uyeda and Ben-Avraham (1972). In their model (Figure 3) the Central Basin Fault (Philippine Ridge) is treated as a mid-oceanic ridge (Ben-Avraham et al., 1972) connected to the Kula-Pacific Ridge System by a long transform fault. Between 80 and 90 m.y. the Kula-Pacific Ridge subducted under Japan. At ~40 m.y. a change in Pacific Plate
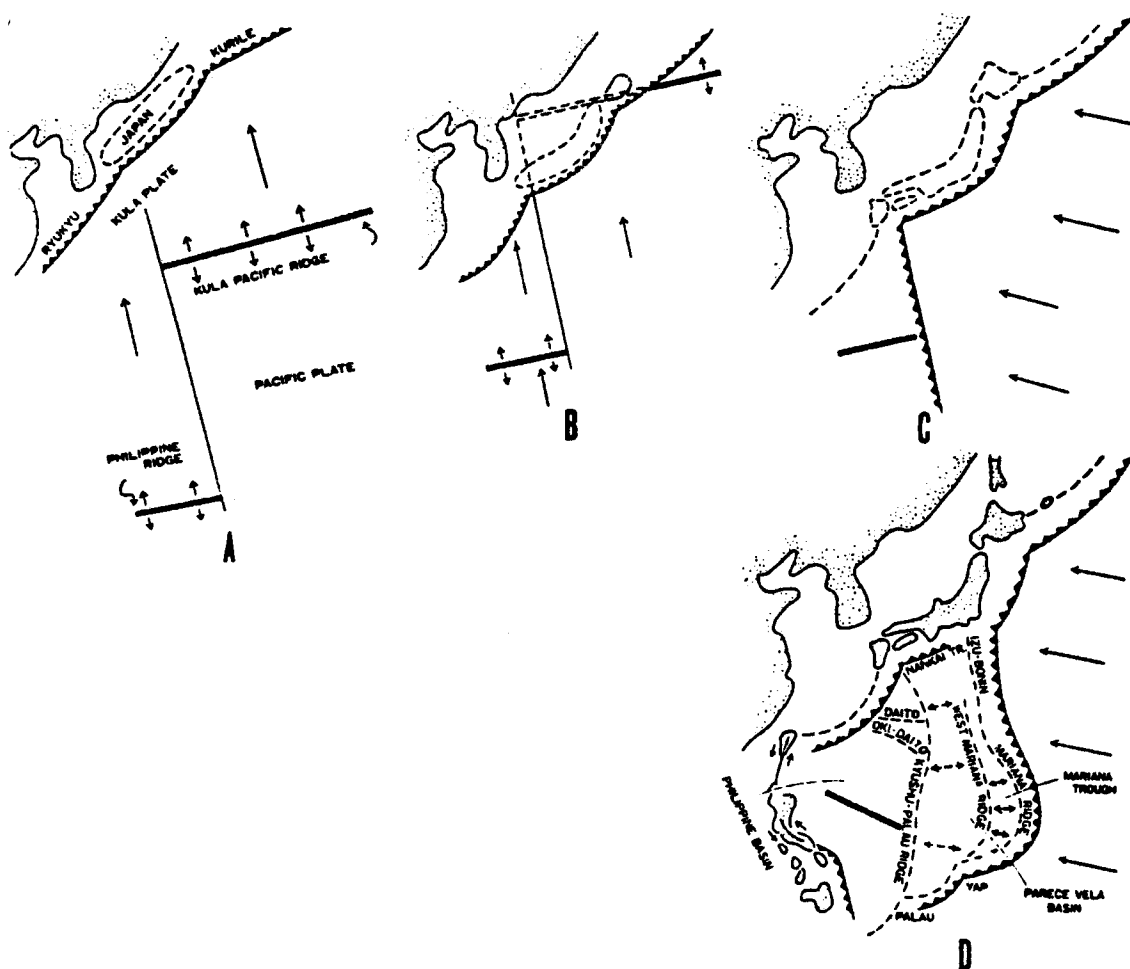
Figure 3. Schematic sketch of possible history of the Philippine Sea (after Uyeda and Ben-Avraham, 1972). A, Plate motion and arrangement at -100 m.y. B, Kula-Pacific Ridge submerges under Japan (80-90 m.y.). C, Change in Pacific plate motion at -40 m.y.; subduction begins at transform fault. D, Present state of the Philippine Sea. Back arc extension formed Parece Vela Basin and Mariana Trough.

motion to a more westerly direction caused subduction to occur at the transform fault. The eastern marginal seas were then formed by extension, contemporaneous with either a clockwise rotation of the basin, or possibly northward movement of the entire Philippine Basin (Ben-Avraham et al., 1972). In this construction model the Palau-Kyushu Ridge probably represents the remnant of the old transform fault, modified by arc volcanism.

Proponents proposing an extensional origin for the basin behind a pre-existing arc system include Karig (1973). It is envisioned by the 'extensionalists' that the West Philippine Basin was created in a similar fashion to the Parece Vela Basin and Mariana Trough, and represents an earlier period of extension behind the Mariana arc system. In Karig's model the Palau-Kyushu Ridge is thought to have been the active arc during an Eocene pulse of extension in the basin (Karig, 1971a). As earlier postulated by Hess (1948), the role of the Central Basin Fault was likened to a strike slip fault and thus identified to be a post feature to basin formation.

More recently Lewis et al. (1982) proposed inter-arc spreading for the West Philippine Basin behind an island arc, but unrelated to the Marianas. The active arc responsible for the basin is thought to have since been plastered onto the Philippine islands; the Oki-Daïto Ridge in the northern part of the basin being the remnant arc that split away.

A hypothesis has also been recently developed and encompasses both entrapment and back arc mechanisms. The theory of Lee (1982) identifies two distinct episodes of crustal extension along the Central Basin Fault. The first pulse occurred as a normal part of the Pacific

basin spreading system. Subsequent to a change in Pacific Plate motion at approximately 45 m.y. the spreading center at the Central Basin Fault changed from NW-SE to E-W, reconfiguring its spreading pattern into short segments. Contemporaneously, subduction began at the Palau-Kyushu Ridge. As spreading continued to 35 m.y. this later pulse of extension on the Central Basin Fault took place in a back-arc environment (Lee, 1982).

The diversity of explanations for the origin of the West Philippine Basin comes in part from the piecing together of an incomplete data set, in addition to the complicated nature of the area. The results of this study have provided additional information to aid in our understanding of this region of the earth. Before a discussion of these results is given a more detailed look at geophysical studies in the area is required.

PREVIOUS STUDIES

Deep Sea Drilling

Coring results from leg 31 and 59 of the Deep Sea Drilling Project (DSDP) from locations in the West Philippine Basin (Figure 2) are summarized in Table I. A more detailed synopsis for each site drilled is given in Appendix I. A DSDP Cruise summary given by Karig (1975) for leg 31 placed the origin of the West Philippine Basin in the late Eocene. The fairly uniform age determined throughout the basin, but not detailed enough to predict a spreading pattern, was interpreted as resulting from rapid extension. The data collected regarding the relationships of the Central Basin Fault to the rest of the basin were inconclusive, although it was thought to have been created by some form of mid-Tertiary tectonism. The volcaniclastics retrieved in the eastern part of the basin are thought to be from arc volcanism and subduction occurring at the Palau-Kyushu Ridge in the early Oligocene.

Bathymetry and Gravity

The main bathymetric feature in the West Philippine Basin is the NW-SE trending Central Basin Fault (Figure 2). Bathymetric profiles across the fault are similar to those of mid-ocean ridges. The fault exhibits a rift valley, 25 km in width, approaching depths of nearly 7 km at the center of the valley and rising to under 4.4 km at the walls of the valley (Ben-Avraham, 1972). As described by Sclater (1976), a zone of very rough topography with an echelon pattern, possibly related to a change in spreading direction

Site	Depth Drilled (m)	General Description	Average Sonic Velocity (km/s)	Estimated Basement Age
290 (17°44.85'N; 133°28.08'E)	255	0-90m Quaternary to Late Oligocene silt-rich clays + zeolite + ash 90-139 Late Oligocene nannofossil ooze 139-223 Early to Late Oligocene volcanic silt and clay 223-255 Very Late Eocene, Early Oligocene vol. conglomerate	1.7	Late Eocene
291 (12°48.43'N; 127°49.85'E)	120	0-62 Late Oligocene-Pliocene silt rich clay 62-80 Early to Late Oligocene clayey nannofossil ooze 80-102 Late Eocene-Early Oligocene clayey radiolarian + nanno-fossil ooze 102-118 Late Eocene, Mid Early Eocene nannofossil/radiolarian silty caly to zeolite-rich clay 118-120 Tholeiitic, fine grained basalt	1.5	?
292 (15°40.11'N; 124°39.05'E)	444	0-368 Late Eocene-Late Pleistocene (holocene) nannofossil ooze, chalk + volcanic debris 368-444 Tholeiitic, subophitic basalt	1.7	Mid-Late Eocene 36.1-39.2 my (K-AR)

Table I. DSDP (leg 31 and 59) coring summary of site locations in the West Philippine Basin.

Site	Depth Drilled (m)		General Description	Average Sonic Velocity (km/s)	Estimated Basement Age
293 (20°21.25'N; 124°05.65'E)	476+	0-244	Late Pliocene-Pleistocene sand-silt turbidites	1.6	? (Late Eocene+)
		244-400	Pliocene mudstone turbidites + reworked Late Cretaceous foraminifera		
		400-429	Mudstone + reworked Late-Mid Eocene nannofossils		
		429-476+	Basaltic breccia, Miocene		
294-5 (22°34.74'N; 131°23.13'E)	118(294)	0-98	Pleistocene silt-rich clay	1.5	Eocene - Paleocene
		98-112	Eocene(?) ferruginous silty clay + reworked paleocene foraminifera		
		112-118	Tholeiitic basalt		
447 (18°00.88'N; 133°17.37'E)	296.5	0-47	Late-Mid Oligocene to Early Miocene clays	2.3	Mid Oligocene +
		47-113	Middle Oligocene volaniclastic breccias - Polmictic conglomerate + tuffs		
		113-282	Tholeiitic basalts (Pillow lavas) and flows		

Table I. (continued)

(Lee, 1982), surrounds the fault. To the south the topography becomes smoother and pelagic sediment cover more uniform in thickness. North of the fault, the zone of rough topography extends further into the basin and sediment cover is thus much more irregular (Sclater, 1976).

Gravity profiles in the West Philippine Basin are similar to slow spreading mid-ocean ridge systems (Ben-Avraham et al., 1972; Talwani et al., 1965). Free-air anomalies less than 42 mgal are observed at the Central Basin Fault and are less than 15 mgal in the rest of the basin. Since the mean gravity field is generally less than 10 mgal (Sclater, 1976), it has been postulated (Louden, 1980; Sclater, 1976) that the basin is compensated, despite the ~1 km deeper water depths than for comparably aged crust in the Western North Pacific (Sclater, 1971). The thin crust can account for part of the observed depth anomaly (Louden, 1976; Sclater, 1976) but other mechanisms such as anomalous upper mantle densities (Watanabe et al., 1977; Yoshii, 1973) are also needed to explain the gravity field.

Heat Flow

Karig (1971b) classified the West Philippine Basin as exhibiting normal heat flow for Eocene age crust. Measurements of heat flow, taken on leg 13 of expedition Antipode and leg 7 of expedition Tasaday helped to corroborate this. Median heat flow values of 1.17×10^{-6} cal/cm^2 sec in the northwest and 1.64×10^{-6} cal/cm^2 sec in the southwest Philippine Basin were discovered (Sclater, 1976). The standard deviations from the 14 measurements located south of the Central Basin Fault and 10 measurements made north of the fault

are rather high; .86 cal/cm^{2}sec and .69 cal/cm^{2}sec, respectively (Sclater, 1976). In the grading system of Sclater (1976) where only reliable measurements such as those occurring in well sedimented areas in regions of smoothed topography are analyzed, scatter decreases. A median value of 1.68 cal/cm^{2}sec with a standard deviation of .16 cal/cm^{2}sec for 6 reliable environments in the southwest Philippine Basin was determined (Sclater, 1976). No reliable measurements for the rougher and less uniformly sedimented northern section are reported.

The relation between heat flow and age for the basin when compared to well sedimented area of deep-ocean floor are similar (Sclater, 1980). The heat flow-depth relationship, however, shows the basin to have higher than normal values for oceanic crust of the same depth (Sclater, 1972), although it may not be considered significant (Sclater, 1976).

Magnetics

One of the earliest magnetic interpretations for the West Philippine Basin comes from Ben-Avraham et al. (1972). In their study symmetric anomalies across the Central Basin Fault were identified. The magnetic anomalies were modeled by a ridge striking N10°W at a latitude of 15°N, or at the present strike of the fault, ∿ N50°W, but at a much lower latitude at the time of crustal generation, close to 8°N. A comprehensive examination from a limited number of profiles existing for the region is given in Louden (1976). In this study spreading about the Central Basin Fault at a rate of ∿ 4 cm/yr and a paleolatitude south of equator, between 0°-16°S,

ceasing ~40 m.y. was determined. The anomalies (Table II) get pro-
gressively younger as the fault is approached. The orientation
of magnetic lineations in the southern part of the basin, being nearly
parallel, suggests that symmetrical crustal extension occurred (Louden,
1976). The symmetry of crustal spreading in the northern section is
not well defined.

Seismic

Table III summarizes seismic profiles investigating crustal
structures in the West Philippine Basin. Louden (1980), Henry
et al. (1975) and Murauchi et al. (1968) report layer 2 thicknesses
with a mean of .5 - 1.0 km thinner and layer 3 thicknesses between
1.0 and 2.0 km thinner than similarly age crust in the Western
North Pacific (Raitt, 1963).

Crustal trends across the basin are not well documented with
such limited data in the area, but there is evidence for consider-
able thinning of the transitional layers towards the eastern areas
(L.D. Bibee, personal communication). Seismic velocities for layer
2 are slightly lower than for average crust (Murauchi, 1968) but re-
gions of anomalously high transitional layer velocities in the north-
ern section of the basin, approaching the Oki-Daito Ridge have been
found (Louden, 1980; Henry et al., 1975). Typical oceanic layer
velocities and mantle velocities have been found to exist in the
basin (Murauchi, 1968).

Investigations into upper mantle structures from surface wave dis-
persion studies across the Philippine Sea (Abe and Kanamori, 1970;
Seekins and Teng, 1977) have shown the area to have anomalously low

Anomaly	Average Distance from Central Basin Fault (km)	Age, my	
		Heirtzler et al., (1968)	Sclater et al., (1974)
Beginning of 21	513	54.2	50.7
20	339 ± 11	49.6	46.4
19	211 ± 11	47.0	44.0
Between 17 and 18	95^{+11}_{-15}	44.1	41.4
End of 17	28^{+4}_{-2}	42.3	39.7
Between 15 and 14		39.5	37.1
or	-80^{+5}_{-17}		
17 and 18		44.1	41.4
19		47.0	44.0
or	-202^{+5}_{-17}		
13		38.0	35.8
Beginning of 20	-302 ± 5	49.6	46.4

Table II. Age of magnetic anomalies identified in the West Philippine Basin and their distance from the Central Basin Fault (from Louden, 1976). (-) signs refer to anomalies south of the fault.

Lat. (°N)	Long. (°E)	Water H(km)	Sediment v(km/s)/ H(km)	Layer 2 v(km/s)/ H(km)	Layer 3a v(km/s)/ H(km)	Layer 3 v(km/s)/ H(km)	Mantle H(km/s)
			Indopac, Philippine Sea (Louden, 1980)				
18°03'	133°49'	5.89	2.0*/0.28			6.28/3.49	7.97
				5.4*/1.38	--	6.28/2.93	7.97
18°03'	133°48'	5.90	2.0*/0.42			6.69/3.01	8.03
				5.4*/1.85	--	6.69/2.43	8.03
18°03'	133°08'	6.04	2.0*/0.36			6.54/2.69	8.11
				5.4*/1.65	--	6.54/2.11	8.11
18°03'	133°08'	6.04	2.0*/0.35			6.57/2.90	7.98
				5.4*/1.57	--	6.57/2.37	7.98
21°04'	126°30'	5.57	2.0*/0.42	5.81/1.36	--	6.98/5.42	8.68
21°04'	126°27'	5.50	2.0*/0.23			5.98/4.17	8.22
21°12'	125°41'	5.28	2.0*/0.31	5.68/1.29	--	7.02/2.48	7.72
			Tasaday, Philippine Sea (Henry et al., 1975)				
22°30'	131°24'	5.77	1.6*/0.24	5.76/0.63	6.23/0.22	6.69/3.52	7.99
17°10'	128°11'	5.40	1.6*/0.20	5.04/1.22	6.30/1.90	7.12/ --	--
			All Philippine Sea (Murauchi et al., 1968)				
				4.85/1.27	--	6.70/4.29	8.23
			Western North Pacific (Riatt, 1963)				
				5.02/2.05	--	6.73/5.08	8.21

*Assumed velocities

Table III. Compilation of refraction results in the West Philippine Sea stemming from Indopac and Tasaday expeditions. Alternate solutions for Indopac surveys are given (Louden, 1980). Average crustal section for the Philippine Sea and Western North Pacific are also shown.

Rayleigh and Love Wave group velocities compared with normal oceanic lithosphere (Forsyth, 1975), indicating an anomalously thin lid over-lying a low velocity mantle. The bottom of the lithosphere is identified by a decrease in shear wave velocities at 30 km depths (Figure 4), about 40 km less (Seekins and Teng, 1977; Abe and Kana-mori, 1970) than beneath normal ocean of Eocene age (Forsyth, 1975). The bottom of the asthenosphere, as indicated by an increase in shear wave velocities, is also anomalously shallow when compared to similar age regions in the Pacific Ocean (AMB model of Seekins and Teng, 1977).
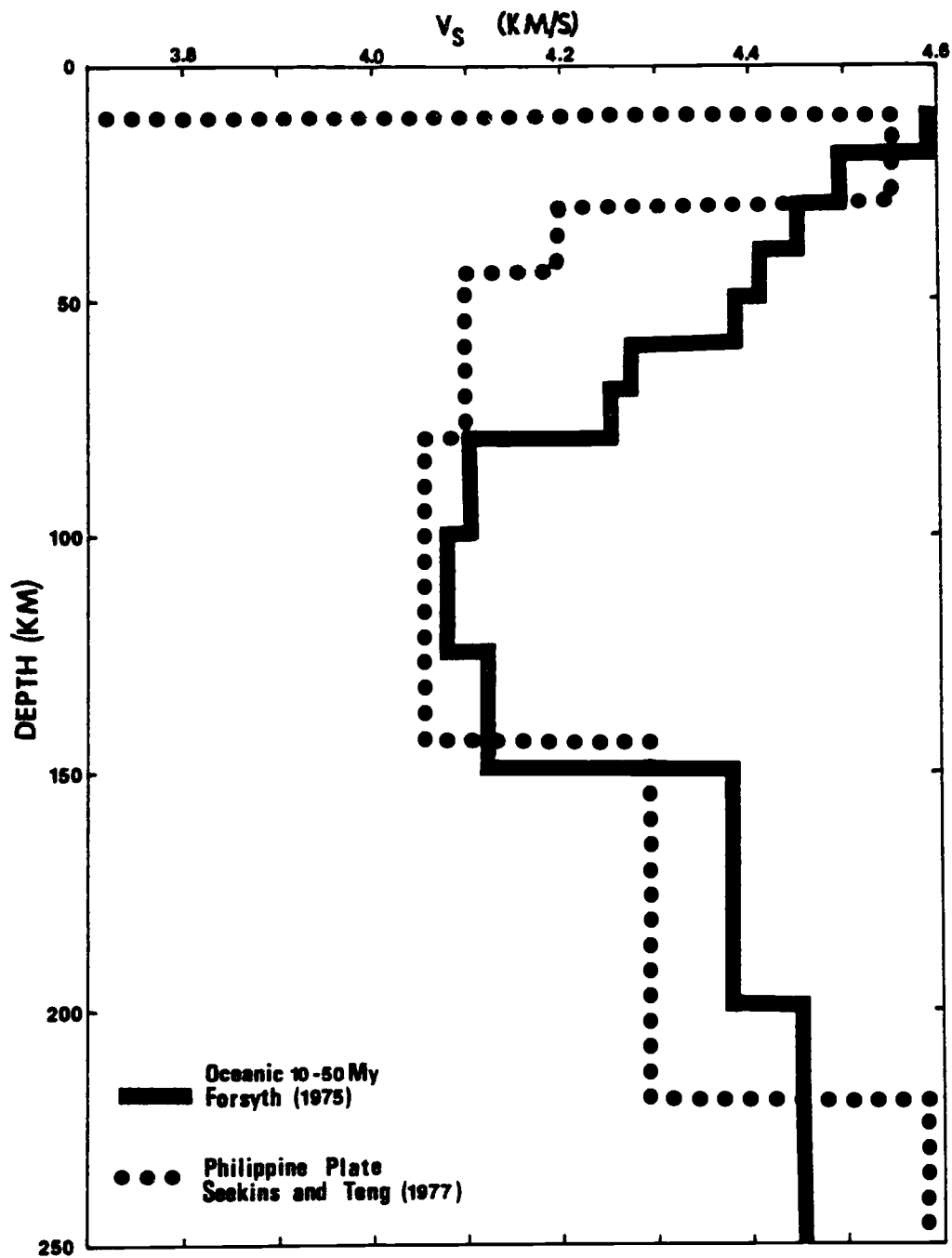
Figure 4.   Comparison of shear wave velocities beneath the Philippine
Sea and 10-50 million year old average ocean.

DATA ACQUISITION

OBS Instrumentation

The objectives of this project were to investigate seismic structures in the West Philippine Sea and their affect on the propagation of acoustic energy. The detection and analysis of naturally and artificially generated seismic waveforms which are reflected, refracted or transmitted from the ocean floor forms the basic method of obtaining this information. Because phase and amplitude of seimsic arrivals are the main parameters of interest, extremely sensitive recorders are needed for measuring these signals. The device essential to this purpose is the ocean bottom seismometer.

The ocean bottom seismometer (OBS) developed by the Marine Seismology group at Oregon State University and used in this study is a 4 channel, direct analog recording device, containing acoustic and timed-release systems for free-fall deployments. The OBS is equipped with horizontal and vertical geophones that have a natural frequency of 3 Hz, and a pressure-compensated hydrophone with a flat frequency response between 1 and 30 Hz. One data channel is a time signal, in which a series of variable length pulses provide a complete time readout coded once each minute (Johnson et al., 1977). To meet the demands of low power consumption for a self-contained battery operated instrument with 17 days of recording capability and up to 35 days of operation, CMOS electronics were used in the board design. Included in the electronics are two independent timed-release circuits, one of which is used as a backup release, and has a completely separate battery supply.

The entire instrument package is encapsulated in a cylindrical aluminum pressure case that can withstand water depths of more than 7 km. The pressure case is mounted to a rectangular frame onto which two small pressure cases, housing high-torque d.c. release motors are attached. These release motors turn shafts connected to levers supporting an expendable, cement, iron-reinforced anchor that is cylindrically shaped to improve ground coupling. The floatation devices used are two Benthos glass spheres mounted in a frame attached to the instrument frame. For those instruments equipped with acoustic releases, (developed at Scripps Institution of Oceanography) the electronics are situated within one of the glass floatation spheres and connected via external Mecca hookups, as are all external connections. An acoustic transducer, hydrophone, radio beacon and flasher are mounted directly onto the OBS frame, composed entirely of aluminum and anodized to prevent corrosion.

There are several advantages to this instrument design. Foremost, it is necessary that only one of the two release motors work for a liftoff should one fail (as has occurred). Furthermore, since the instrument is in a continuous recording mode and supports an acoustic release system, significant flexibility is given to the underway experiment design. In addition to being a cost-effective instrument and requiring only a few hours of engineer checkout time, its' overall design makes for relatively easy launch and recovery procedures. One disadvantage is that the fidelity and dynamic range

reproduced in the analog recording of ground velocity is generally not as good as that afforded in a digital instrument.[1]

Underway Operations

The field program to investigate long-range propagation of acoustic energy in the West Philippine Sea was conducted in a three phase experiment during February and March of 1981, in cooperation with Scripps Institution of Oceanography. During the first phase of the study carried out on the RAMA expedition leg 9 (Guam-Guam), one of two 17-day cruises aboard the R/V THOMAS WASHINGTON, a long-line refraction profile extending to 500 km was conducted. 0.9 - 1.8 ton Tovex water gel explosives were used as sources and ocean bottom seismometers as receivers. A total of seven Oregon State continuous recording seismometers were deployed for this experiment. Satellite navigation was inoperative during RAMA 9 and was most likely responsible for the loss of two of these instruments. A map of the locations of recovered instruments and the shot line is shown in Figure 5. Underway operations for RAMA 9 included 3.5 and 12 KHz bathymetry echo sounding as well as sea-going gravity and magnetics acquisition.

For phase two of the experiment, seismometers were left between cruise legs to monitor earthquakes. In this way travel paths across the basin could be extended to 1000 km using events occurring at the surrounding trench systems. (Data analysis for this study which is being done at Scripps is continuing presently.)

---

[1] A prototype digital ocean bottom hydrophone to aid in the measurement of explosive source spectrums was developed for the cruise and deployed, but recorded no useable data.
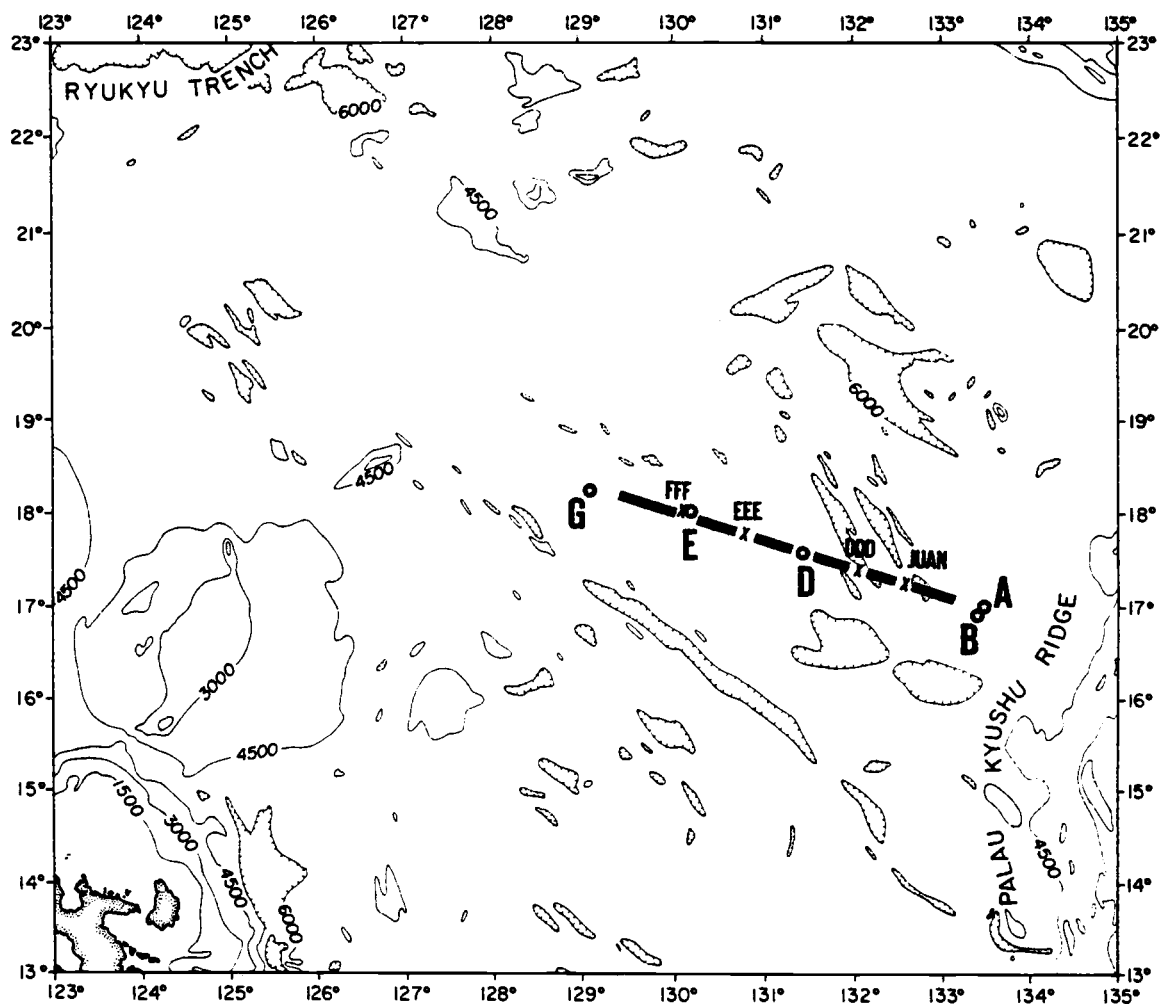
Figure 5. OBS station locations in the West Philippine Sea used
in this study. Instruments A, B, D, E, and G are from
RAMA 9 and DDD, EEE, FFF and Scripp's OBS JUAN are from
RAMA 11.

During the RAMA expedition leg 11 (Guam-Cebu), the third phase of the experiment was run. The initial plan was to recover instruments deployed at the end of RAMA 9 for earthquake investigations. Three of five Oregon State OBS' were recovered; the most likely cause for the two losses attributed to battery power drain from the lengthy 6-week deployment period. The recovered instruments along with two additional seismometers were launched along the same refraction line shot in the first phase in order to perform a shallow crustal examination and anisotropy experiment. Shot sizes ranged from 1 - 240 lbs. of Tovex and were densely spaced along the shot line. A location map of the instruments used in this study is provided for in Figure 5. One instrument was lost for unknown reasons. Data gathering for this study also included continuous airgun reflection profiling, airgun to OBS shooting, 3.5 and 12 KHz echo sounding. In addition, Navy sonobouys were used as receivers. However, because of the degraded quality of this data set relative to the data recorded on the ocean bottom seismometers, the sonobouy data was not included in this analysis.

World-wide standard time transmitted from stations in Colorado and Japan were monitored throughout the experiment so that OBS clock drift corrections could be made.

RAW DATA REDUCTION AND PROCESSING

Digital Conversion

The 4-channel analog data recorded by Oregon State OBS's are
converted into the digital domain for ease of information handling
and manipulation. A flow chart of the processes involved in the
conversion of raw data to the finalized ROSE format (LaTraille et al.,
1982), a standardized data format adopted by many oceanographic in-
stitutions, is shown in Figure 6.

The seismic signals, initially recorded on magnetic tape, are
played back through a stereo reel-to-reel tape transport modified for
slow speed, a four channel head and low noise preamps. To make sure no
skew occurs, calibrations were placed on channels 1 - 3 prior to
OBS deployment. During playback then, tape heads could be adjusted
for skew simply by phasing channels 1 - 3 at the lowest frequencies
first, and progressively at the higher frequency calibrations. Tape
tracks were centered on the playback head by adjusting for maximum
voltage output. Output from the tape deck was then connected to
amplifiers with differential inputs. Gain settings used placed the
background noise at about .05 V. (This would correspond to about
10 counts on a 12-bit A/D converter.) Next, amplifier outputs were
fed into antialiasing filters set at 2 - 25 Hz. Since an attempt
is made to digitize at 100 samples/sec, the Nyquist frequency is
about 50 Hz, or twice that of the high frequency filter setting.
Signals between 2 - 25 Hz are thus fairly well recovered with little
aliasing noise from higher frequencies. Filtered output from channels
1 - 3 subsequently were fed directly into a 12 bit A/D converter.
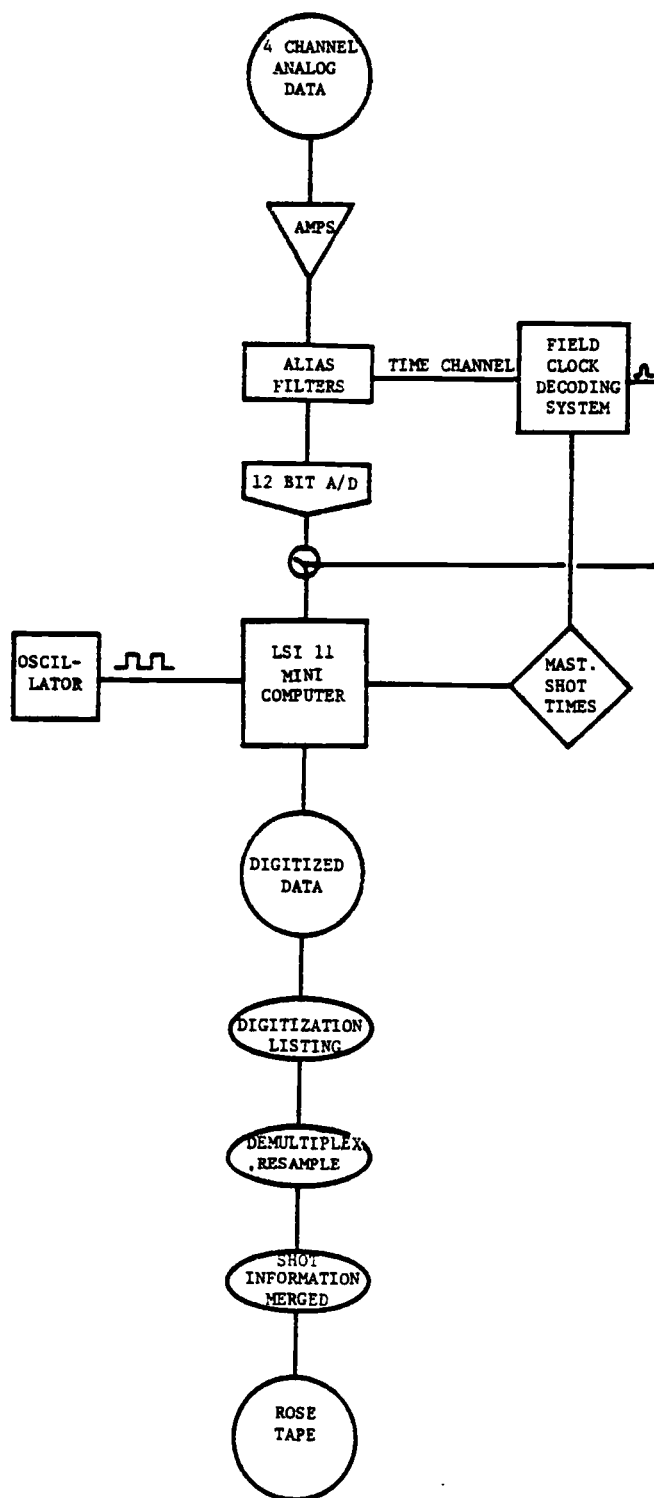
Figure 6. Flow chart of raw data reduction procedures; from raw
analog data to ROSE tape format (LaTraille, 1982).

Channel 4, which contains the time signal, was first input to a time decoding system before being connected to the A/D.

At this point digitization control is taken over by a high-level software program run on an LSI-11 mini-computer. Digitization times are read by the A/D program from a master shot file and sent to the clock decoder for comparison. On a pulse from the comparator, digitizing begins, with the rate set using an external oscillator. In order to increase signal/noise, a playback speed of 30 x real time is used. The digital information is written to 9 track magnetic tape in multiplexed form. After this process is complete a listing of digitization results is compiled in order to check for timing errors. Because of variabilities in instrument recording speed due to battery power drain during prolonged deployments as well as other factors, the actual number of samples digitized in each second varied. For this reason the data was resampled to 100 samples/sec after being demultiplexed. The final reduction programs corrected for OBS clock drift and placed shot information into the headers of each event, consistent with ROSE format.

Shot and Receiver Range Determination

In performing a seismological study in the marine environment poor navigation can undermine the success of a project. Throughout the entire duration of RAMA 9, the first cruise of this study in which the long-line refraction experiment took place, satellite navigation was not available due to a malfunction in the shipboard computer. Fixing by LORAN C was marginal to fair at times but was generally regarded as unworthy by the mate on watch. Navigation by

LORAN is usually good in this region, with adequate areal coverage provided by slave stations located at Iwojima, Guam and Yap islands. However the Yap station was inoperative and only a sketchy two-line position could be made. The ship was not equipped for OMEGA radio-ranging, hence this could not be used as a backup navigational aid. For these reasons the primary navigation from which most of the positioning was logged came from dead-reckoning off star fixes, made at morning and evening twilights, and occasional LORAN fixes.

Navigation by this method proved to be inadequate, with DR positions considerably off the latest star fix. In one instance a search for a surfaced OBS was being conducted. When a star fix became available several hours later it was learned the assummed position was 24 miles in error. Because of the scheduling of instrument surface times, the additional steaming time necessary to check the new position could not be afforded. This instrument was therefore lost. Errors in navigation were more than likely the cause of the loss of another of our OBS's as well as one from Scripps. Nonetheless, OBS recovery was still better than 70%, with 5 out of the 7 Oregon State OBS's retrieved from deployments during the first leg.

Severe inaccuracies in navigation during the shooting run were also discovered. Shot and receiver positions can be corrected however, if the water velocity is known as a function of depth and water-borne arrivals can be observed on the instruments. Accordingly, given the acoustic velocity, $V(z)$, the total travel time for a ray departing at an angle θ_s and shot depth Z_s, and arriving to a bottom depth Z_b, is

$$T = \int_{Z_s}^{Z_b} \frac{dz}{V(z)\cos[\sin^{-1}V(z)p]} \tag{1}$$

where $p = \sin\theta_s/V(Z_s)$, the ray parameter. In application, the travel time from this equation is adjusted using the independent variable, ray parameter p, to match observed arrival times of water-borne energy arrival. The corrected shot-receiver range is then given by

$$X = \int_{Z_s}^{Z_b} \frac{dz}{\tan[\sin^{-1}V(z)p]} \tag{2}$$

In obtaining ranging information from water waves, additional complications arise from the fact that the observable energy from the water waves, at larger shot-receiver distances, have gone through multiple reflections off the sea surface and bottom. The distance at which the first reflection becomes the first observable energy is determined using the ray parameter that is just turning at the ocean bottom (i.e., $p = 1/V_b$, where V_b is the velocity at the ocean floor and $\theta = 90°$ for a turning ray). Using the water velocity model secured for our study area in the West Philippine Sea (Table IV) and a nominal depth of 3000 fathoms, this distance was calculated to be about 32 km. Hence at distances greater than this no direct water waves are observed at the sea floor. At distances larger than about 3 times this, or 96 km, the first bounce, which includes one reflection off the sea bottom and sea surface, also dies out. Similarly, the nth bounce dies out at $\sim(2n+1) * 32$ km.

Depth (m)	Sound Velocity in water (km/sec)*
0	1.5299
16	1.5305
30	1.5306
50	1.5311
78	1.5308
100	1.5267
130	1.5243
172	1.5206
218	1.5172
270	1.5150
400	1.5089
487	1.5011
566	1.4920
727	1.4814
918	1.4815
1472	1.4837
2086	1.4923
2500	1.4991
3153	1.5095
3686	1.5184
4754	1.5378
5288	1.5477
5821	1.5572

*Courtesy of Scripps Institution of Oceanography

Table IV. Water velocity vs. depth.

The generalized equation for travel time and horizontal range traversed are thus better described:

$$T = \int_{Z_s}^{Z_{b_0}} \frac{dz}{V(z)\cos[\sin^{-1}V(z)p]} + 2\sum_{i=1}^{n} \int_{0}^{Z_{b_i}} \frac{dz}{V(z)\cos[\sin^{-1}V(z)p]} \quad (3)$$

$$X = \int_{Z_s}^{Z_{b_0}} \frac{dz}{\tan[\sin^{-1}V(z)p]} + 2\sum_{i=1}^{n} \int_{0}^{Z_{b_i}} \frac{dz}{\tan[\sin^{-1}V(z)p]} \quad (4)$$

where Z_{b_i} is the depth at the ith bounce. For simplicity in ray tracing for ranges, Z_{b_i} was set to the average bathymetric depth measured across the shot line.

Because satellite navigation was operational during RAMA 11, the number of bounces the water waves had gone through was clearly depicted on record sections. Choosing the water path was also aided by a fairly continuous and dense array of shots, with charge sizes small enough such that crustal arrivals did not obscure contemporaneous arrivals from the water column. This was not the case for RAMA 9, however. The number of bounces the water waves had experienced was not readily apparent on the record sections made from the 5 OBS data tapes collected. Some shots were so inaccurately navigated that the water waves did not appear on reduced sections comprising 20 seconds of travel time. Furthermore, because of the large shot size of 1 - 2 tons, water waves from shots within about 70 km of an OBS were masked by large amplitude crustal arrivals. Digital high-pass filters, 15 to 32 Hz, were applied to the

data in hopes of alleviating this problem; since the water waves generally have more power at higher frequencies. This was met with limited success.

An initial estimate of the number of multiple water wave reflections that occurred was made using the uncorrected range from navigation and the corresponding first observable bounce path at that range. Hence shot ranges between 32 - 96 km were given one bounce, 96 - 160 were assigned two bounces, etc. Existing ray tracing programs had to be modified for handling up to 7 water bounces to accomodate the long-line data from RAMA 9.

Next, an attempt was made to get relative locations of shot and receivers using a two-dimensional inversion relocation program. There was essentially a two-fold purpose in applying this program: first to calculate distances to shots that could not be ray traced due to the overshadowing effect at close ranges, and second, to provide for final analyses a consistent model of shot location and ranging so the travel time data would be consistent between instruments. Solutions from the two-dimensional relocation never converged. This was not too surprising since the experimental design of RAMA 9 was to have, as closely as possible, shots and receivers along a common line. Thus the solutions would not be constrained very well in the dimension perpendicular to the array. For this reason, one-dimensionality was assumed and a simple least squares method, solving simultaneously for shot and reveiver locations was applied. The simplicity of this relocation has some inherent problems in that the least square ranges for close range shots may be off the actual

range if shooting, deviated significantly from the OBS line because
of navigation.

Residuals from the linear fit showed the ranges, and therefore
possibly the number of bounces for some shots were off. Adjusting
the number of bounces was done in a somewhat iterative fashion. The
shots with the largest residuals were given alternate bounce paths.
A new least squares relocation model was determined and iteratively
adjusted in the same fashion. This proceeded quite successfully
until all residuals got to within about 1.5 km, after which no
progress was made.

From a desire to produce a positioning model with less error,
a program was written to calculate travel time versus distance from
the first water arrivals for each bounce path. The output of this
program was a travel time plot made at the same scale of the reduced
sections used in picking water waves. The plot was then used as an
overlay on the sections to help determine the bounce path by looking
for later water wave arrivals and the time between various bounce paths
in respect to distance. The graph also included the travel time for
reflected energy beginning at a nominal shot depth, $\sim$ 100 m for 1
ton shots, and that takes an initial bounce off the sea surface.
Several modifications to the number of bounces for some shots were
made possible using this travel time overlay. The final model cal-
culated had residuals which were all less than 0.6 km.

For ROSE format cataloging purposes and for locations given in
this study, absolute geographic positions were referenced with respect
to OBS G, and using an initial angle along a great circle to OBS B.

SEISMIC REFRACTION

General Theory

The technique of refraction seismology involves measuring the arrival time of acoustic wave energy which propagates in the earth from a source point to a receiving station. The seismic energy, either initiated artificially using explosives or from naturally occurring earthquakes, is recorded on devices such as ocean bottom seismometers for marine work or on land base seismometers for investigations on continents. The benefits of the method are that information regarding the acoustic structures at depth are manifested in the seismic signals. To interpret these signals requires and understanding of the phenomena of refraction.

The first physical description of refraction, quantized into Snell's Law, was developed from experimental work by the man of the same name, Willebrod Snell (1591 - 1626)[2]. The law states that "when a wave crosses a boundary between two isotropic media, the wave changes direction such that the sine of the angle of incidence... divided by the velocity in the first medium equals the sine of the angle of refraction divided by the velocity in the second medium" (Sheriff, 1973). The mathematical expression describing ray bending (refraction) depicted in Figure 7a is

$$\frac{\sin\theta_1}{V_1} = \frac{\sin\theta_2}{V_2} .$$

(5)

---

[2]The experiments which led Snell to develop the law of refraction were motivated from an earlier corpuscular theory of light by René Descartes (1596-1650). In France, Snell's law is known as Descartes law.

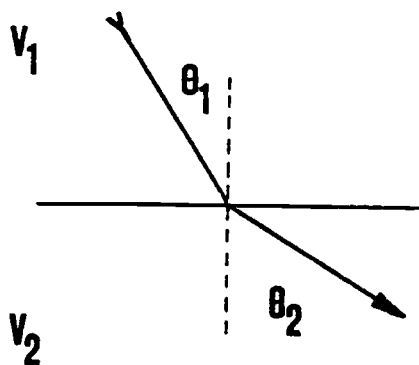Figure 7a. Geometry of a refracted ray.
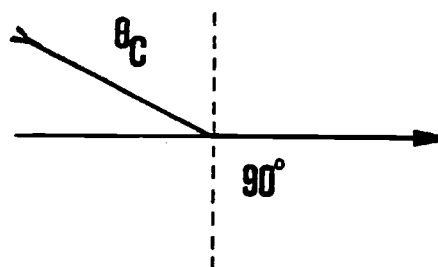
Figure 7b. Geometry of a critically refracted ray.
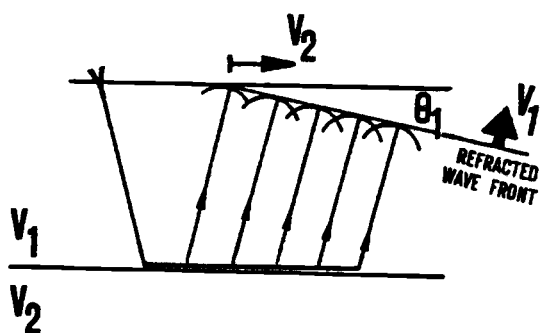
Figure 7c. Geometry of the wavefront produced by refraction (for a layer over a half-space).
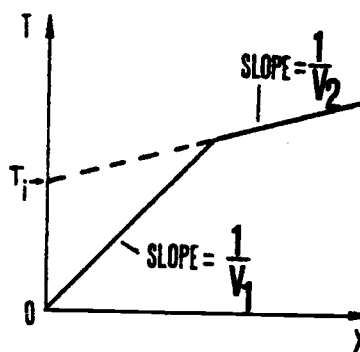
Figure 7d. Travel time curve for a horizontal layer over a half-space.
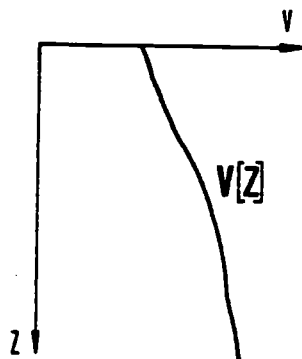
Figure 7e. Continuous velocity increase with depth.
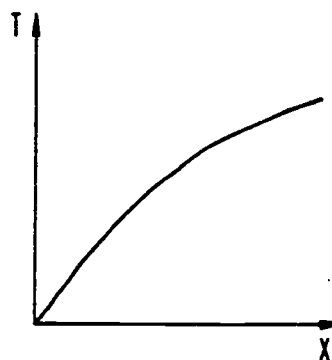
Figure 7f. Travel time curve (simulated) for continuous velocity increase with depth.

In applying our knowledge of ray paths of seismic energy to the study of the earth we make use of 'critically refracted rays'. Critical refractions are for rays traveling at an angle, $\theta_1 = \theta_c$, such that $\theta_2 = 90°$, i.e. $\sin\theta_c/V_1 = \sin\theta_2/V_2 = \sin 90°/V_2 = 1/V_2$. The critical angle, θ_c is thus given by $\sin^{-1}(V_1/V_2)$. For the simplest case of a layer over a half space with $V_2 > V_1$ (Figure 7b) this is the ray traveling along the interface between the acoustically defined media. The critically refracted ray also acts as a new spherical wave source as stated by the Huygens' principle. When combined with other rays leaving the interface the net effect is to produce a flat wave front traveling at speed V_1 and inclined at an angle θ_1 from the horizontal (Figure 7c). The wave front although traveling at V_1 is observed to travel at a phase velocity V_2 at the surface of the earth when measured by a set of receiving stations strung out on a common line with the source point. This can be compared to a wave at sea which angles into the beach, although traveling at a constant velocity, its' effects are felt much faster along the coastline.

The travel time of first observable energy with distance from the source point for the horizontal plane layer structure (Figure 7c) is shown in Figure 7d. The inverse slopes of the two lines are the velocities of the two isotropic media. The break point in slope, known as the crossover distance, occurs when the refracted or head wave overtakes the direct wave traveling strictly along the surface of top media, and becomes the first observable energy at the surface. The depth to the interface Z_1, which also defines the crossover distance, is found from extension of the later arriving phase to the

origin. The intercept time T_i is given by $2Z_1\cos\theta_1/V_1$; and the depth to the layer 2 refractor is thus $T_iV_1/2\cos\theta_1$. Hence, knowledge about a structure at depth is learned.

The method can also be extended to a multi-layered system where velocity increases in each consecutive layer downward. For earth structures having a continuous velocity gradient (Figure 7e), evident in a travel time curve with continous curvature (Figure 7f) an alternate method for interpretation is needed. A commonly used travel time inversion for data of this kind is the Herglotz-Wiechert inversion and is discussed in a later section.

The inadequacy of the horizontal plane layer solution for interpretation becomes apparent when seismic discontinuities are not laterally homogenous. For velocity horizons which dip in one direction, graphical solutions, similar to those of the flat plane layer solution, are available and are well known to the practicing geophysicist. This method along with the horizontal plane layer method are rather limited however in real earth situations--the real earth being neither perfectly layered horizontally or perfectly layered with a dipping structure. A method which unifies both of these methods and yet allows for further freedom in mapping seismic structures at depth is discussed subsequently.

Delay-Time-Function Method

It is not well documented when the first creative thought for partitioning travel time using "delay" or "time terms" was conceived, but it was in operation at least as early as 1931 by the

Imperial Geophysical Experimental Survey to map subsurface structure. It has been applied in various forms since then (Gardner, 1939; Scheidegger and Willmore, 1957; Willmore and Bancroft, 1960; Berry and West, 1966; Morris, 1972) and most recently by Ganoe (1983) to study P_n wave propagation in Oregon and by Cook (1981) to investigate crustal structures in the Gorda Basin using sonobouy refraction data. The delay time analysis used in this study and developed by Morris et al. (1969) and Raitt et al. (1969) is the Delay-Time-Function method.

Theory

The travel time from a shot to a receiving station can be described as

$$T_{IJ} = \Delta_{IJ}/V_n + \tau_I + \tau_J \tag{6}$$

where Δ_{IJ} is the shot-receiver distance, V_n is the velocity at the refracting surface, and $\tau_{I,J}$ are the delay times beneath receiving and shot stations, respectively.

The delay times, geometrically depicted in Figure 8, represent the difference between the total travel time and the travel time of a ray propagating along the refracting interface for the entire shot-receiver distance. If the velocity is taken to be a continuous function of depth $V_i(z)$ at the ith point, then the one-way delay time at the ith coordinate can be shown to be
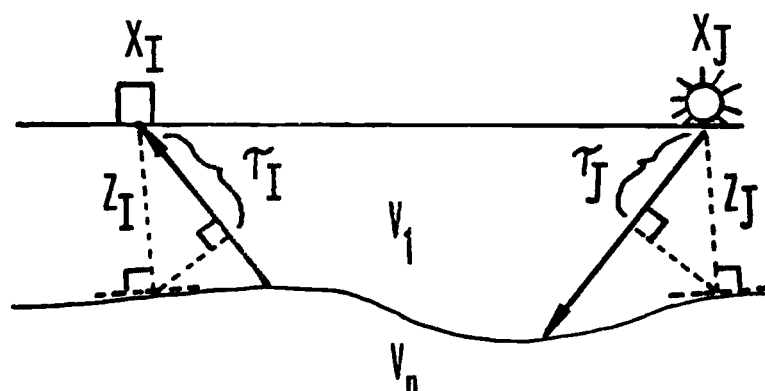
Figure 8. Geometrical description of delay time.

$$\tau_i = \int_0^{Z_i} [\frac{(1-V_i(z)^2/V_n^2)^{1/2}}{V_i(z)}] \, dz \ . \tag{7}$$

Transforming this equation into discrete layer velocities, yields

$$T_i = \sum_{\ell=1}^{n-1} Z_{i\ell}/V_\ell (1-V_\ell^2/V_n^2)^{1/2} \tag{8}$$

where V_ℓ is the velocity of layer ℓ and $Z_{i\ell}$ is the thickness at the ith coordinate.

Some of the inherent assumptions in this method are that velocities are dependent on a single spatial coordinate, i.e. no lateral heterogeneity of seismic velocity for a distinct layer is allowed. In addition to the assumption that seismic arrivals are

refracted head waves, it is necessary for refractor undulations to be small since delay times are taken to be directly below the receivers and shots. When these conditions are satisfied, delay times can be formulated to be solely a function of position. The process employed by Morris (1969) and Raitt (1969), the Delay-Time-Function method, is to represent the delay time position dependence using low order polynomial functions. The travel time for head waves traveling on the ℓth layer is

$$T(XI,XJ)_\ell = G_\ell \Delta_{IJ} + [2a_{0_\ell} + a_{1_\ell}(XI + XJ)$$
$$+ a_{2_\ell}(XI^2 + XJ^2) + \ldots a_{n_\ell}(XI^{n_\ell} + XJ^{n_\ell})] \quad (9)$$

where XI and XJ are shot and receiver positions, G_ℓ is the slowness (= $1/V_\ell$), and $(a_0, a_1, a_2, \ldots a_n)_\ell$ are coefficients of a n_ℓ^{th} order polynomial for the ℓth layer. The delay surfaces can also be described using a linear combination of Fourier terms and polynomial terms (Cook, 1981; Morris, 1969; Raitt, 1969).

The benefits of using these descriptions of travel time is that the delays to the refracting horizon are allowed to vary laterally. This is not allowed for in typical plane layer models. Furthermore, no information on upper layer velocities is required to determine the delay times. If upper layer velocities are known then it is very easy to invert the delay surface into depth using equation (8).

In calculating the delay surface a simple least squares method can be applied. Letting D be a vector containing m travel time observations of critically refracted rays from the ℓth layer, i.e.

$$D = \begin{bmatrix} T_{1_\ell} \\ T_{2_\ell} \\ \cdot \\ \cdot \\ \cdot \\ T_{n_\ell} \end{bmatrix} \qquad (10)$$

and designating M to be the vector containing the unknown coefficients of a $n_\ell{}^{th}$ order delay surface and velocity of the ℓth layer, i.e.

$$M = \begin{bmatrix} 1/V_\ell \\ a_{0_\ell} \\ a_{1_\ell} \\ \cdot \\ \cdot \\ \cdot \\ a_{n_\ell} \end{bmatrix} \qquad (11)$$

then,

$$D = AM \qquad (12)$$

where A is a matrix which transforms M into D and is given by

$$A = \begin{bmatrix} \Delta_{IJ_1} & 2\ (XI + XJ)_1 & (XI^2 + XJ^2)_1 & \cdots & (XI^{n_\ell} + XJ^{n_\ell})_1 \\ \Delta_{IJ_2} & 2\ (XI + XJ)_2 & (XI^2 + XJ^2)_2 & \cdots & (XI^{n_\ell} + XJ^{n_\ell})_2 \\ \cdot & \cdot & & & \\ \cdot & \cdot & & & \\ \cdot & \cdot & & & \\ \Delta_{IJ_m} & 2\ (XI + XJ)_m & (XI^2 + XJ^2)_m & \cdots & (XI^{n_\ell} + XJ^{n_\ell})_m \end{bmatrix} \qquad (13)$$

Since it is a necessary condition to have more observations than unknowns, $m > n_\ell + 1$, the problem in practice is an overdetermined one. The solution to the problem is thus a least squares solution given by

$$(A^T A)^{-1} A^T D = M \tag{14}$$

where A^T is the transpose of A and $(A^T A)^{-1}$ is the inverse of the symmetrized matrix $A^T A$.

Longline Refraction Results

Record sections from 3 instruments: OBS B, E and G, deployed during RAMA 9 are shown in Figures 9, 10 and 11. Results from OBS's A and D were not used in the final analyses since signal to noise was too low for picking first arrivals accurately (even though the water wave information from these instruments was used in the least square ranging solutions). All sections have been reduced at 8 km/sec. Each individual shot has been topographically corrected to a common datum using the delay time of a layer over a half-space according to the equation

$$T_{cor} = \frac{(h_{datum} - h_{shot})}{V_w} \cos\left(\sin^{-1} \frac{V_w}{V_{ref}}\right) \tag{15}$$

where V_w is the sound velocity in water and V_{ref} is the phase velocity at the shot-receiver range. The motivation for initially correcting shots to a datum rather than to the sea floor is that the phase velocity of the first arriving energy from a shot to the receiver is masked by bathymetric variations between shots. By correcting
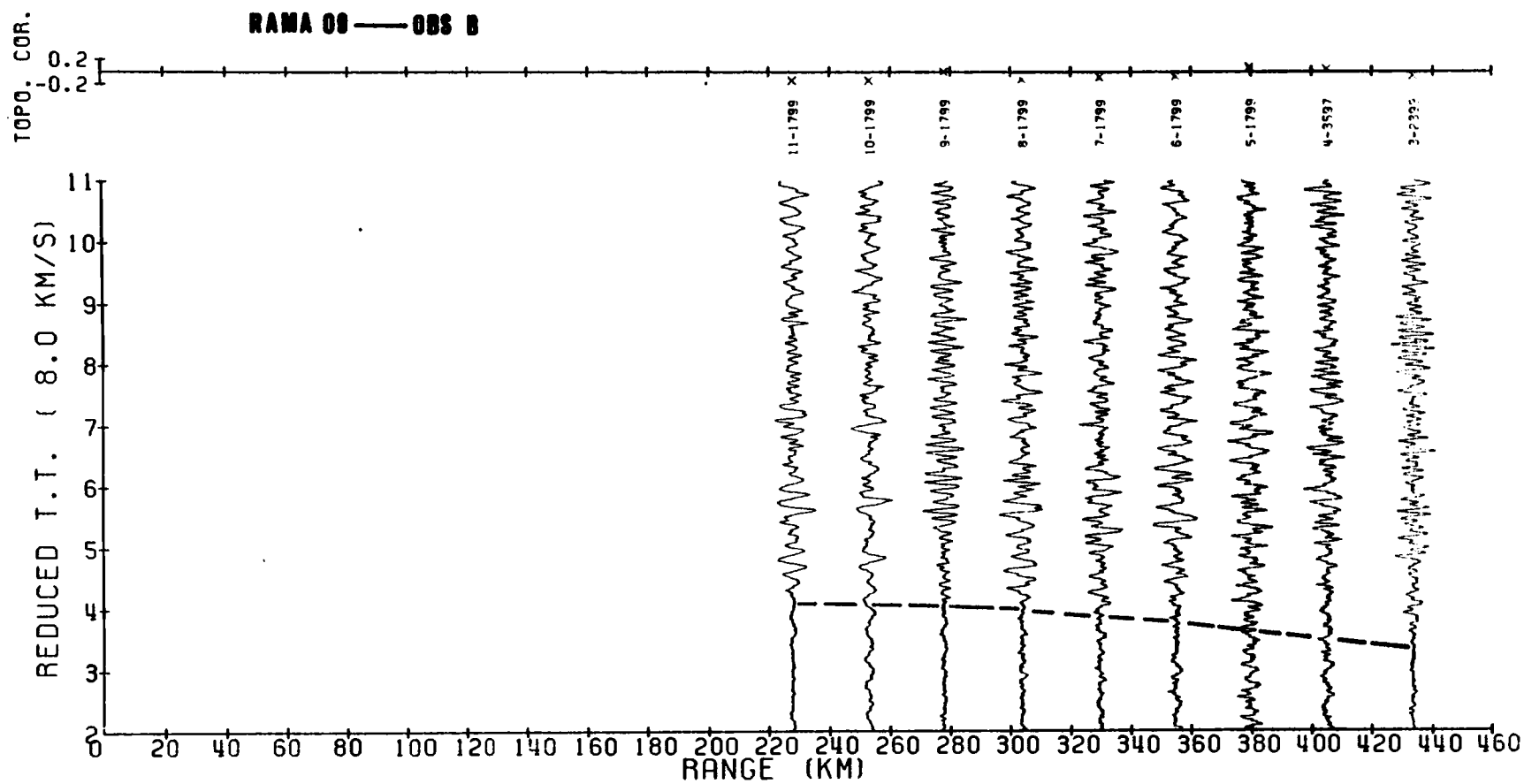
Figure 9.   Long-line record section from OBS B.
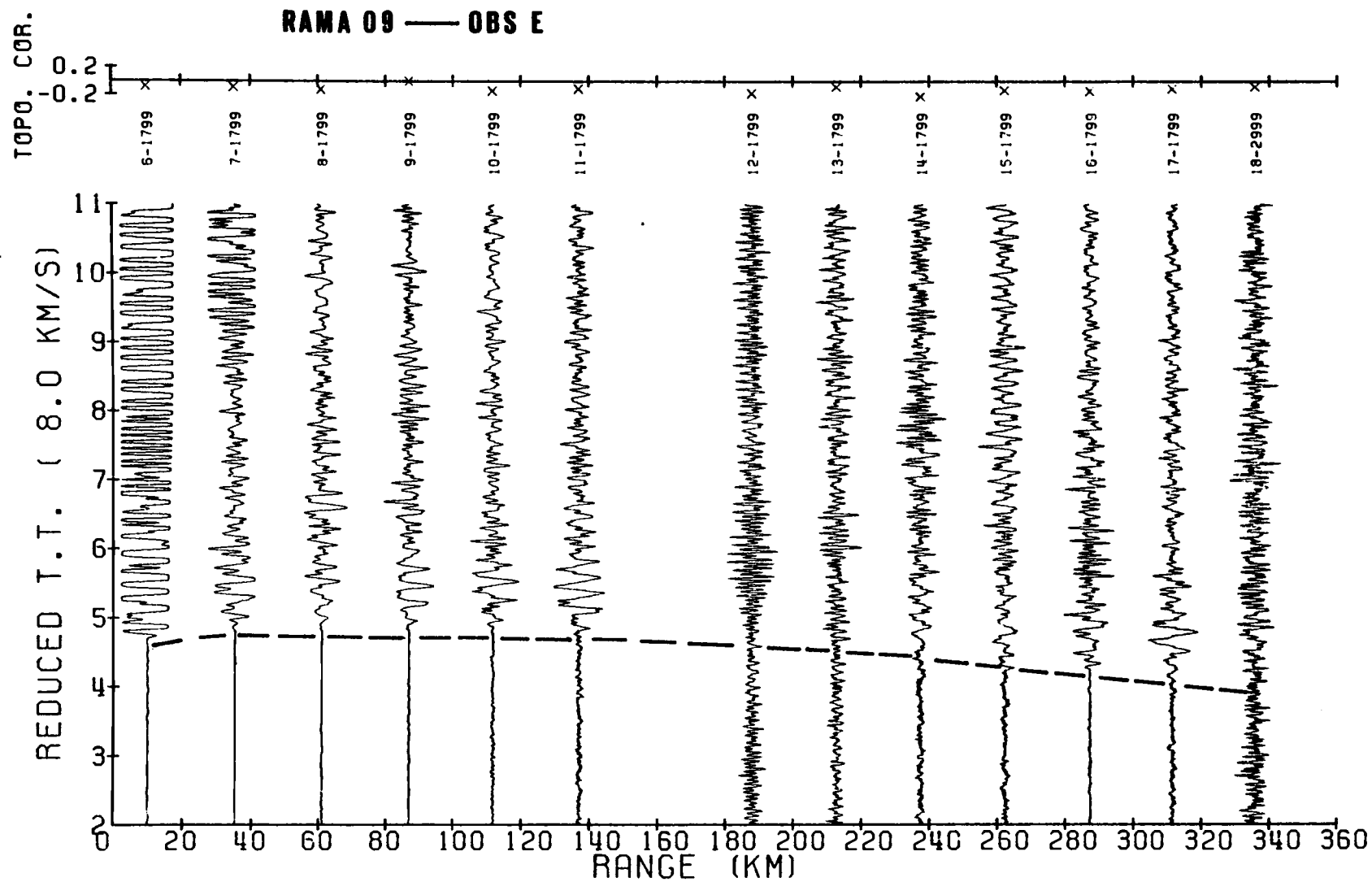
Figure 10. Long-line record section from OBS E.
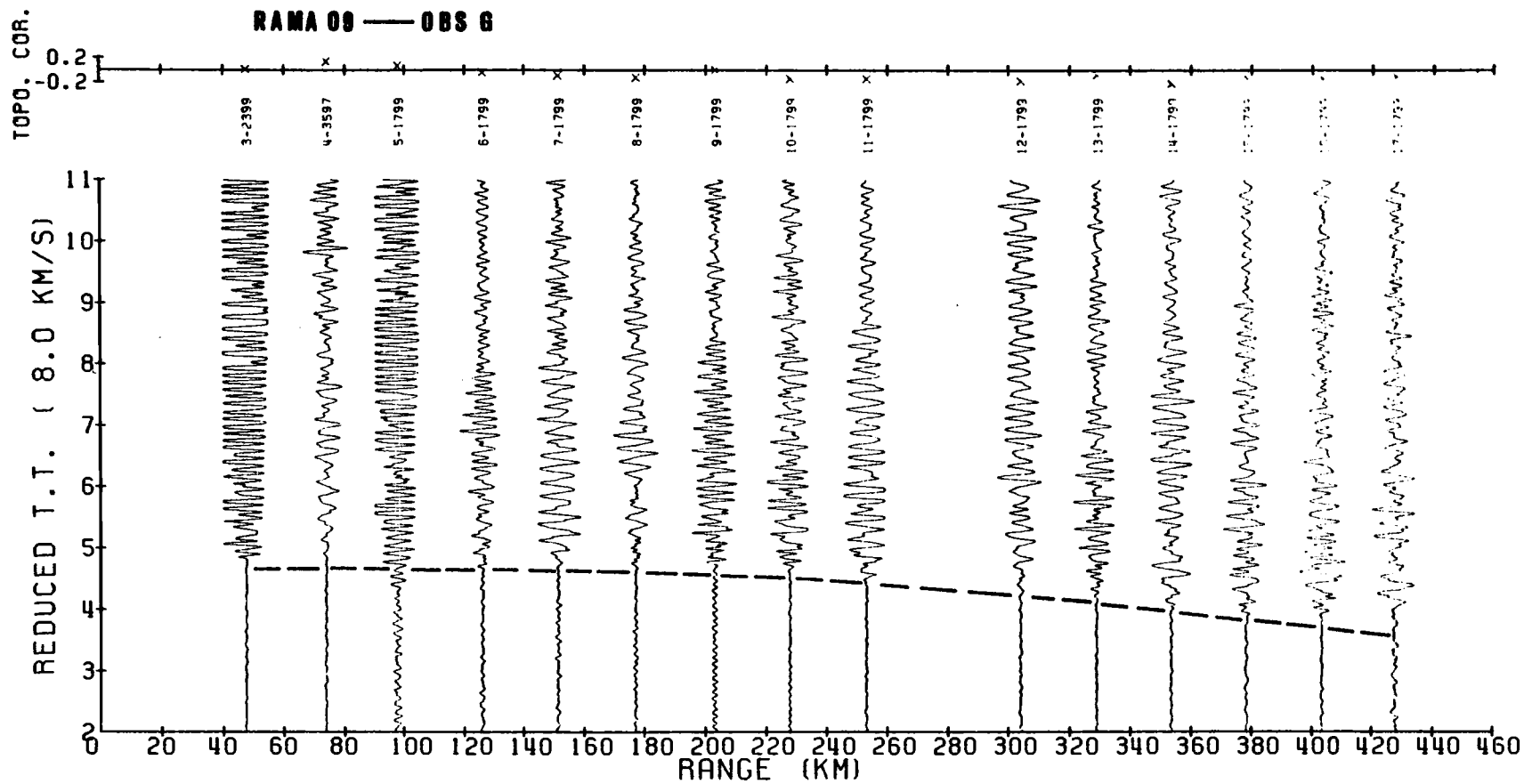
Figure 11. Long-line record section from OBS G.

shots to a common datum and thus removing topographic effects the
phase velocity at each individual shot can then be measured.
The proper phase velocity can then be incorporated into a simi-
lar expression to (15) for reducing travel times the rest of the way
down to the sea floor. In practice V_{ref} is taken to be a nominal
phase velocity across the section since the actual phase velocity
from the raw data is usually not available. A small error is
introduced by using a constant reference velocity in correcting to
the datum, however by choosing a datum close to the average shot
depth the error can be minimized. A phase velocity of 8 km/sec for
a reference velocity and a sonic velocity in water of 1.5 km/sec were
used in the topographic correction. The record sections thus contain
a one-way travel-time in the water column to the datum, which was set
to 3000 Fathoms.

Sections shown are from the vertical channel from each instru-
ment, these being the clearest for picking first arrivals. Hydro-
phone channels were too noisy for this purpose since gains were set
too high. Horizontal channels are designed for measuring shear waves
and are not good recorders for first-arriving compressional phases.
Shot number and shot weight in pounds is also provided.

Short Range Refraction Results

Record sections from 3 of the instruments, DDD, EEE and FFF
recovered from RAMA 11 are shown in Figures 12 - 17.[3] Both incoming

_____

[3]Record sections from Juan were not available at the time of
this publication.
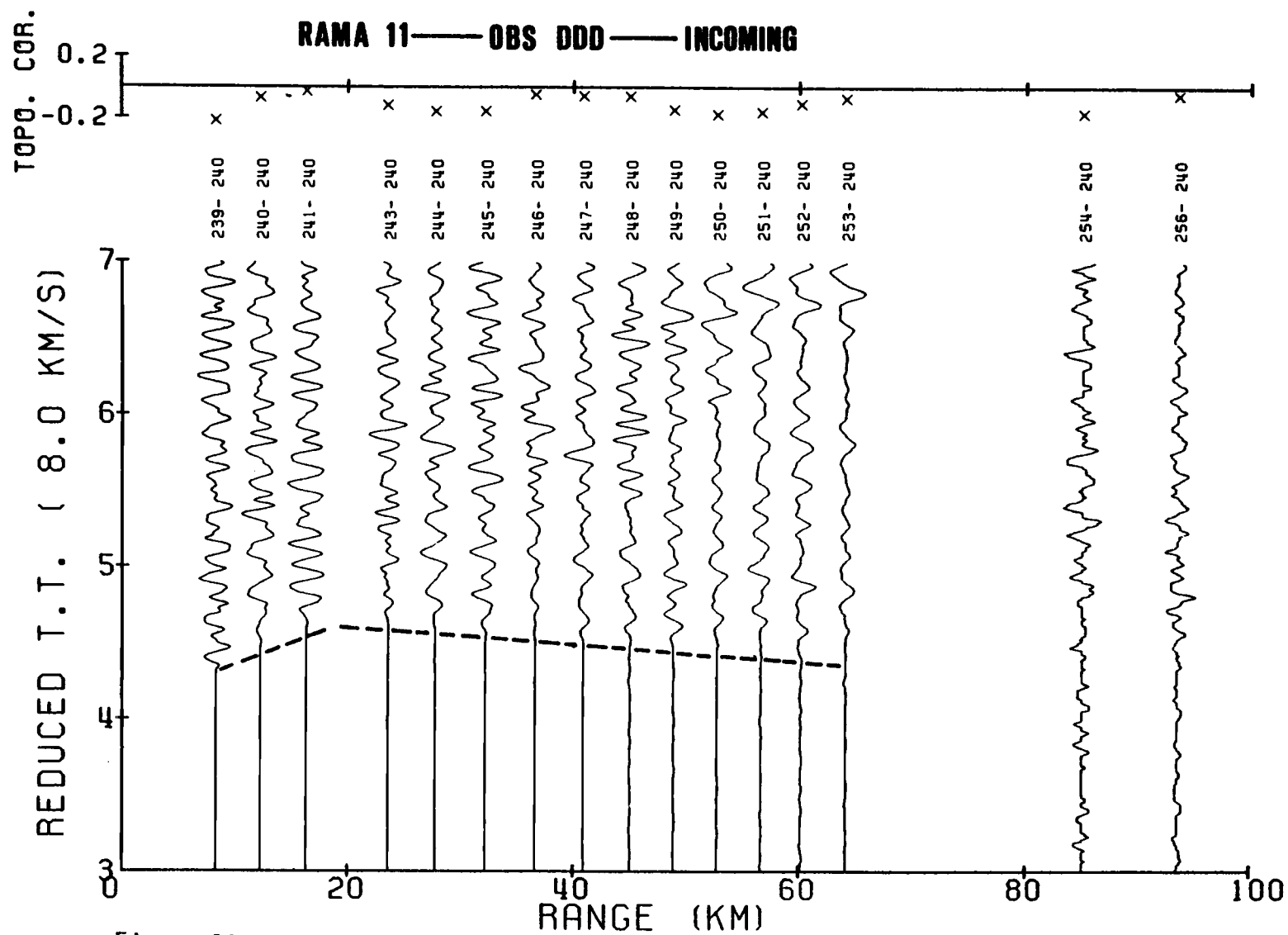
Figure 12. Short range record section from incoming run to OBS DDD.

Figure 13.   Short range record section from outgoing run to OBS DDD.
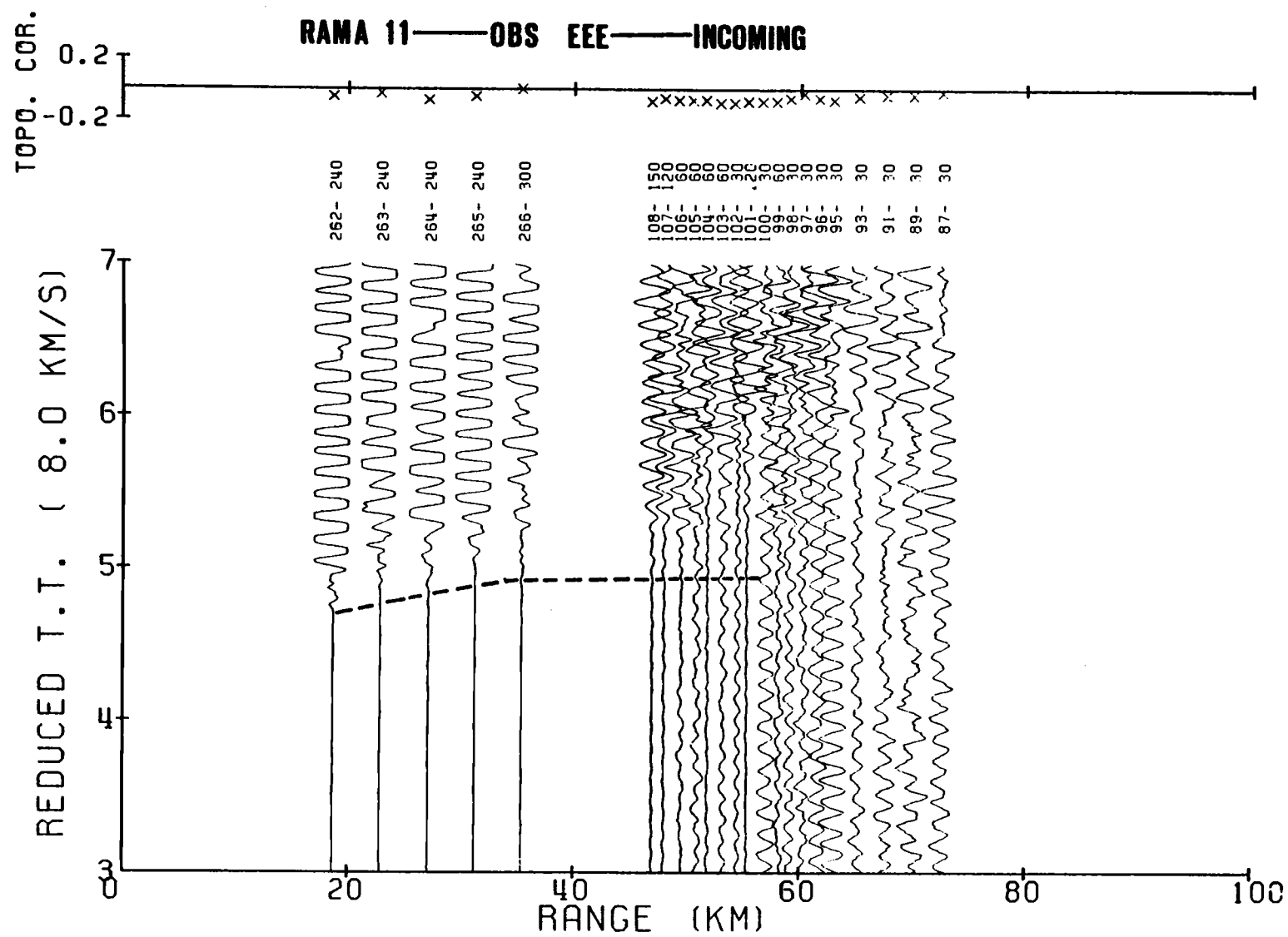
Figure 14.   Short range record section from incoming run to OBS EEE.
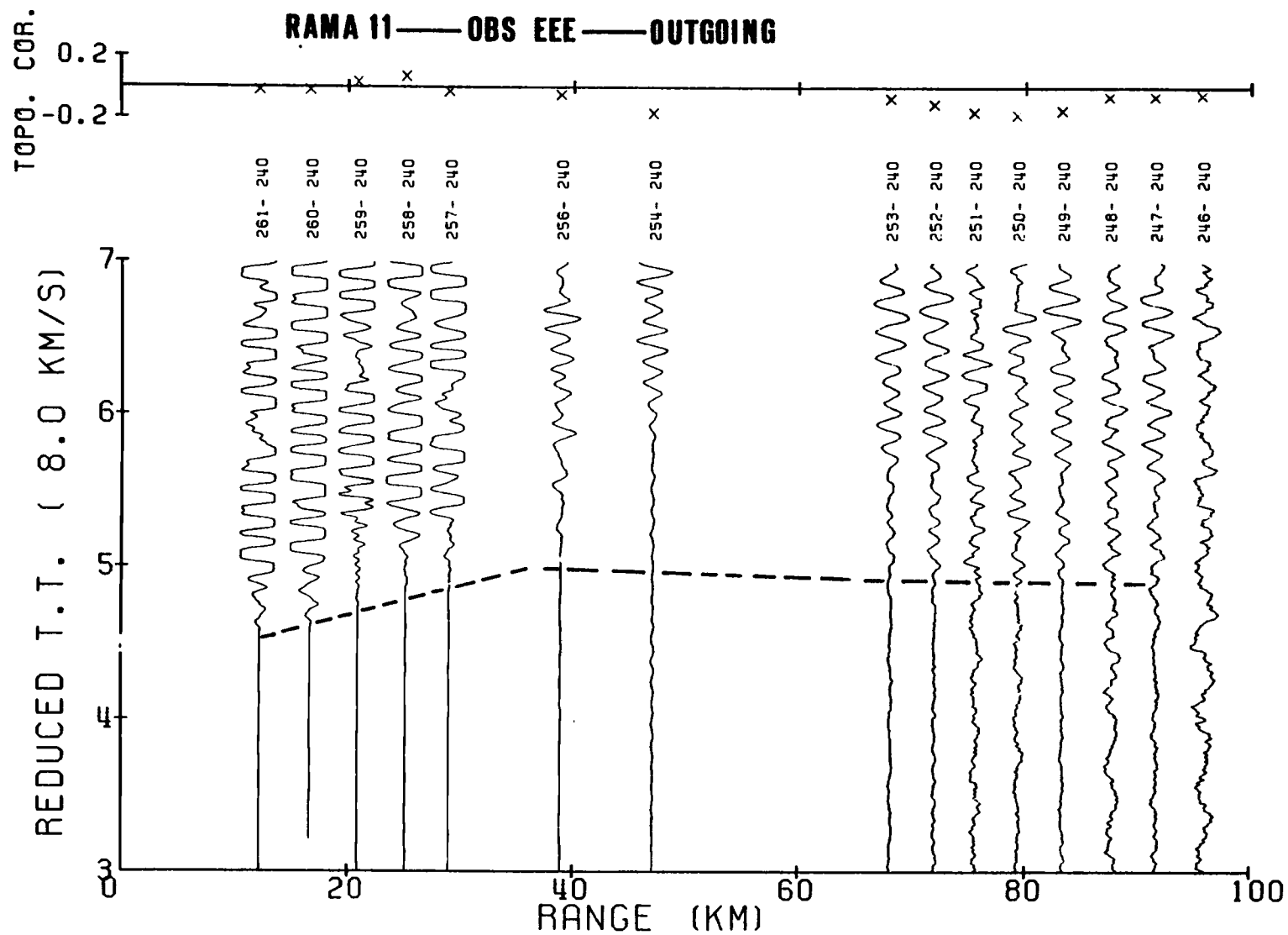
Figure 15. Short range record section from outgoing run to OBS EEE.
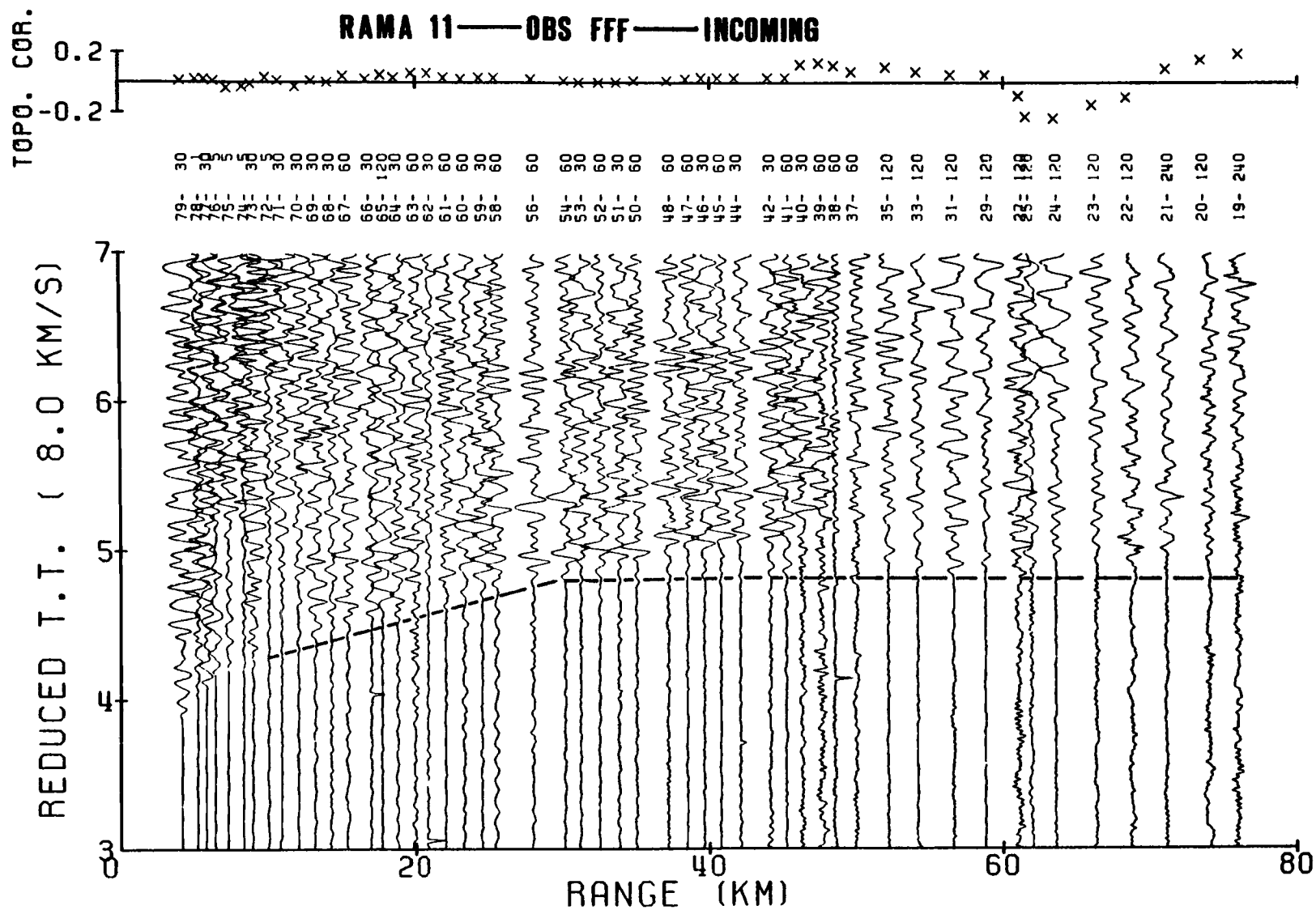
Figure 16. Short range record section from incoming run to OBS FFF.
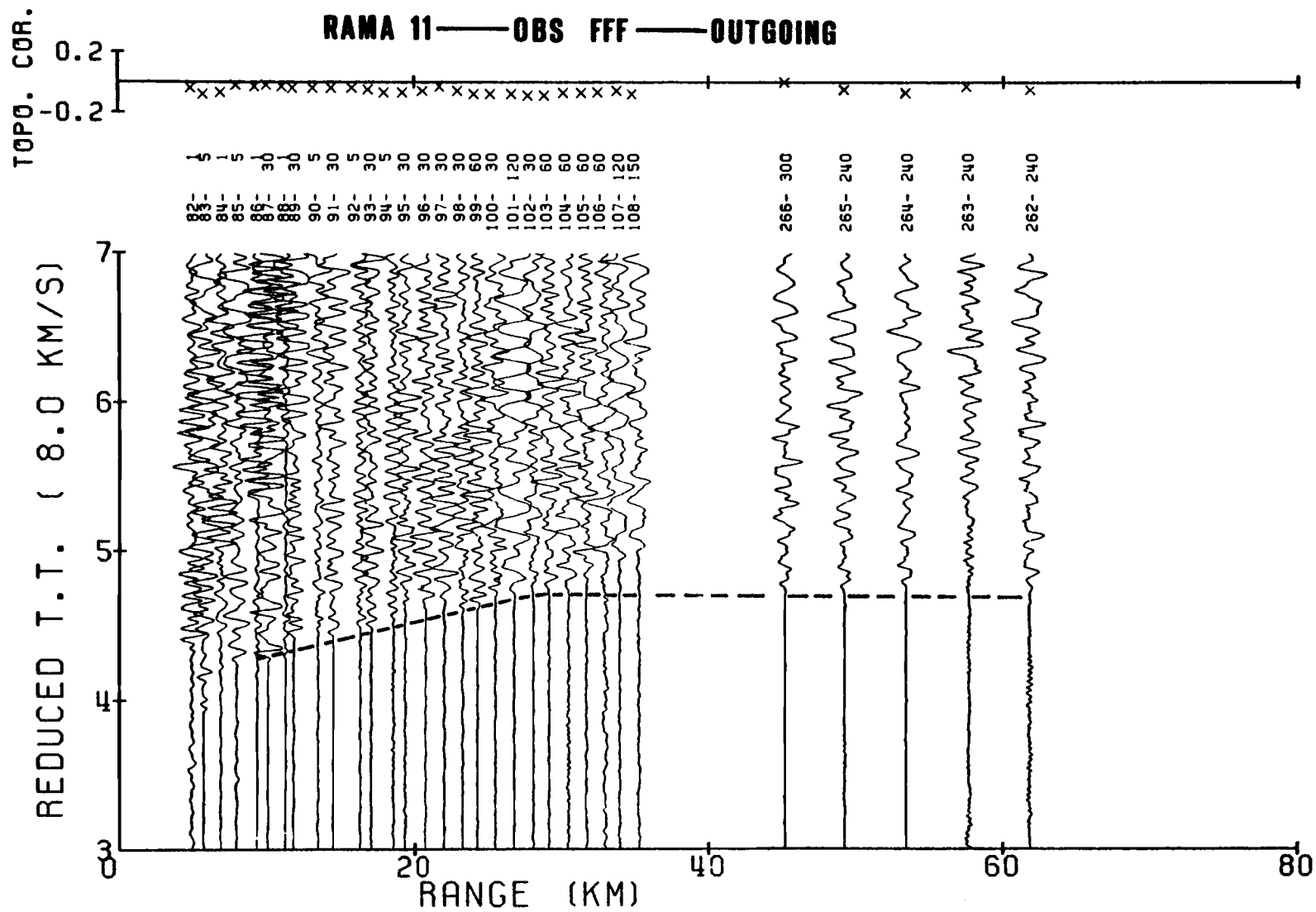
Figure 17. Short range record section from outgoing run to OBS FFF.

and outgoing sections are given, and refer to shots made to the west
and east of each instrument, respectively. The data was corrected
in an identical manner as the long-line data, the sole difference
being that the ranges shown for each shot are actual water wave
ranges determined separately for each instrument. The clearest chan-
nel on instruments EEE and FFF were the vertical and on OBS DDD, the
hydrophone.

Justification

The motivation for using the delay-time-function method is
that variations in travel time can not be adequately predicted
using horizontal or dipping plane layer solutions. The character
of the data from this study complies well with this criterion. Shown
in Figure 18 is a composite travel time plot from instruments involved
in the shallow crustal examination, RAMA 11. Large variations in
travel time data across the receiving stations are seen. The data
certainly cannot be fit satisfactorily by horizontal or dipping
plane layers. The later is displayed by the fact that travel
times from instruments FFF and JUAN, which are located at the ends
of the shot line do not bound the travel times from the other in-
struments. In contrast, we observe that crustal delays are highest
at OBS EEE and lowest at OBS DDD which is what we would expect if
they were located at the ends of the shot line and seismic
structures dipped strictly in one direction.

Velocity gradients, which would nullify a delay time analysis
approach for interpreting travel time data relevant to this study,
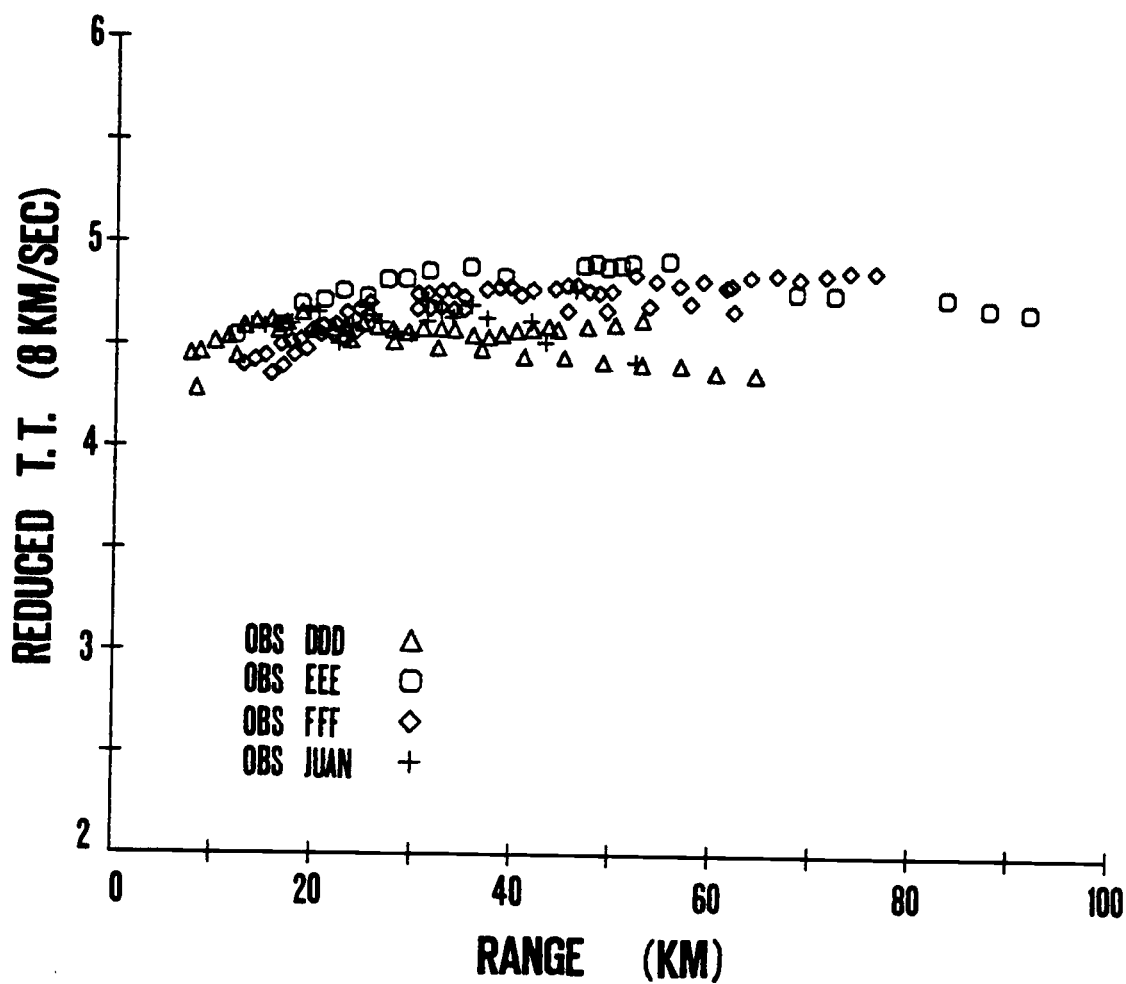
Figure 18. Composite travel time plot of instruments involved in the short range (crustal) refraction experiment from RAMA 11. Lower crustal (oceanic) data and mantle travel times are shown.

do not appear to be of considerable magnitude. Rather sharp discontinuities in phase velocities for lower crust and mantle arrivals from a single OBS are observed (Figure 18). In addition, phase velocities are fairly constant between the abrupt slope changes and suggests that velocity gradients are negligible. However, to accurately test for velocity gradients requires a detailed examination of wave amplitudes. Some initial work in this area indicate there may be some subtle amplitude buildups from crustal arrivals and just beyond the critical distances for mantle arrivals. The amplitude buildups may signify the existence of gradients at depth, reflections off of refracting horizons, or a combination of these two. Nonetheless, if velocity gradients are rather moderate within the discrete layers, the travel time of head waves will still closely match those of refracted rays that dive deeper into the graded layer.

Using a discrete delay time analysis where actual crustal delays at shot and receiver positions are measured can not be used since data overlap is insufficient. To apply a discrete analysis requires a minimal 3 shot overlap between instruments. There are then 6 equations with 6 unknowns. For two complementing stations A and B with shots 1, 2 and 3 we have:

$$T_{A1} = G\Delta_{A1} + \tau_A + \tau_1$$

$$T_{A2} = G\Delta_{A2} + \tau_A + \tau_2$$

$$T_{A3} = G\Delta_{A3} + \tau_A + \tau_3$$

$$T_{B1} = G\Delta_{B1} + \tau_B + \tau_1$$

$$T_{B2} = G\Delta_{B2} + \tau_B + \tau_2$$

$$T_{B3} = G\Delta_{B3} + \tau_B + \tau_3$$

To apply these equations to strictly one set of travel times delineating a particular phase is suitable for predicting total delay down to the refracting horizon. Problems arise however in inverting delay times into depth. The velocity-depth relationship above the refracting horizon must be known. If other refractors have been identified which are shallower, then their delays too, must also be amply described at the same shot locations, and preferably from discrete analysis. This requires there to be data overlap from upper refractors as well. The data from the uppermost crustal refractor (defined in the next section) identified on the record sections lacked data overlap between instruments. There does exist some data overlap in sparse areas in the middle of the shot line from the deeper refractor. However in the final analysis, to mix solutions, delay-time-function method and discrete analysis is an unreasonable approach for depth inversion. The small scale variations in delay through the upper refractor which remain unpredicted as a result of a smooth functional delay fit would eventually be incorporated into the lower layer thicknesses, and would transform into a larger thickness variation since velocities are much higher here. Had overlap existed for the upper refractor instead of for the lower one, then mixing solutions would be appropriate and desirable. Nevertheless, this is not the case.

Application

The delay-time-function method was implemented to study the crustal structures across the West Philippine Basin using the following set of procedures:

1. Travel times of first arriving compressional phases were classified according to the refracting surface the head wave traveled on. Energy arriving at phase velocities close to 6.8 km/sec were identified as layer 3 (also known as the oceanic layer) refractions and correspond to the layer 3 of Hill (1957). Mantle or moho (or layer 4 of Hill (1957)) arrivals were identified for phase velocities in the proximity of 8.0 km/sec. Both layer 3 and mantle phases were detected on incoming and outgoing runs from all the instruments.

2. a) One-way delay time from the ocean surface to the datum (see section on Refraction Profiles) was removed from the data according to the expression

$$T_{datum} = \frac{h_{datum}}{V_w} \cos\left(\sin^{-1} \frac{V_w}{V_{ref}}\right) \qquad (16)$$

similar to equation (15). Since phase velocities were relatively constant for layer 3 as well as mantle arrivals it was unnecessary to estimate phase velocities at each shot in removing water delays. Constant delays were removed with V_{ref} = 6.8 km/sec for layer 3 and with V_{ref} = 8.0 km/sec for mantle travel times, both of which described the mean velocity of their refractor.

b) Delay time through an assumed, constant sediment cover of 100 meters (Karig, 1975) and a sonic velocity of 1.7 km/sec for sediments was subtracted out. This correction was applied twice to the travel time data, once for the

receiver and once for the shot position. The two-way sediment correction was calculated separately for each set of classified arrivals, layer 3 and mantle, at their respective phase velocity.

3. A delay surface for layer 3 travel times corrected for water and sediment delays was fit with a 0th order polynomial (a constant) (Figure 19).

4. Delay surfaces for mantle travel times corrected for water, sediment and delays to layer 3 were computed at 0th - 2nd order polynomials (Figure 19).

Attempts were made to fit the data with higher order polynomials but large fluctuations in the delay surface in regions lacking data were discovered. A Fourier description (Raitt, 1969; Morris, 1969) was tried but also yielded unrealistic fluctuations due to incomplete areal coverage.

For the inversion of delay surfaces into crustal depths, the constant fit to layer 3 seemed the most reasonable. In the sense that the delay-time function method was employed, using only a 0th order polynomial in describing delay time to layer 3, the problem reduced to a least squares solution for a horizontal plane. A physical explanation for choosing the less than desired quality of solution for Layer 3 involved the areal coverage of the shot data. The delay surface was constrained by only 46 points occurring in several dense packets spread sparsely over 400 km, with no overlap in shot data between instruments. In addition, regions of rapidly varying topography, such as near OBS DDD, which was dropped into a bathymetric depression
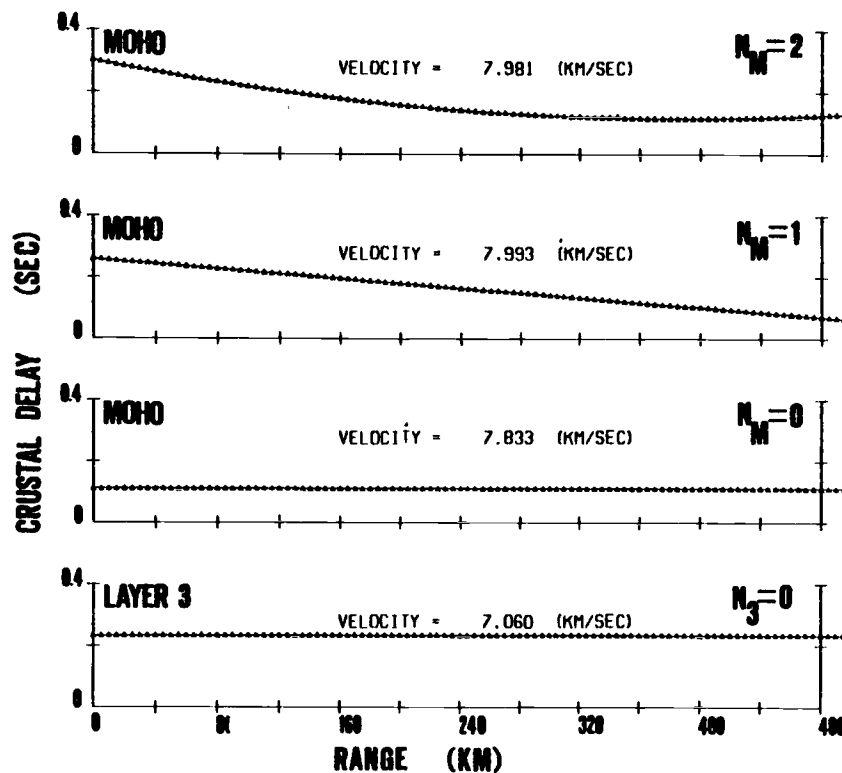
Figure 19. Delay surfaces for 0th order fit to layer 3 data and 0th - 2nd order for moho data, as computed from standard delay-time-function method. Ranges shown are W.R.T. OBS G.
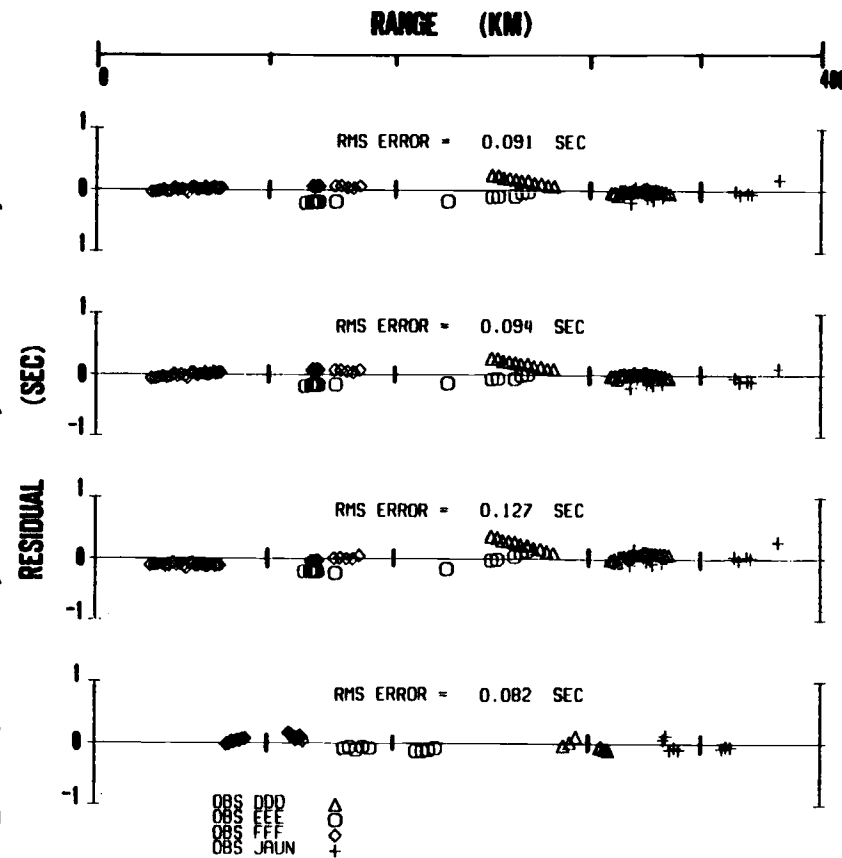
Figure 20. RMS residual plots from standard delay-time function method.

and had rather large topographic corrections for close in shots, have also depreciated the quality of the solutions compromised for layer 3. Last of all, but nonetheless important, regards the fact of lumping arrivals refracted at layer 3 as traveling through a homogenous upper layer of constant velocity. Results from airgun reflection suggest the upper layer, corresponding to layer 2 of Hill (1957) and also known as the transitional layer, exhibits velocities which are not continuous between instruments. Hence in the inversion of delay times for crustal thicknesses the most cautious model was chosen. In any case, the RMS error of .082 sec for the 0th order fit (Figure 20) is rather good and is slightly better than a $\pm$ .1 sec confidence in travel time picks.

A 2nd order fit, having a RMS of .091 sec (Figure 20) was used for inverting delay time into Layer 3 thickness. In examining the residual plots some local variations in predicted travel time are apparent. A small error in the receiver delay at OBS EEE is shown by the DC offset in the residuals for this instrument. On the incoming run, west of OBS DDD, actual travel times are progressively lower at further ranges. This might be explainable by a shorter wavelength structure in the area. If the delay surface and hence layer 3, were downwraped in this region such that OBS DDD were looking downdip, then the apparent phase velocities would be higher, as the trend of the residuals indicate. This explanation is offered in conjunction with using low order - low resolving power polynomials. An alternate explanation is discussed in the next section.

Modified Delay-Time-Analysis

In the conventional application of the delay-time-function method, as was done previously, seismic velocities are taken to be constant along the entire length of the refracting surface. For short-range seismic surveys this is a reasonable assumption. However, for longer range data extending over several hundred kilometers the validity of the assumption breaks down. Seismic structures traversing such large ranges may vary significantly laterally. In some applications to relax this condition data sets are segmented. However this may cause problems in linking solutions together again. Morris (1972) in his application of the delay-time-function method, allowed for lateral gradients in basal refractor when describing delay times for data traversing ranges up to 800 km.

Since the West Philippine Sea data in this study extends to over 450 km, it is desired to relax the condition of velocity constancy as does Morris (1972), (although he does not formally present the mathematics of the problem) without losing continuity in the delay functions. Accordingly, if $G(x)$ describes the slowness as a function in x along a refracting surface (Figure 21) then the travel time is given by

$$T(XI, XJ) = abs\left[\int_{XI}^{XJ} G(x)dx\right] + \tau_I + \tau_J \qquad (17)$$

where XI, XJ are receiver and shot positions and τ_I and τ_J are their respective delay times to the basal refractor. The first term in this equation is the integrated travel time along the refractor
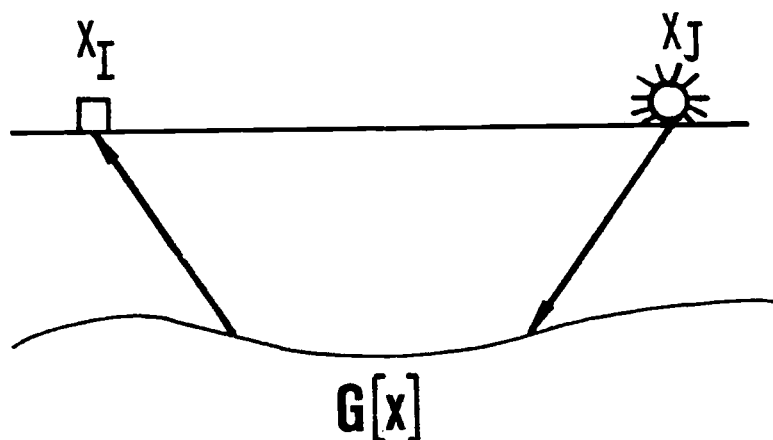
Figure 21. Refractor with slowness as a function of position.

from the shot to the receiver, replacing the $G_\ell \Delta_{IJ}$ term from equation (9) used in the traditional application. The absolute value of the integral insures that a positive number is obtained from the integration (as XI can be greater than or less than XJ).

A simple approach to solving this problem is to assume that G(x) can be described by a low order polynomial in x. Accordingly if

$$G(x) = b_0 + b_1 x + b_2 x + \ldots b_k x^k \tag{18}$$

then the total time for a head wave to travel from a shot to a receiving station is given by

$$T(XI,XJ) = [b_0(XI - XJ) + \frac{b_1(XI^2 - XJ^2)}{2} + \frac{b_2(XI^3 - XJ^3)}{3}$$
$$+ \ldots \frac{b_k(XI^{k+1} - XJ^{k+1})}{k}] + \tau_I + \tau_J. \tag{19}$$

The unknown coefficients describing velocity can also be solved for in a least square sense. The A matrix to be inverted now transforms to

$$
A = \begin{bmatrix}
|XI-XJ|_1 \cdots \dfrac{|XI^{k+1}-XJ^{k+1}|}{n}\bigg|_1 \; 2\,(XI+XJ)_1 \cdots (XI^{n_\ell}+XJ^{n_\ell})_1 \\
\vdots \\
|XI-XJ|_m \cdots \dfrac{|XI^{k+1}-XJ^{k+1}|}{n}\bigg|_m \; 2\,(XI+XJ)_m \cdots (XJ^{n_\ell}+XJ^{n_\ell})_m
\end{bmatrix} \quad (20)
$$

where n_ℓ is the order of polynomial describing the delay surface and m is the number of travel times used in the regression. The model vector corresponding to the transforming matrix is thus

$$
M = \begin{bmatrix}
b_{0_\ell} \\
\cdot \\
\cdot \\
b_{k_\ell} \\
a_{0_\ell} \\
\cdot \\
\cdot \\
a_{n_\ell}
\end{bmatrix} \quad (21)
$$

An inherent assumption involved in this method, just as in the standard method, is that the first arrivals are taken to be head waves traveling along the refractor interface. Because of the freedom given in describing the velocity of the refractor, an additional assumption is required. Velocities at the top of the refracting horizon must be vertically homogeneous within the refractor layer as well. Continuing the velocities downward within the discreet layer will insure that first arrivals have traveled as head waves along the top of the refractor.

Results from applying this method to the data are shown in
Figure 22. Velocity was taken to vary linearly along layer 3 and
moho. Results from the standard method suggested that a 0th order
in the delay surface for layer 2 was the most reasonable solution and
thus is used to describe the 'structural' delay part of the solution
for this layer.[4] From the bottom diagram of Figure 22 it is seen that
layer 3 velocity decreases toward the eastern portion of the West
Philippine Basin, with a value of 7.05 km/sec beneath OBS FFF and
6.82 km/sec at instrument JUAN. The RMS error for this solution is
.076 sec (Figure 23), which is slightly better than the RMS for the
standard 0th order solution.

Total crustal delays using mantle data were computed at 0th, 1st
and 2nd orders for the delay surface (Figure 22), in conjunction with
a linear dependence in refractor velocity. The RMS error at pro-
gressively higher order fits to the structural delay (Figure 23) do
not decrease at least out to 3 decimal places, remaining stable at
.088 sec. (Some changes in the standard error of the coefficients was
noted and actually increased slightly for the 1st order fit, but de-
creased somewhat for the 2nd order fit, as compared to the 0th order.)
These results indicate delay time variations through layer 3 are thus
much better described by allowing for changes in moho velocities.
As more weight is given to the structural delay, $V(x)$ is seen not to
change very much. A small degree of flattening in the $V(x)$ curve is

---

[4]It is referred to as the 'structural' delay since it represents
the delay solely due to structural thickness of the overriding layer,
whereas the delay surface from standard calculations include non-
structural delays as a result of a single least squares velocity.
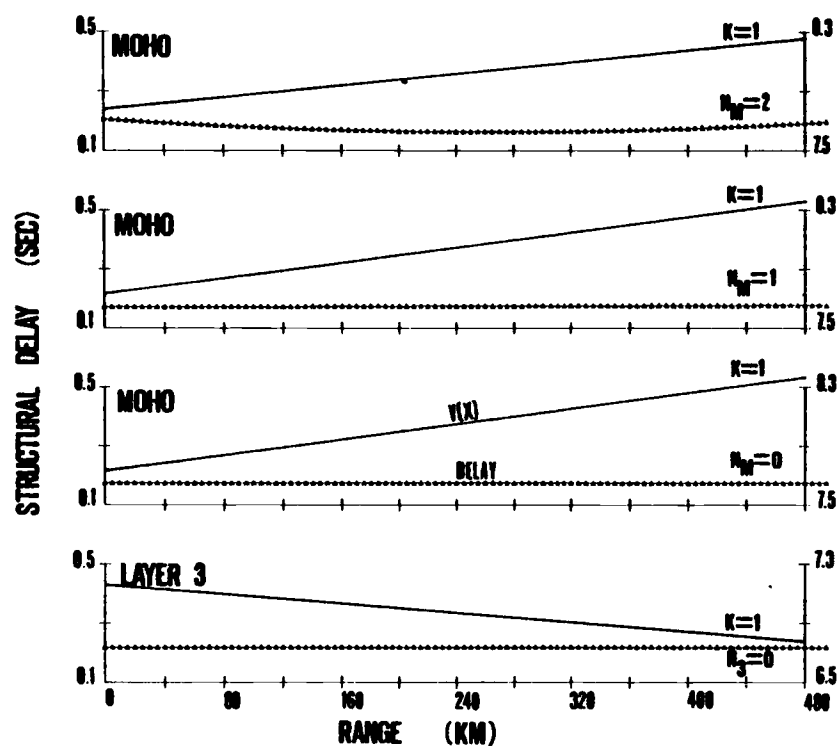
Figure 22. Structural delay surfaces and velocities from modified delay time analysis. Structural delay fits of 0th - 2nd order for moho data, and 0th order for oceanic data were used in conjunction with a 1st order dependence in refractor velocity. Ranges shown are W.R.T. OBS G.
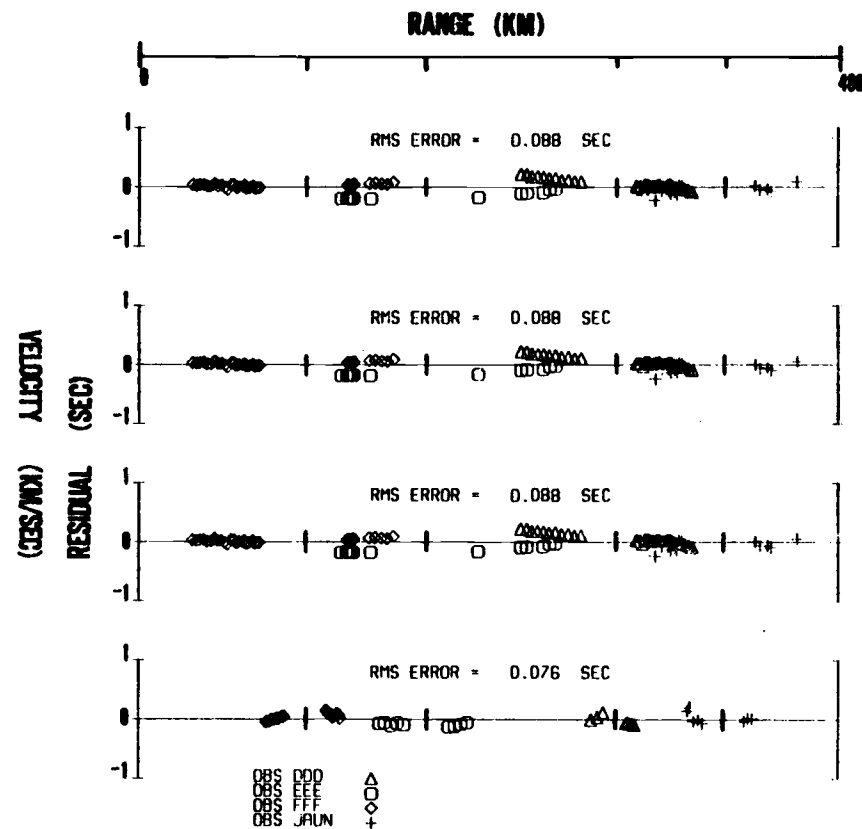
Figure 23. RMS residual plots from modified delay time analysis.

observed for the $N_M = 2$ structural delay solution, which is expected
as the weight of velocity coefficients in the least square solution
is decreased. Nonetheless, modified delay-time analyses strongly
suggest that mantle velocity increases toward the eastern section of
the basin.

In applying this method it was hoped that large residuals, such
as those discovered in the incoming run to OBS DDD, could be removed.
The trend of residuals, which exemplify the fact that larger, apparent
phase velocities were measured in this region may be actual velocities
of the moho, and not to be adequately explained by a sloping inter-
face. The resolving power of a first order dependence in velocity
probably can not describe variations in seismic velocity especially
if they are of a local nature. A parabolic dependence was tried and
reduced the residuals in this area. However, 2 degrees of freedom
for determining velocity may not be justified, at least given the
qualities for this data set.

Crustal Structure Summary

The crustal models derived from the delay-time function method
and the modified version are shown in Figure 24. Crustal thickness
of layer 2 from the standard method was .found to be 1.62, and nearly
a constant depth, at 1.46 km beneath OBS FFF and at 1.51 km below JUAN
for the modified version. For the conversion of delay time into
depths a layer 2 velocity of 4.85 km/sec (Murauchi, 1968) was
assumed. Layer 3 thicknesses decrease eastward as seen from both
methods, but more rapidly from the standard delay application.
Thicknesses determined from the standard and modified methods are
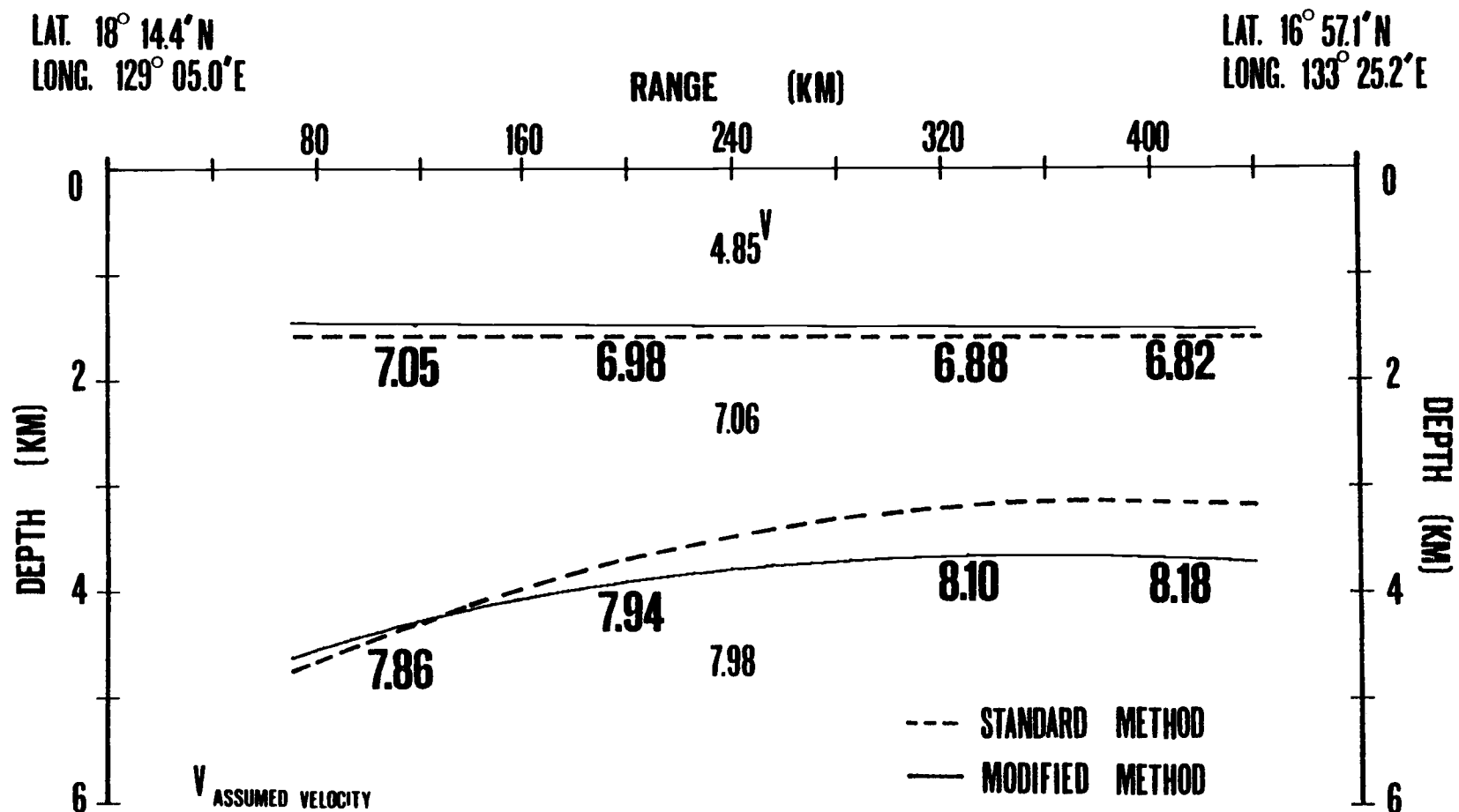
Figure 24. Crustal thicknesses of transitional and oceanic layers across the West Philippine Sea. Latitudes and longitudes are from OBS's G and B.

2.73 km and 2.85 km beneath OBS FFF grading to 1.52 km and 2.17 km beneath OBS JUAN, respectively.

Velocities given are those found at instrument stations from the modified technique and the single value computation from the standard method. Regional layer 3 velocities decrease eastward while moho velocities decrease westward.

Herglotz-Wiechert Inversion

As was discussed earlier, velocities measured within the upper crust were not consistent between instruments. Airgun results from instruments DDD and FFF showed phase velocities from first observable crustal refractions to be different. Phase velocities for these initial refractions were found to be 5.20 km/sec for DDD and 4.38 km/sec for FFF. A complete description of the velocities from the upper crust could not be obtained from the airgun data however, because some crustal arrivals were masked by reflections from multiple water column bounces. Nonetheless on the record sections for FFF some transition layer is present. This was the only instrument to have a relatively complete sampling of first arrivals from the transitional layer. Instrument JUAN and EEE lacked very close-in shot data and thus had no travel time data here. Instrument DDD had some close-in shot data. However, because of the large topographic variations at small shot ranges, the quality of these data are questionable. In applying delay time analysis to the travel time data from this study, only the lowermost crustal arrivals were used to determine delay through the transition layer. These arrivals exhibited fairly constant phase velocities across the record section, and were

identified as oceanic layer arrivals since their phase velocities
were close to 6.8 km/sec. Travel time data from FFF at small shot
ranges were not included into layer 3 arrivals; only those data which
showed a fairly constant phase velocity were used.

Because a complete sampling of shot-receiver ranges from FFF is
available, it is to our advantage to treat the data from this in-
strument individually, and compute velocity-depth functions. To
treat the data in this manner requires us to make the assumption
of lateral homogeneity. Results from surface fitting travel time
data to layer 3 suggested that a constant delay solution was the most
reasonable. This is not to imply that crustal delays through the
transition layer are constant everywhere in the basin, since some
scatter is apparent here (Figure 18); the constant delay solution
was chosen mainly because of insufficient areal coverage of shallow
crustal data. Lateral homogeneity can nonetheless be invoked in
interpreting this data if we assume that laterally heterogeneity
in the West Philippine basin crust, measured over 450 km ranges,
is locally homogenous when only a small portion of it is analyzed.

Theory

The travel time data from the incoming and outgoing profiles
for OBS FFF show some curvature at small shot ranges (Figure 25).
To invert for velocity-depth functions for travel time data exhibiting
a continual change in phase velocity, we make use of the Herglotz-
Wiechert inversion. The equation for a flat earth is

$$z_1 = \frac{1}{\pi} \int_0^{x_1} \cosh^{-1}\left(\frac{c_1}{c(x)}\right)dx \qquad (22)$$

where z_1 is the depth a ray arriving at x_1 with velocity c_1 bottomed at. The phase velocity at x_1 is determined from the travel time data and is given by

$$c_1 = \frac{1}{(dT/dx)_{x_1}} \qquad (23)$$

The Herglotz-Wiechert equation essentially represents a seismic application to Abel's problem in 1826, whose task it was to find the shape of a hill when only the total travel time of a particle to go up and to return is known as a function of its' initial velocity.

The Herglotz-Weichert formulism of Abel's problem is only valid, in the flat earth approximation, for $dc/dz > 0$ and for c monotonically increasing with depth. Thus, low velocity zones can not be mapped using equation (22). The formula is applicable however, in the case of strong velocity gradients, causing a triplication in the travel-time curve (Aki and Richards, 1980).

Application for Crustal Data

To apply the Herglotz-Wiechert inversion technique, the split-spread shot data from OBS FFF (Figure 25) was linked together. A high order polynomial was fit through the data. Water and sediment delays were then removed by allowing for a variable reference velocity determined from the polynomial for each individual shot. Another polynomial, zeroed through the origin was then fit to the corrected
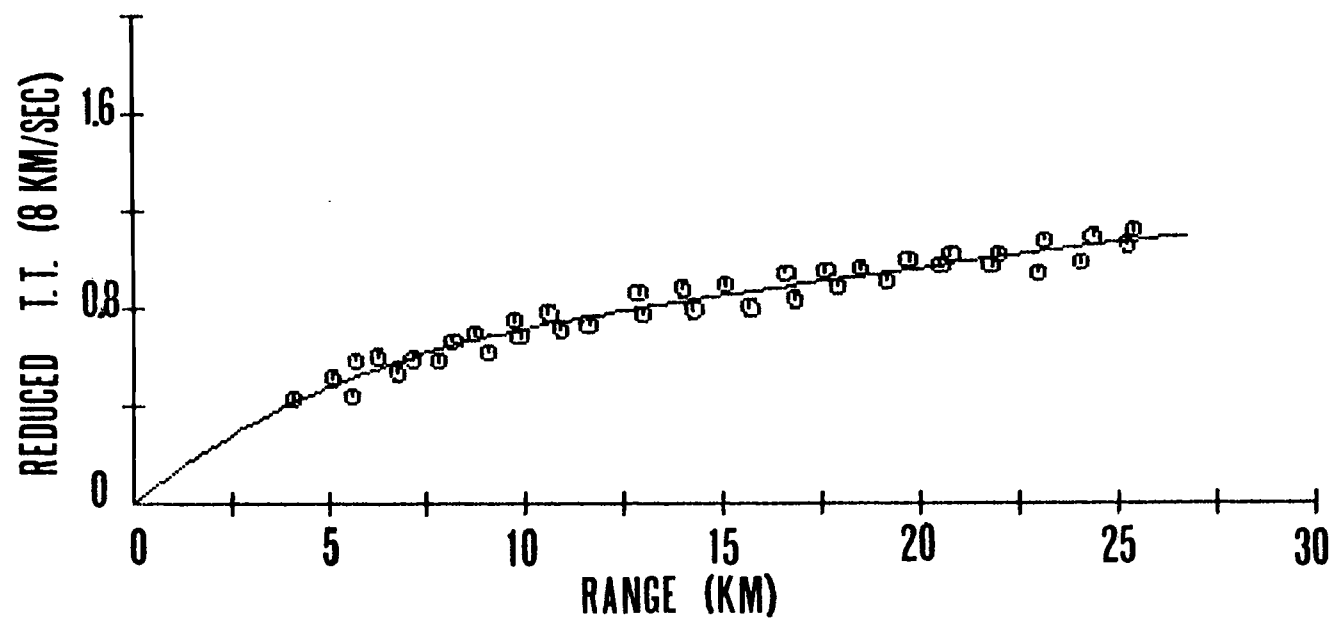
Figure 25. Crustal travel time data from incoming and outgoing runs to OBS FFF. A 4th order polynomial zeroed through the origin, and used in Herglotz-Wiechert velocity-depth inversion is shown.

travel time data (Figure 25). This polynomial was used to invert for the velocity-depth function, the results of which are shown in Figure 26.

Velocity gradients are shown to be rather significant in the top 2 km of crust. The gradients decrease gradually at depth, and are nearly constant below 3 km.

Long-Line Data Travel Time Reduction

The method for determining upper mantle structures in the West Philippine Basin requires removal of all crustal delays to the long-line refraction data, as variations in crustal delays along the shot line affect the phase velocities and travel times measured.

The long-line data acquired in the RAMA 9 cruise leg extend beyond the line shot during RAMA 11, with instrument G being 45 km further west and OBS B being 30 km further east of the closest available shot data. For this reason, in removing crustal delays from the long-line refraction travel times it was necessary to describe a generalized delay surface for the West Philippine Basin, one in which some degree of confidence, especially for predicting receiver delays at OBS' B and G can be made. In this respect, a first order, all-encompassing crustal delay surface was found using only the moho data from RAMA 11. In practice this delay surface (standard method) when operated on the long-line data gives identical results using the $N_3 = 0$ layer 2 model along with the $N_M = 1$ layer 3 delay model to the data. The higher order model, $N_M = 2$ used in the crustal inversion could not be applied to the RAMA 9 data since predictability of crustal delays would be destroyed by the instability of the polynomial beyond
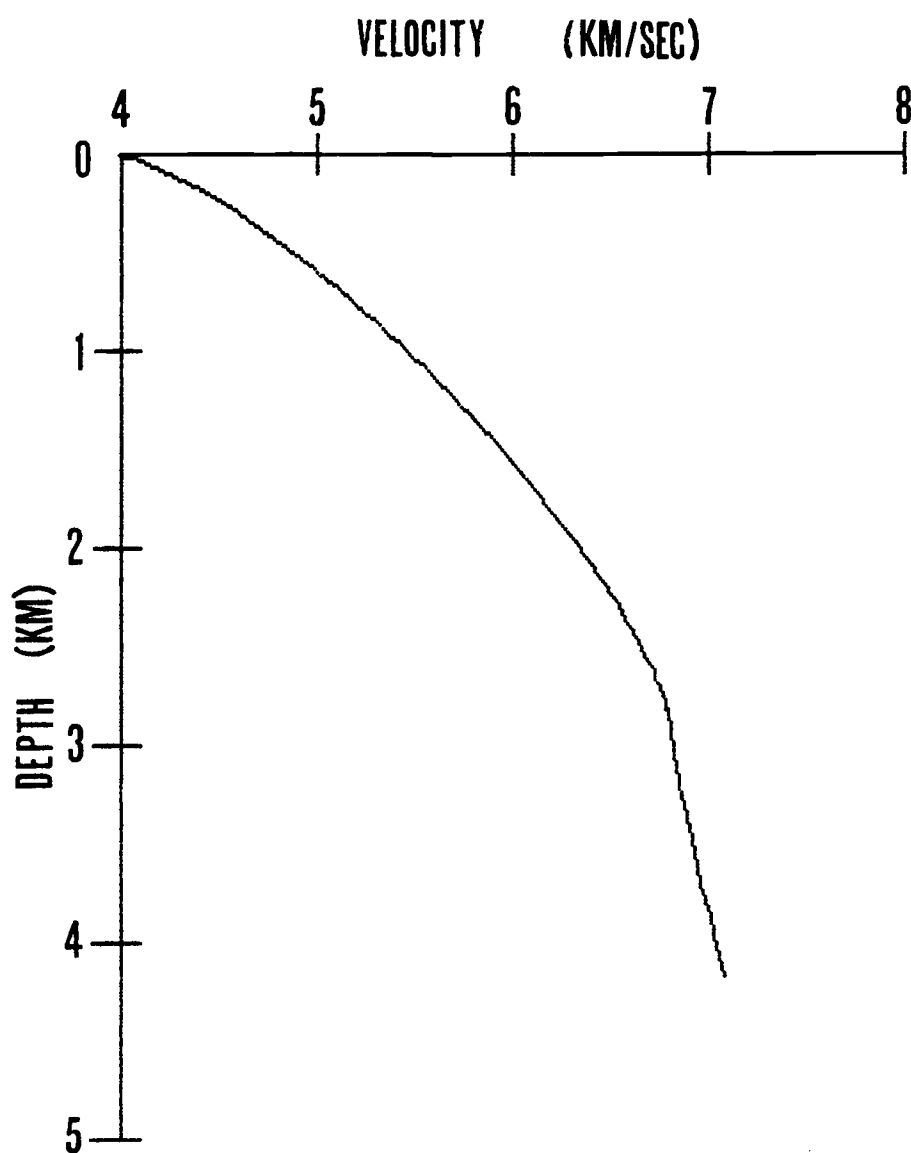
Figure 26. Herglotz-Wiechert travel time inversion of crustal data from OBS FFF.

the area extent of the data, and stability is least likely to be lost with a 1st order fit.

An inherent assumption in removing crustal delays to the long-line data is that crustal delays are described using a single moho velocity, and as such, variations in crustal delays for rays with higher phase velocities from rays diving deeper into the mantle are not considered. This is not an unreasonable simplification of the problem since crustal delays do not change significantly for small changes in mantle phase velocities. To demonstrate the magnitude of this, the difference in delay time for rays traversing the average crustal structure for the West Philippine Basin, at phase velocities of 8.0 km/sec and 8.5 km/sec was computed and found to be only about 0.05 sec. This is well within the error assigned to the travel time data from making handpicks.

Figure 27 shows original travel time data before and after crustal (and water) delays were removed. It is observed that the 1st order model is a good estimator of crustal delays, i.e. observed travel times are predicted. A slight DC offset in OBS B travel times implies a small error in the predicted receiver delay for this instrument. The actual crustal delay at OBS B is less than that found from the extrapolated polynomial, since corrected travel times are lower overall. This suggests that thinner crust (or possibly higher crustal velocities, or a combination of both of these), than that predicted exists beneath this easternmost instrument.
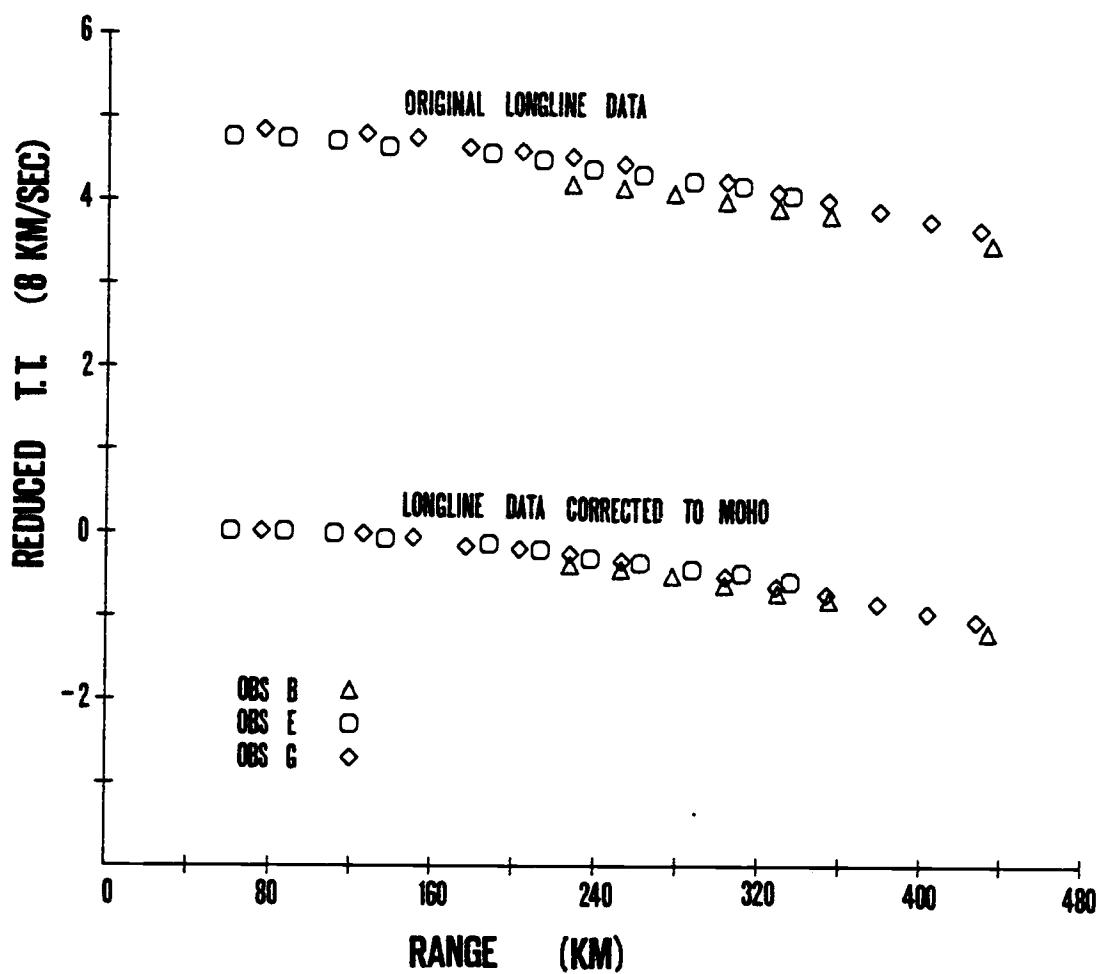
Figure 27.   Travel time data from RAMA 9 before and after
being corrected for water and crustal delays.

Application for Mantle Data

To invert the long-line refraction data, making use of the Herglotz-Wiechert formula, the travel times, corrected down to the moho were first fit with a polynomial. The 2nd order polynomial used in the inversion, having a RMS of .05 sec, was forced through the origin, since this is a necessary condition if crustal delays have been properly extracted from the data. Numerical integration was carried out using coarse elemental ranges, i.e. $dx = 2$ km, because hyberbolic cosine functions are rather slow varying functions. The results of these integrations, velocity versus depth from the moho, are shown in Figure 28.

Velocities at the top of the mantle were found to be 7.98 km/sec. 8.39 km/sec phase velocities measured at the maximum range of the data, 433 km, were found to correspond to bottoming depths of just over 29 km. Velocity gradients are fairly constant below 5 km from the moho discontinuity and are somewhat higher at shallower depths.

Validity of Flat Earth Approximation--Spherical Herglotz-Wiechert

For refraction surveys carried out over short ranges the assumption of flat earth geometry is generally taken to be a reasonable approximation, simplifying both raw data reduction and inversion mathematics. Since the data used in this study is rather unique in that the refraction profile was done over several hundred kilometers, it is necessary to check if flat earth geometry is still applicable. To aid in this investigation the Herglotz-Wiechert formulation in spherical coordinates is used. The equation, which
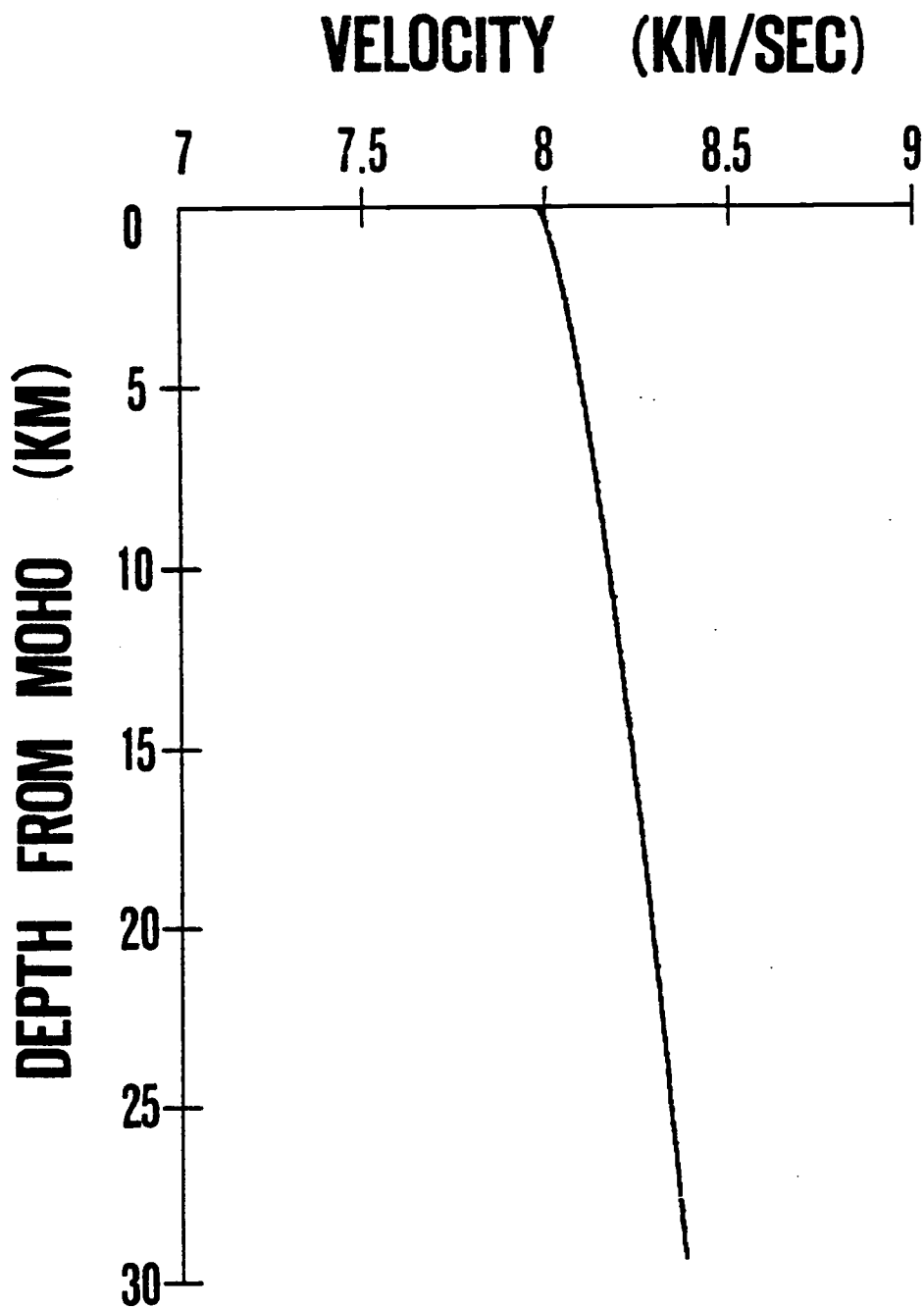
Figure 28. Upper mantle velocity-depth structure in the West Philippine Basin.

makes use of Snell's law in a spherical geometry is

$$\ln \frac{r_o}{r_1} = \frac{1}{\pi} \int_o^{\Delta_1} \cosh^{-1} (\frac{s_1}{s(\Delta)}) d\Delta \qquad (24)$$

where Δ = angle (in radians) ray subtends

$s_1 = (1/(dT/d\Delta))_{\Delta=\Delta_1}$, measured from T.T. curve.

r_o = radius of the earth

r_1 = radius where ray bottoms.

The actual velocity in a spherical earth corresponding to a ray bottoming at r_1 is

$$V_1 = r_1 s_1 \qquad (25)$$

The condition for a ray to bottom in spherical earth is different than those for flat earth geometry. The necessary condition is that ray angle θ must increase with depth r, i.e. $d\theta/dr < 0$. To find what condition this places on velocity, the spherical ray parameter $p = r \sin\theta/V$ is introduced. Then

$$\frac{dp}{dr} = \frac{\sin\theta}{V} + \frac{r \cos\theta}{V} \frac{d\theta}{dr} - \frac{1}{V^2} r \sin\theta \frac{dV}{dr} = 0 \qquad (26)$$

since the ray parameter is constant along the ray path. Solving for $d\theta/dr$,

$$\frac{d\theta}{dr} = - \frac{1}{r} \frac{\sin\theta}{\cos\theta} (1 - \frac{r}{V} \frac{dV}{dr}) \qquad (27)$$

thus, the condition for $d\theta/dr$ to be less than 0 is

$$-(1 - \frac{r}{V} \frac{dV}{dr}) > 0 \qquad (28)$$

or

$$\frac{dV}{dr} < \frac{V}{r} \qquad (29)$$

This condition (29) states that the rate of change of velocity with depth must always be smaller than the absolute velocity-depth relationship (ratio).

It is important to note the consequences of this condition. If $\frac{dV}{dr}$ is greater than 0, i.e. velocity decreases with depth, but condition (29) is still satisfied, then ray bottoming can still occur in a low velocity zone. Therefore, a shadow zone would not be present in the travel time curve if rays had bottomed in the (spherical earth) low velocity zone. Solutions for modeling velocity-depth functions beyond this region, however, become nonunique therafter (Aki and Richards, 1980). In any case, since no low velocity zones were identified in the long-line refraction records, velocity-depth relationships were assumed to satisfy both flat and spherical earth conditions of monotonic increase in velocity with depth.

Table V shows a comparison of velocities and depths determined for the two geometry's. The 'measured phase velocity' corresponds to the flat earth depth determination (as well as being involved in the spherical velocity calculation). At the maximum shot range, $\sim$ 430 km, the difference in predicted velocity from the two methods is $\sim$ 0.04 km/sec. The difference in depths for this range is less than 70 meters. The general trend from spherical calculations is for lower overall velocities and slightly lower depths, but with larger depths

Range (km)	Measured Phase Velocity (km/sec)	Flat Earth Depth (km)	Spherical Earth Velocity (km.sec)	Spherical Earth Depth (km)
0.0	7.976	0.000	7.976	0.001
10.0	7.985	0.091	7.985	0.093
20.0	7.994	0.276	7.994	0.277
30.0	8.004	0.515	8.003	0.516
40.0	8.013	0.798	8.012	0.800
50.0	8.022	1.120	8.020	1.121
70.0	8.040	1.863	8.038	1.864
90.0	8.058	2.724	8.055	2.725
110.0	8.077	3.687	8.072	3.688
130.0	8.095	4.745	8.089	4.744
150.0	8.114	5.889	8.106	5.888
170.0	8.132	7.115	8.123	7.112
190.0	8.151	8.417	8.140	8.413
210.0	8.170	9.792	8.157	9.786
230.0	8.189	11.237	8.174	11.229
250.0	8.208	12.749	8.191	12.737
270.0	8.227	14.325	8.208	14.310
290.0	8.246	15.963	8.225	15.944
310.0	8.265	17.662	8.242	17.639
330.0	8.285	19.420	8.259	19.392
350.0	8.304	21.235	8.276	21.201
370.0	8.324	23.106	8.294	23.065
390.0	8.343	25.032	8.311	24.984
410.0	8.363	27.011	8.328	26.955
430.0	8.383	29.043	8.345	28.978

Table V. Comparison of spherical earth and flat earth Herglotz-Wiechert travel time inversion.

than those predicted by the flat earth approximation at similar velocities.

The degree of accuracy to which the long-line refraction data should be inverted, for a desired accuracy of 0.1 km/sec in seismic velocity and along with the inherent errors in travel time picks, the flat earth approximation suffices. At least for the structures determined from the travel time data herein, flat earth geometry is a reasonable simplification; alternate velocity-depth functions may have invalidated this assumption.

Crust-Moho Transition

Given the velocity-depth function determined using the short range crustal data from FFF, it is in our interest to append the upper mantle velocity structure. Assuming that the velocity structure found from the long-line refraction data is a good indicator of upper mantle velocities existing beneath FFF, then to proceed with appending this velocity structure, we need to make sure that crustal delays at this instrument, as measured by delay time analysis, are accounted for. Accordingly, in calculating the bottoming depth for a ray having a phase velocity of 7.98 km/sec, the uppermost mantle velocity determined from the flat earth Herglotz-Wiechert inversion, a depth of 4.17 km is found. The total travel time and horizontal range traversed to this depth is 1.13 sec and 5.45 km, respectively. The delay time to this depth is thus 0.45 (=1.13 - 4.17/7.98) sec. In comparison, the delay time for mantle arrivals measured at FFF from delay time analysis

(standard method) yield a 0.59 sec delay. There is therefore a 0.14 sec of delay between 4.17 km and the uppermost mantle velocity, determined from the long-line data.

The discrepancy in delay comes from the fact that the crustal velocity structure extends to slightly deeper depths than those measured at FFF. Knowledge about the velocity structure above the 7.98 km/sec refracting horizon, which could account for the extra delay, is manifested in the area where the travel time curve bends sharply, or in second arrival data. Since we have no travel time data for this region and second arrival phases are not easily identified, we need to make an assumption to allow processing of the deeper data. Several reasonable alternatives exist:

1) Assume that velocity at 4.17 km continues down to a dis-
    continuity (moho) and then increases to mantle velocity.
    This transition model assumes the extra delay is soaked up
    in a homogenous layer. The thickness of a homogenous layer
    needed to generate the delay for $V_3(4.17) = 7.09$ km/sec is

$$h = \frac{\tau V}{\cos(\sin^{-1} \frac{7.09}{7.98})} = 2.20 \quad km \tag{30}$$

    This implies that the moho occurs at a 6.36 km depth
    (minimum depth solution).

2) Assume that a linear gradient is present between $V_3(4.17$
    and the mantle velocity of 7.98 km/sec. Equivalent to the
    problem of calculating the gradient of a layer of constant
    gradient when the bounding velocities and delay time are

known we have

$$\tau(\frac{1}{V_m}) = \frac{1}{G} [\ln(\frac{V_m}{V_3} (1 + (1 - \frac{V_3^2}{V_m^2}) ^{1/2})) - (1 - \frac{V_3^2}{V_m^2})^{1/2}] \quad (31)$$

The gradient from this is $G = .26 \ sec^{-1}$, which gives a transitional zone thickness of 3.44 . Moho does not strictly occur in this case since there is no discontinuity, but manifests as a high gradient zone from a depth of 4.166 km to a depth of 7.60 km. This is in general the smoothest and close to the maximum depth solution.

3) A third model assumes that the velocity gradient just above 4.17 km depth continues down to a discontinuity at which the velocity jumps to mantle velocity. The velocity gradient just above 4.17 km is $G = .24 \ sec^{-1}$ which is slightly less than that calculated for case 2. The solution for layer thickness can be solved iteratively using equation (31). The result gives a thickness of 3.00 km and a velocity at the discontinuity of 7.79 km/sec. The jump in velocity at the discontinuity is only .19 km/sec. The discontinuity depth for this transitional model is thus 7.17 km (intermediate between case 1 and 2).

The velocity-depth functions for these three models, describing the crust-moho transitional region, are shown in Figure 29. The linear gradient model (M2) and the crustal-gradient-continuation model (M3), are closely matched through the transition zone. The minimum depth solution calculated from a homogenous transition layer model
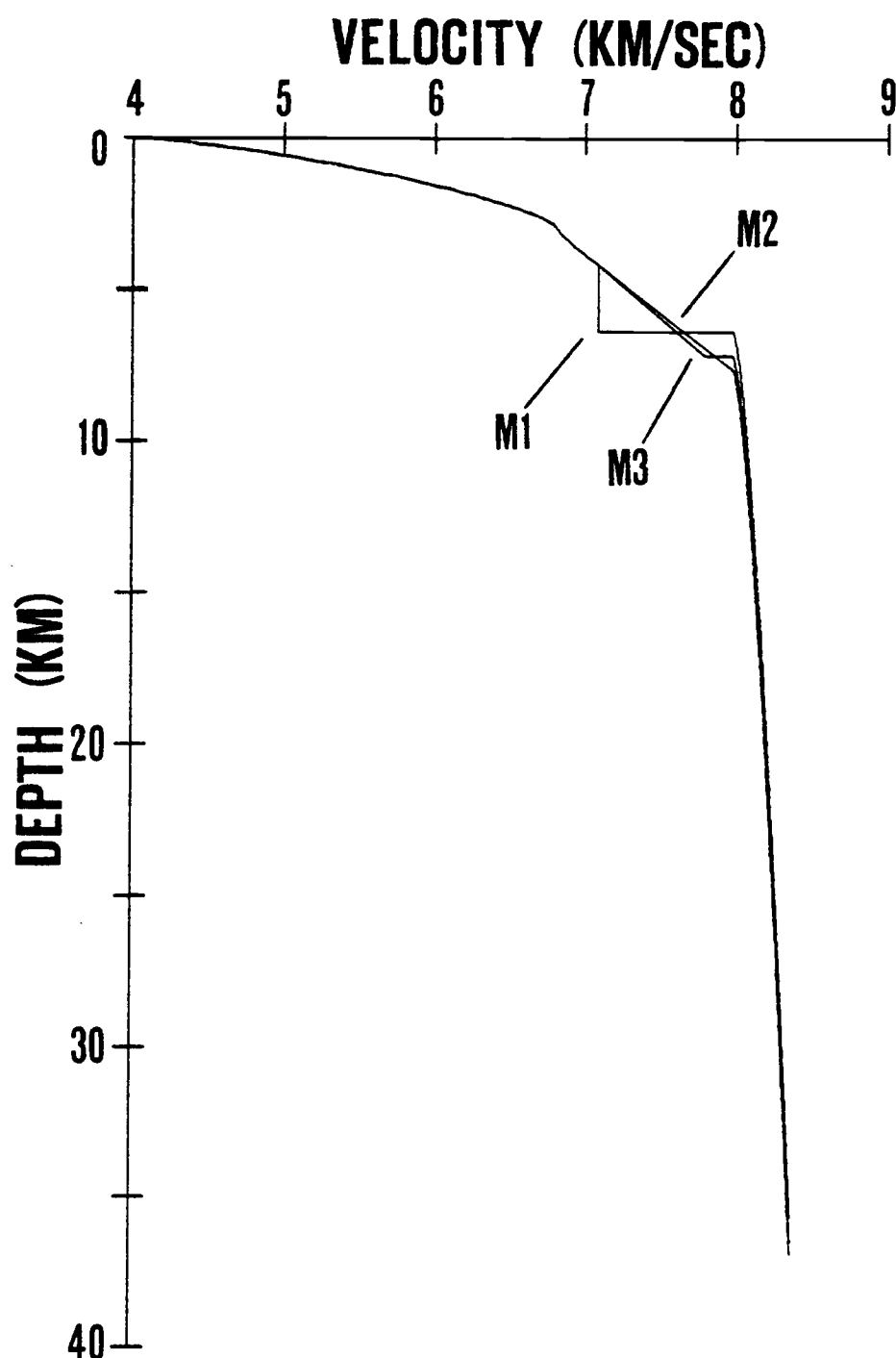
Figure 29. Appended crustal velocity structure from OBS FFF and upper mantle velocity structure for a homogenous layer transition zone (M1), a linear gradient transition zone (M2) and a crustal-continuation-gradient model (M3).

(M1), although it produces a velocity-depth function that is significantly different in the transition zone, its' upper mantle velocity profile is indistinguishable from the M2 and M3 models.

INTERPRETATION

Temperature-Pressure Modeling

Given the seismic structure determined for the upper mantle and published results from experimental testing of compressional wave velocities at high temperatures and pressures, it is useful to examine what constraints are placed on upper mantle composition in the West Philippine Basin. To proceed in this manner a generalized density model was chosen for the West Philippine Basin (Figure 30). With the density model, seismic velocities versus depth were converted to pressure dependent velocities using the simple overburden formulation

$$P = \rho gh \qquad\qquad (32)$$

where   P = pressure

        g = acceleration of gravity at surface of the earth

        h = thickness of overburden

        ρ = density

The resultant velocity-pressure data, V(P), are shown in Figure 30 plotted with various rock types from Christensen (1974) thought to represent possible mantle constituents. Velocity-pressure data for the mantle rocks are from tabulated values in Christensen (1974) for measurements made at 2 Kbar intervals with velocities uncorrected for length changes and uncompensated for temperature related effects. It is observed that the slope of V(P) for the West Philippine Sea is slightly higher than those determined for either of the ecologites, pyroxenites, or the dunite.
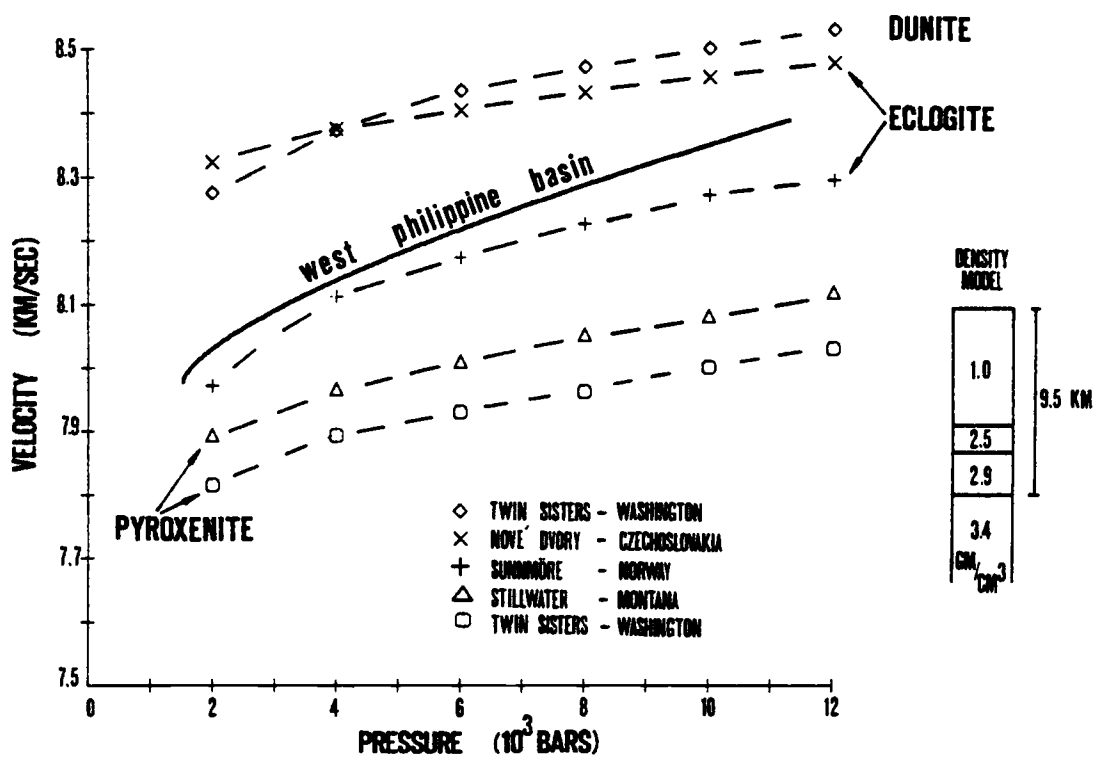
Figure 30. Upper mantle velocity versus pressure for the West
Philippine Basin and possible mantle constituents from
Christensen (1974).

The discordancy of slope becomes even more pronounced when the velocities of the mantle rocks are corrected to the temperature field in the West Philippine Basin. To estimate the temperature-depth function two methods were examined:

1. A steady state model which assumes constant conductivity, and neglects mantle heat production due to the decay of radioactive elements or possible convective processes in the mantle, gives an estimate of the temperature profile according to

$$T = T_o + \frac{dT}{dz}(z) \qquad (33)$$

where

$$\frac{dT}{dz} = \frac{q}{K} \, . \qquad (34)$$

The temperature gradient, dT/dz, was estimated using a heat flow value for q of 1.17 H.F.U. determined by Sclater et al. (1976) for the northeast part of the basin. This value is less than the average value for the entire basin, 1.48 H.F.U., but is more applicable to our region of study. Mantle conductivity (K_m) of 7 x 10^{-3} cal/cm sec°C was used, and is similar to values from Sclater and Francheteau (1970). Transitional and oceanic layer conductivities were also assumed (K_t = 4 x 10^{-3} cal/cm sec°C; K_o = 5 x 10^{-3} cal/ cm sec°C, Clark (1966)). The temperature profile for this model, when T_o is taken to be 0°C at the ocean bottom, is shown in Figure 31.
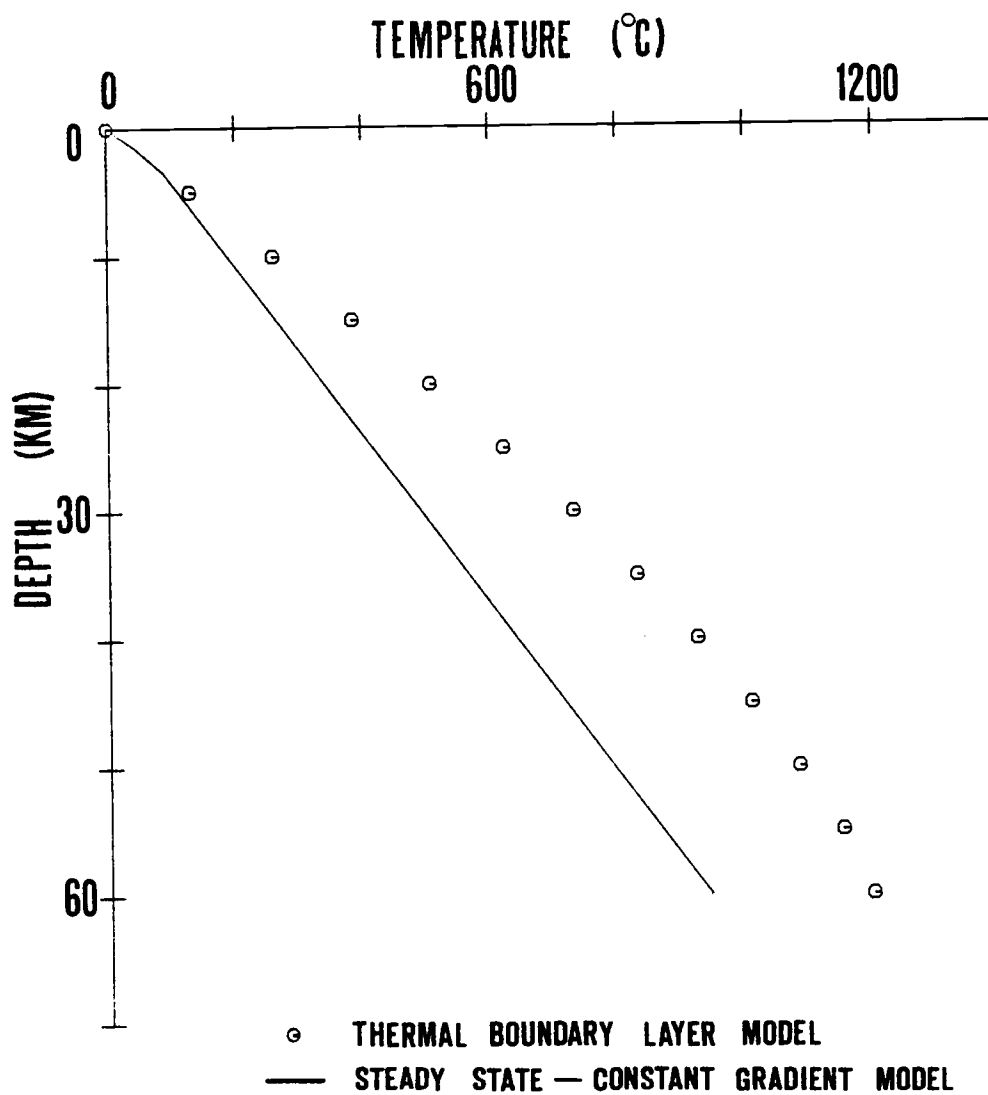
Figure 31. Temperature-depth profile for the West Philippine Basin from steady-state and thermal boundary layer models.

2. A thermal boundary layer model (Parker and Oldenburg, 1973)
in which the melting point isotherm deepens with age from
the ridge, gives an estimate of the temperature field ac-
cording to

$$T(x,z) = \frac{T_m \; erf \; \dfrac{Z/d}{2\sqrt{at/d^2}}}{erf(\alpha)} \; . \tag{35}$$

This equation solves a time-independent Laplacian equation
for heat transport in a solid slab. A diffusivity (a)
of $8.23 \times 10^{-3} \; cm^2/sec$, a time (t) of 40 m.y. since crustal
generation, and a convenient scaling depth (d) of 1 km were
used in estimating the temperature-depth function. An α
of .917 determined from the boundary value problem was also
used. The temperature profile using these model parameters
is shown in Figure 31.

Temperature gradients from the thermal boundary layer model of Parker
and Oldenburg (1973) are much steeper than those predicted by the
steady state model. In correcting the seismic velocities, only
the temperature profile from the steady state calculation was used.
The reason for choosing this model over Parker and Oldenburg's
model is that the minimum effect of temperature on seismic velocity
will be represented. In addition, the assumption of a thermal bound-
ary layer model for the West Philippine Basin may be errant since
the ridge that created the basin (possibly the Philippine Ridge)
is extinct. The time since crustal creation (which is also related

to the spreading rate and distance from the ridge) may therefore have less significance in this model.

Using the temperatures for the steady state - constant gradient model and a single value for $(\partial V_p/\partial T)_p$ of -5.5 x 10^{-4} km/sec °C suggested by Christensen (1979) to be representative of velocity-temperature dependence for most rock types, seismic velocities were adjusted. The value of $(\partial V_p/\partial T)_p$ of -5.5 x 10^{-4} km/sec °C is close to the experimental value found for the Nove' Dvory eclogite $(\partial V_p/\partial T)_p$ = -5.6 x 10^{-4} km/sec °C and the Twin Sisters dunite, $(\partial V_p/\partial T)_p$ = -5.3 x 10^{-4} km/sec °C (Christensen, 1974). Compressional wave velocity temperature derivatives for the other mantle rocks are not provided. $(\partial V_p/\partial T)_p$ used in the temperature correction is applicable to temperature in the range of 25 - 300°C and for pressures between 3 - 5 Kbar. Somewhat higher numbers were found for the Nove' Dvory eclogite and the Twin Sisters dunite at higher temperatures and pressures, but their significance is questionable in temperature modeling of the upper mantle.

Critical temperature gradients yielding velocity inversions are slightly exceeded in each of the single-phased mantle rock species (Figure 32) using the temperature-depth function found for the basin. For velocity to increase with depth as was found to 29 km, a single-phased co positional mantle is unlikely for the West Philippine Basin. From the trend and positioning of V(P), the upper mantle probably has a composition which progressively increases in denser phases having higher seismic velocities at greater depths.
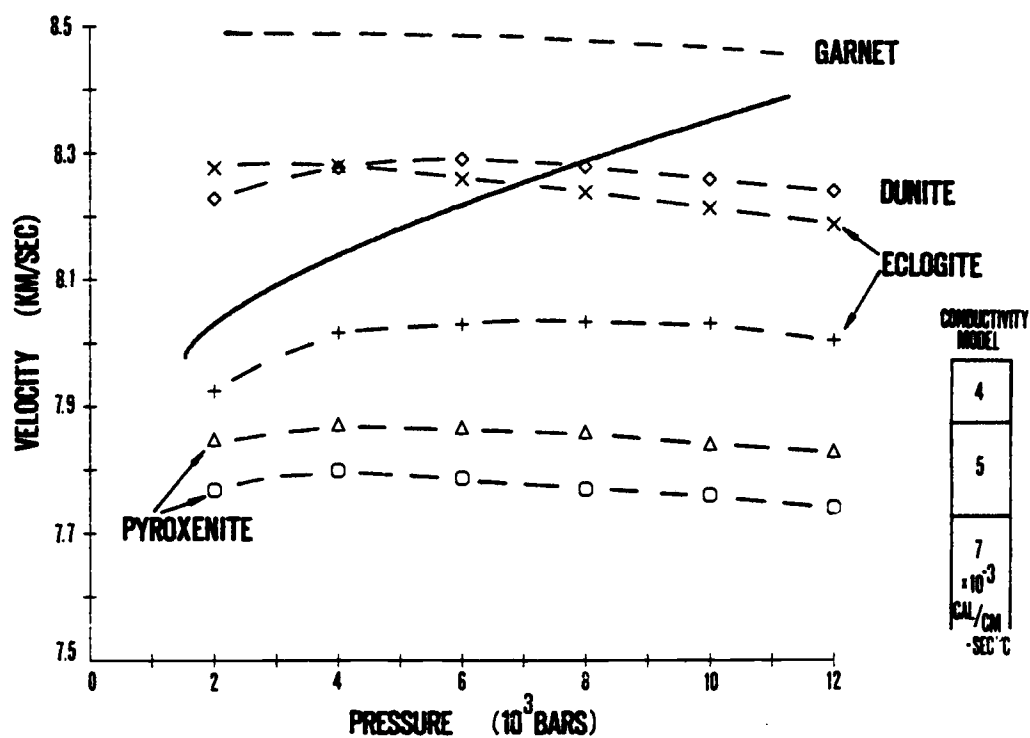
Figure 32. Upper mantle velocities determined from this study
and velocities of the mantle constituents corrected
to the steady-state temperature field estimated for
the West Philippine Basin. Garnet curve is deter-
mined from experimental values in Soga (1967).

It is also of interest to see how predicted travel times for the mantle rocks compare with those measured. To approach this problem pressures were first converted to depth using the generalized density model for the basin. Velocity at the top of the mantle was interpolated for 1524 bars, between the 10 and 2000 bar data given in Christensen (1974). With $c(z)$ thus obtained the Herglotz-Wiechert forward problem was then solved:

$$x = 2 \int_0^{z_1} \frac{c_1/c(z)dz}{\sqrt{1-c_1^2/c(z)^2}} \; ; \tag{36}$$

$$t = 2 \int_0^{z_1} \frac{dz}{c_1\sqrt{1-c_1^2/c(z)^2}} \tag{37}$$

Figure 33 shows the travel time curves for the mantle rocks, uncompensated for the temperature field of the basin. The long-line refraction data with all crustal delays removed and the polynomial used in the depth inversion are also provided. The results from transforming pressure-velocity data into travel time data are somewhat less convincing for a multi-phased mantle beneath the West Philippine Sea. Although only the predicted curve for the Sunnmöre eclogite comes close to the observed data, overall curvature is still flatter and the deviation becomes larger at larger ranges.

The travel time data can be modeled using a 'single'-phased mantle composition mostly of the Sunnmöre eclogite but having characteristics of the Nove' Dvory eclogite at deeper depths. The major
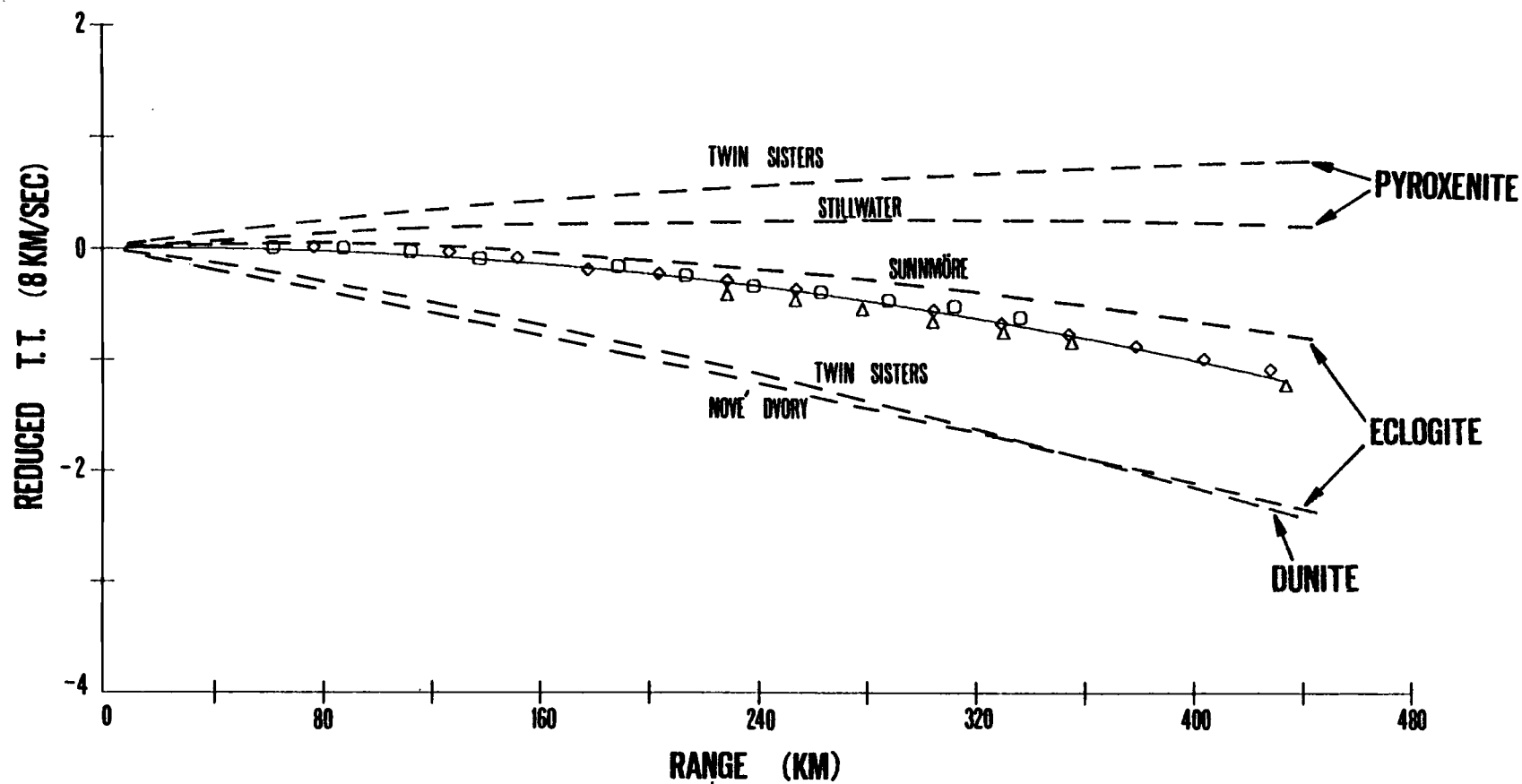
Figure 33. Comparison of travel time data from RAMA 9 (corrected to moho) and predicted travel times for mantle constituents of Christensen (1974).

characteristic mineral assemblages, densities and grain sizes from these two eclogites are:

Nove' Dvory (Czechoslovakia)	Sunnmöre (Norway)
density - 3.559 g/cm^3	density - 3.504 g/cm^3
grain size - .5 mm	grain size - .8 mm
53% garnet	48% garnet
44% omphacite	46% omphacite
1% opaque	3% hornblende
2% plagioclose-	2% phlogopite
diopside symplectite	1% opaque

The main difference separating the two eclogites, as far as the bulk seismic velocity of the rocks is concerned, is the garnet compositions. An increase of approximately 1 - 2 % garnet in the Sunnmöre eclogite could conceivably depress the travel time curve somewhat, and match the observed travel times for rays traversing through mantle in the West Philippine Basin.

Compensation in the West Philippine Basin

It has been reported by several investigations (Watanabe et al., 1977; Louden, 1976; Sclater et al., 1976; Sclater, 1972) that predicted water depths for the West Philippine Basin are shallower than observed depths, by as much as 1 km, when compared to crust of similar age in the Pacific. Theoretical compensation depths also are shallower than observed bathymetric depths.

To find the theoretical, water compensation depths we make use of the crustal structures determined from delay time analysis for the basin and averaged crustal structures reported by Raitt (1963)

for the Western North Pacific from which layer 2 thicknesses are
2.05 km and layer 3 are 5.08 km. The problem then in finding water
compensation depths involves solving algebraic expressions for
column thickness and mass relationships:

$$h_w + h_2 + h_3 + \Delta h_m = 2.05 + 5.08 + \bar{h}_p \tag{38}$$

$$h_w \rho_w + h_2 \rho_2 + h_3 \rho_3 + \Delta h_m \rho_m = (2.05)\rho_2 + (5.08)\rho_3 + \bar{h}_p \rho_w \tag{39}$$

where $h_{w,2,3}$ = thicknesses of compensated water depth, and meas-
ured layer 2 and layer 3 thicknesses.

Δh_m = depth into mantle

$\bar{h}_p$ = averaged Pacific Ocean depth of similar age as
West Philippine Sea crust.

$\rho_{w,2,3,m}$ = densities of water, layer 2, layer 3, and mantle

The two unknowns in the expressions are the compensated depths, h_w,
and the depth into the mantle, Δh_m. The problem thus set up has pro-
perties of an Airy isostatic model for the West Philippine Basin in
that calculated water depths, h_w, are reflected by 'anti-root' thick-
nesses into the mantle, Δh_m. It varies in practice from a strict
Airy formulation since thicknesses are held constant.

Figure 34 shows compensated water depth plotted with actual
bathymetry. Computations were done with $\bar{h}_p$ = 4707 m determined from
formula in Parsons and Sclater (1977) for Eocene crust 40 million
years old and densities identical to those used in the previous
section (Figure 30). Results from this analysis indicate $\sim$ .3 km
shallower compensation levels than observed bathymetric depths for
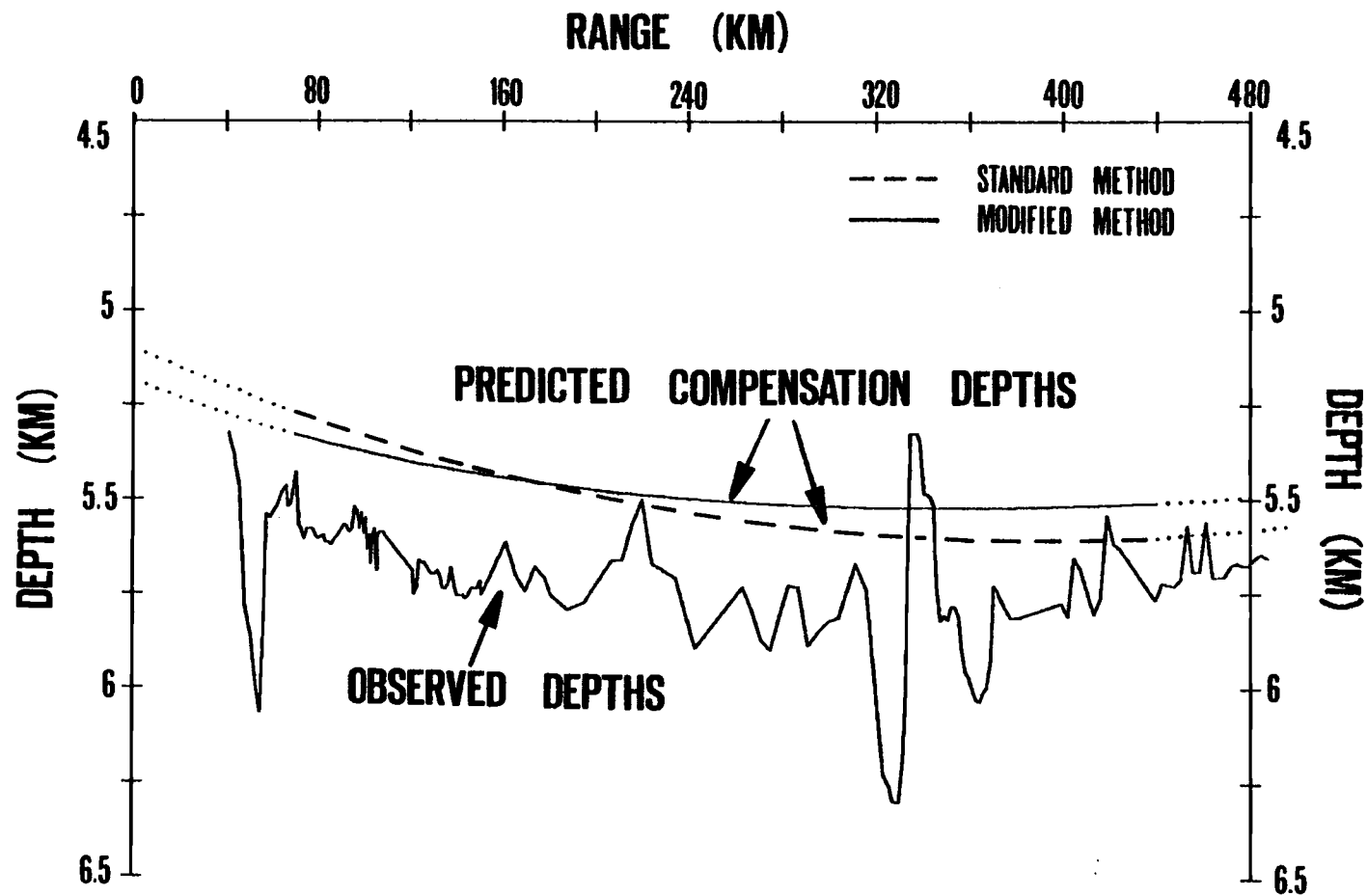
Figure 34. Predicted and observed bathymetric depths along 17 - 18°N in the West Philippine Basin.

the West Philippine Basin when isostatically balanced to Pacific mantle depths. A strong correlation between the computed compensation depth and the measured bathymetry, suggested by the nearly constant offset with the smoothed topography, implys an isostatic response to crustal thickness variations in the basin and are reflected in the generalized bathymetry, but are not sufficient to cause the depth anomaly.

DISCUSSION

Thin Crust

Resultant crustal thicknesses determined from delay time analyses are in excellent agreement with earlier investigations by Louden (1980) as well as Henry et al. (1975), supporting the contention for abnormally thin crust in the West Philippine Basin. Total crustal thicknesses from our line shot along 17° - 18°N in the basin are thinner, however, from those reported in Murauchi et al. (1980) for the entire Philippine Sea marginal basin. A schematic diagram comparing crustal sections from these studies along with Western North Pacific averaged thicknesses (Raitt, 1963) and lithology/seismic structure of the Blow-Me-Down massif, Bay of Islands ophiolite (Salisbury and Christensen, 1978) is displayed in Figure 35.

One hypothesis for explaining thinner crust in the West Philippine Basin may suppose negligible crustal thickening has occurred since basin creation. Syntheses of seismic refraction data in the Pacific relate crustal thickening of the lower crust (oceanic layer) with increasing age (Lewis and Syndsman, 1979, 1977; Christensen and Salisbury, 1975; Goslin et al., 1972; Shor et al., 1968). The magnitude of crustal thickening approaches 2 km with time. Shown in Figure 36 are Layer 3 thicknesses versus age plotted with those determined for the study area, and using results of Louden (1976). As can be seen, layer 3 thicknesses fall well below the theoretical curve for the Pacific Ocean and are still lower than the scatter, which is mostly due to compilation of seismic results encompassing varying rates of spreading. The anomalously thin
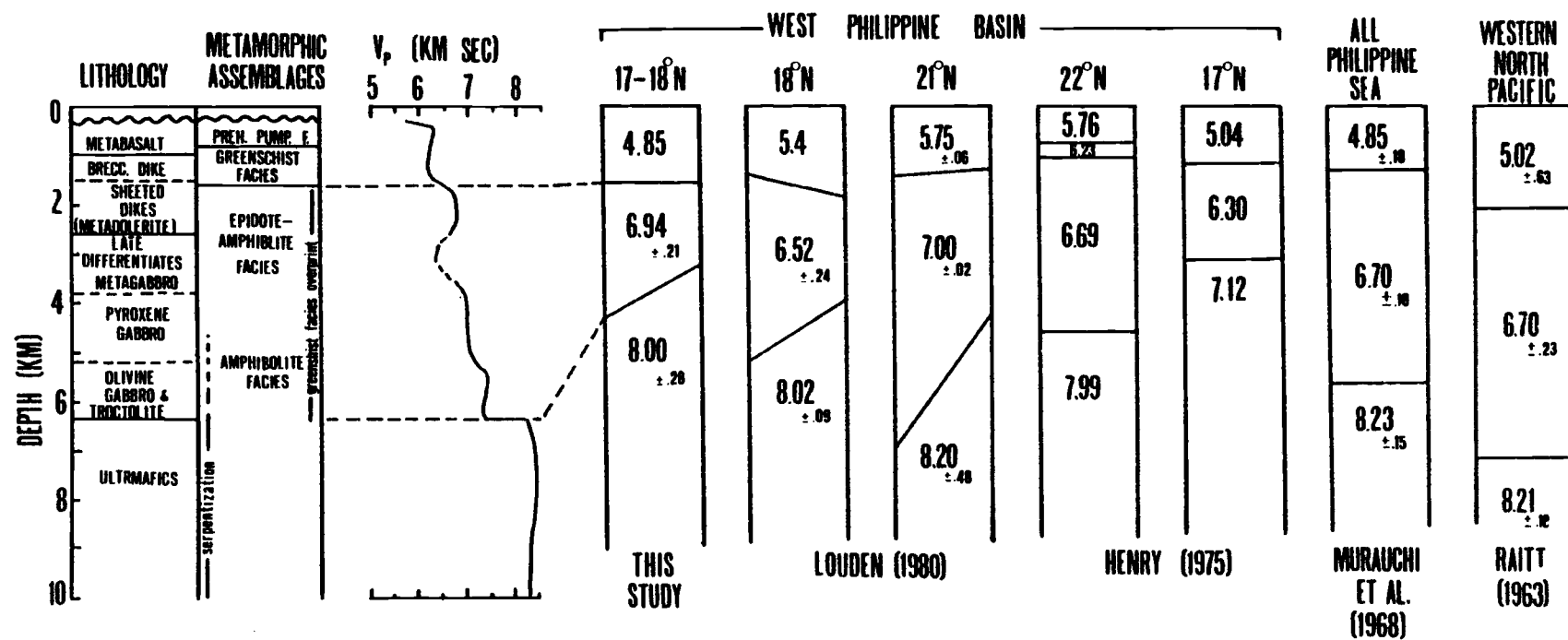
Figure 35. Comparison of crustal measurements made in the West Philippine Basin, entire Philippine Sea, and the Western North Pacific. Lithology and seismic structure of the Blow-Me-Down massif, Bay of Islands ophiolite (Christensen, 1978) is also shown.
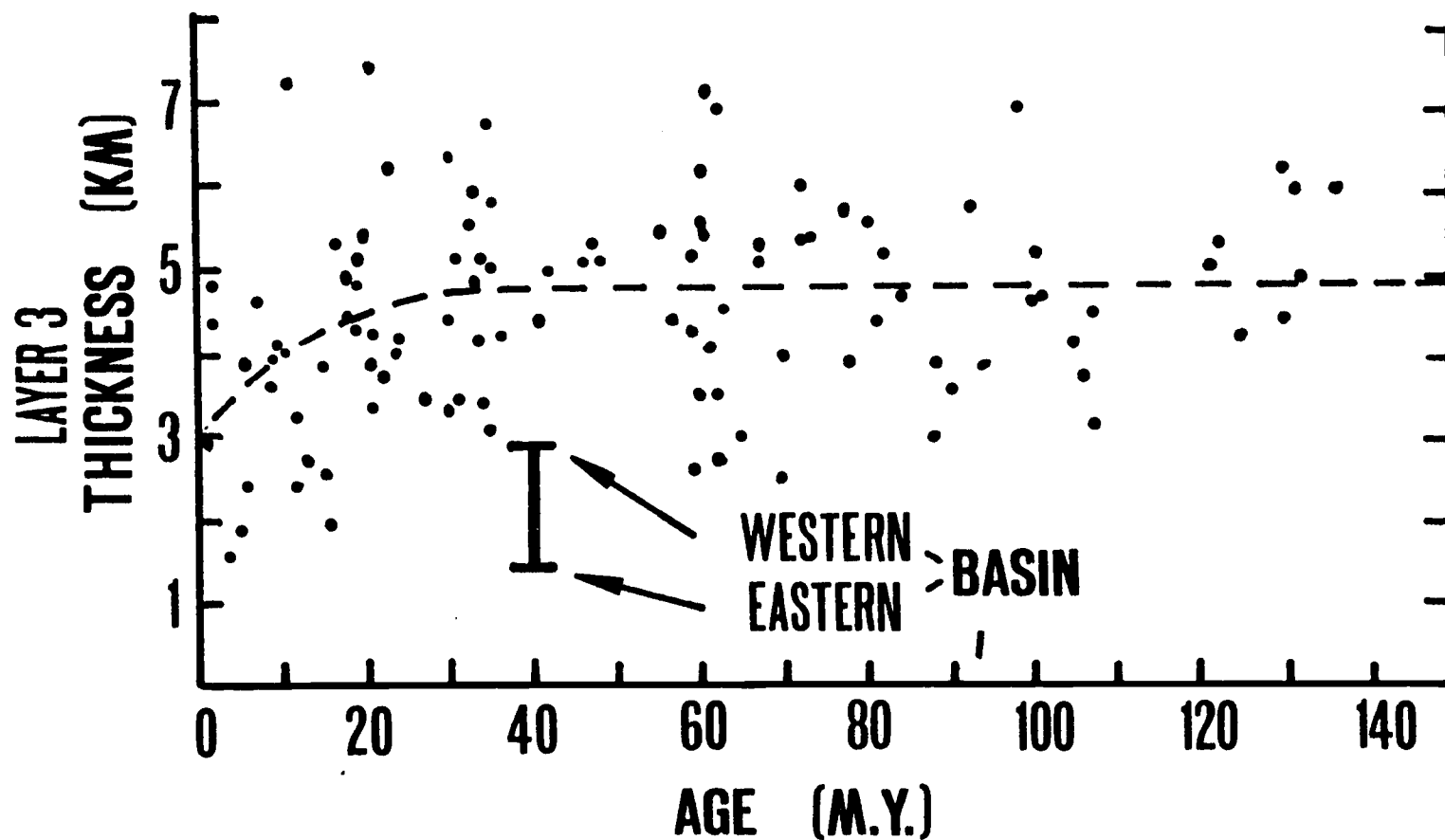
Figure 36. Thickness of the oceanic layer as a function of the age of the crust in the Pacific Ocean (after Christensen & Salisbury, 1975) plotted with layer 3 thicknesses in the West Philippine Basin.

crust in the West Philippine Sea is primarily due to a thinner oceanic layer; transitional layers do not appear to be significantly thinner in the basin (our results and Louden (1976)) when compared to Pacific and Atlantic transitional thicknesses and spreading rate (Figure 37).

The anomalously thin Layer 3 in the West Philippine Basin might be adequately accounted for in the paradigm of Christensen and Salisbury (1975). Crustal thickening of the lower crust in their model, is attributed to off-ridge intrusion, occurring for at least 40 m.y. subsequent to initial production. Upper basalt and dike layers are formed largely at the median valley and are not affected by intrusions into the lower crust. The anomalous mantle, the storehouse for magmatic intrusives, is thought to exist beneath crust to at least 50 m.y. from the ridge axis, but has thinned out considerably thereafter as replacement by solidified, normal mantle ultramafics develops. The lateral extent of this storehouse of magma may be quite large in the mid-ocean ridge environment, and less at ridge or back-arc extensional environments occurring at the margins of continents. The lateral extent of available magma for intrusion might be in direct response to the size of convection cells, if any, in the lower mantle. The sizes of these cells, initiated by the subducting plate in the back-arc situation, may be smaller at margins as they are confined by continental lithosphere thus not allowing for lower crustal, offridge thickening at distance (time) from the active rift. In light of this one might expect crustal thicknesses in all marginal sea basins created in the proximity of a continent to have thinner than normal crust. This remains a problem since marginal sea basins do not all have thin
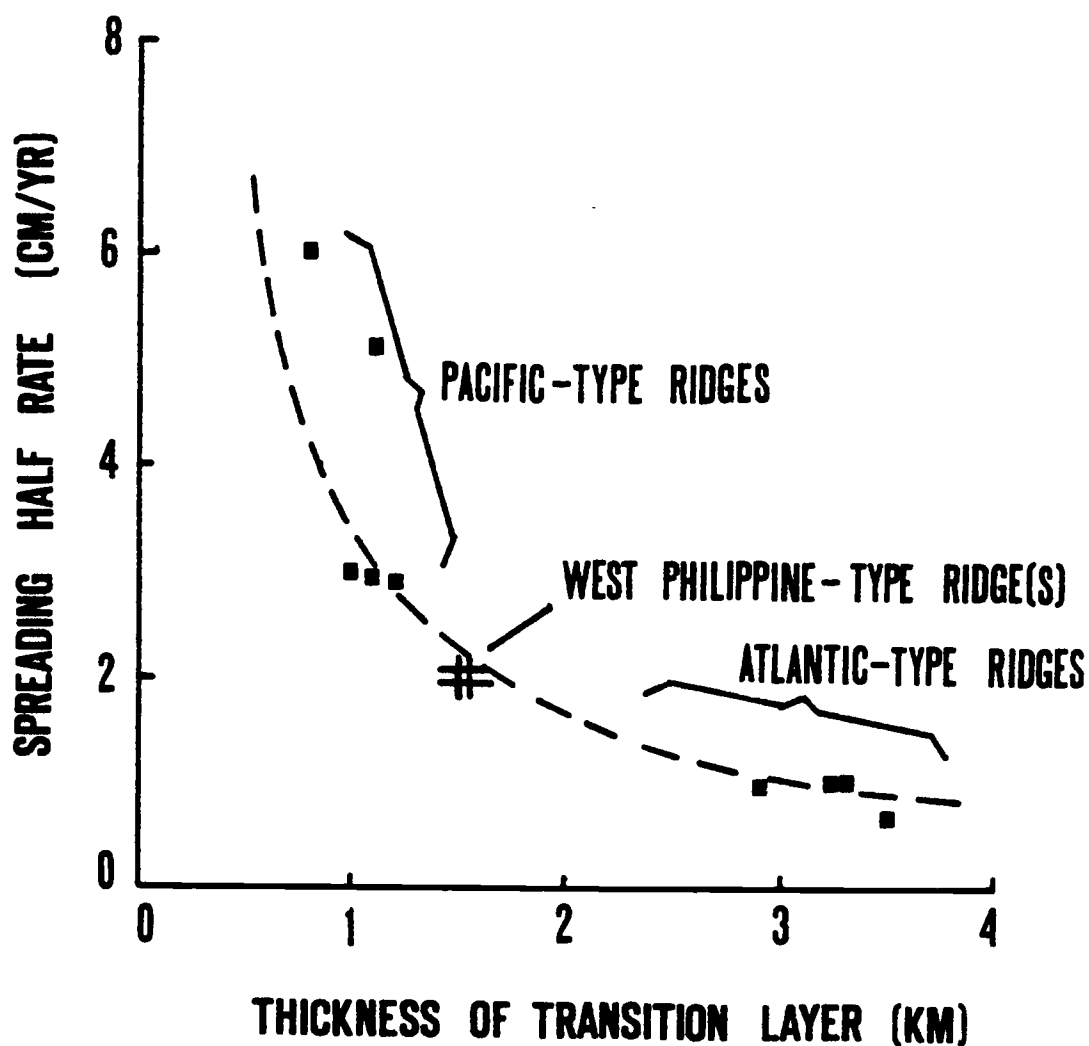
Figure 37. Spreading half-rate as a function of thickness of the transition layer from Shor et al. (1971). Includes seismic results from the present study and spreading rates given by Louden (1976).

crust (Karig, 1971a).

An alternate hypothesis for explaining thin crust would employ the Uyeda and Ben-Avraham model (1972) for the origin of the West Philippine Basin (with the Palau-Kyushu ridge forming along a fossil transform fault). The juxtaposition of the Philippine Ridge with the colder Pacific lithosphere may have caused a lowering in the isotherms beneath the active ridge, thus limiting magmatic intrusives and hence crustal thickness. In light of this one would expect progressively thinner crust toward the Palau-Kyushu ridge since isotherms would be much more depressed as the lithospheric heat sink-Pacific plate were approached. In addition, the dynamic forces associated with transform faulting could also cause considerable thinning, and more so in the proximity of the fault. Detrick and Purdy (1980) have found the crust around transform faults and associated fracture zones to be thinner than normal oceanic crust. Results from our study show the crust to be progressively thinner toward the eastern OBS's, and much thinner beneath OBS B, the easternmost instrument and closest to the extinct transform fault. The crustal structure determined is therefore consistent with the trapped oceanic crust model of Uyeda and Ben-Avraham (1972) for the West Philippine Basin.

Another theory may suppose the West Philippine Basin was initially laid down very thin and has experienced the same thickening processes and temperature distributions during basin creation as that in normal oceans. This would entail developing a significantly different mode of crustal generation for the basin. Karig et al. (1978) in studying back-arc spreading has found dissimilar styles

in extension than at midocean ridges. In the Lawver and Hawkins (1978) model of numerous and contemporaneous areas of mantle upwelling and extension behind island arcs, developed to account for the rougher topography and diffuse magnetic anomalies in marginal basins, also implies that different spreading process are operational in back-arc environments. As one petrologic consequence for having a different spreading mechanism, one might expect variations in the normative mineralogy of the basalts, although this is not observed in the Lau Basin where Lawver and Hawkins (1978) worked. Examination of leg 59 basalts, at site 447 in the West Philippine Basin however, fall well within the petrologic ranges determined for East-Pacific Rise and Mid-Atlantic Ridge basalts (Scheidegger and Corliss, 1981; Zakariadze et al., 1978). Furthermore, magnetic anomalies in the West Philippine Basin are fairly well defined; unlike in other marginal basins. In any case, this theory certainly can not be ruled out; the mode of crustal generation in the basin may not manifest its' difference in the petrology of surface basalts or the resultant magnetic signatures measured.

Depth Anomaly

The compensation model determined from our study corroborates evidence from earlier investiagtions (Louden 1980; Watanabe et al., 1977; Sclater et al., 1976; Sclater, 1972) of deeper water depths than those predicted for the West Philippine Basin.

To account for the depth anomaly while still maintaining a nearly isostatically compensated basin requires there to exist some mass excess at depth in either the crust or upper mantle. It is un-

likely the mass/density anomaly is in the crust since seismic velocities here are comparable to normal oceans. This leads to the conclusion of placing the mass anomaly in the mantle.

A compositional model which might adequately explain the observed depth anomaly in the basin would be to postulate a mantle source composed of garnet lhzerolite. The property of this rock which makes it special is that basaltic depletion of a garnet lhzerolite leaves a fractionated material lighter than the original parental magma (Jordan, 1978). Isostasy can then be afforded by having lower basalt depletion and thinner crust, which results in a relatively denser mantle.

Because very little experimental velocity data regarding garnet lhzerolites is available, were are unable to test the validity of this rock type as being a possible mantle constituent for the West Philippine Basin.

CONCLUSIONS

A summary of the important results from this investigation are
itemized:

1. The upper crust transitional zone in the West Philippine
    Basin is characterized by strong seismic gradients which
    gradually decrease with depth. The lower crust exhibits
    a nearly constant velocity gradient (0.24 $\sec^{-1}$).

2. Crust in the West Philippine Sea is abnormally thin, by
    approximately 2 km as compared to normal oceans. The major
    contributor to the thinner crust between 17° - 18°N in
    the basin is smaller oceanic layer thicknesses.

3. Oceanic thicknesses have been shown to be thinner in the
    eastern than in the western section of the basin. This is
    consistent with a Uyeda and Ben-Avraham (1972) model, sug-
    gesting the West Philippine Sea is a trapped oceanic basin.
    The relatively thinner crust in the eastern regions is
    related to transform faulting (and associated fracture
    zones) occurring along the remnant Kuyushu-Palau Ridge.

4. The West Philippine Basin depth anomaly cannot be fully
    accounted for by the thin crust. The observation requires
    a deeper-seated anomaly to exist in the basin.

5. Temperature/pressure constraints indicate that the upper
    mantle velocity gradients are rather high in the West
    Philippine Basin. Comparison with possible mantle constit-
    uents imply a multi-phased or graded composition may be pre-
    sent, at least to depths of 29 km from the moho in the basin.

The nature of the compressional wave velocities across the lithosphere -asthenosphere boundary and deeper have not been resolved in this study. Ray bottoming depths that only slightly exceed 20 km were discovered from first arriving phases at 433 km shot ranges. This is right at the juncture where shear wave velocities are thought to decrease, marking the upper extent of the low velocity zone.

BIBLIOGRAPHY

Abe, K., and H. Kanamori, 1970. Upper mantle structure of the Philippine Sea, in Island Arc and Ocean, eds., M. Hoshino and H. Aoki, 84.

Aki, K., and P.G. Richards, 1980. Quantitative Seismology Theory and Methods, W.H. Freeman and Co., San Francisco, 2, 643.

Ambos, E.L., and D.M. Hussong, 1978. Crustal structure of the Mariana Trough, J. Geophys. Res., 83, 5899-5912.

Asada, T., and H. Shumamura, 1976. Observation of earthquakes and explosions at the bottom of the western Pacific: structure of the oceanic lithosphere revealed by longshot experiment, AGU Mon., 19, 138-153.

Barazangi, M., and J. Dorman, 1969. World seismicity maps compiled from ESSA, Coast and Geodetic Survey, epicenter data, 1961-1967, Bull. Seism. Soc. Am., 59, 369-380.

Ben-Avraham, Z., J. Segawa, and C.O. Bowin, 1972. An extinct spreading center in the Philippine Sea, Nature, 240, 453-455.

Berry, M.H., and G.F. West, 1966. An interpretation of the first arrival data of the Lake Superior Experiment by the time-term method, Bull. Seism. Soc. Am., 56, 1357-1362.

Bibee, L.D., G.G. Shor Jr., R.S. Lu, 1980. Inter-arc spreading in the Mariana Trough, Mar. Geol., 35, 183-197.

Christensen, N.I., 1979. Compressional wave velocities in rocks at high temperatures and pressures, critical thermal gradients, and crustal low-velocity zones, J. Geophys. Res., 84, 6849-6857.

Christensen, N.I., 1974. Compressional wave velocities in possible mantle rocks to pressures of 30 kilobars, J. Geophys. Res., 79, 407-412.

Christensen, N.I., and M.H. Salisbury, 1975. Structure and constitution of the lower oceanic crust, Rev. Geophys. and Sp. Phys., 13, 571-586.

Clark, S.P., 1966. Handbook of Physical Constants, Geol. Soc. Am. Mem. 97.

Cook, J.A., 1981. Sonobouy refraction study of the crust in the Gorda Basin, M.S. Thesis, Oregon State University.

Detrick, R.S., and G.M. Purdy, 1980. The crustal structure of the Kane fracture zone from seismic refraction studies, J. Geophys. Res., 85, 3759-3777.

Fitch, T.J., 1970. Earthquake mechanisms and island arc tectonics in the Indonesian-Philippine region, Bull. Seism. Soc. Am., 60, 565-591.

Forsyth, D.W., 1975. The early structural evolution and anesotrophy of the oceanic upper mantle, Geophys. J. Roy. Astron. Soc., 43, 103-162.

Ganoe, S.J., 1983. Investigation of P_n wave propagation in Oregon, M.S. Thesis, Oregon State University.

Gardner, L.W., 1939. An areal plan of mapping subsurface structure by refraction shooting, Geophysics, 4, 247.

Gaskell, T.F., M.N. Hill, and J.C. Swallow, 1959. Seismic measurements made by H.M.S. Challenger in the Atlantic, Pacific, and Indian Oceans and in the Mediterranean Sea, 1950-53, Phil. Trans., Roy. Soc. London, A, 251, 23-85.

Goslin, J.B. Beuzart, J. Fancheteau, and X. LePichon, 1972. Thickening of the oceanic layer in the Pacific Ocean, Mar. Geophys. Res., 1, 418-427.

Heirtzler, J.R., G.O. Dickson, E.M. Herron, W.C. Pitman III, and X. LePichon, 1968. Marine magnetic anomalies, geomagnetic field reversals, and motions of the ocean floor and continents, J. Geophys. Res., 73, 2119-2136.

Henry, M., D.E. Karig, and G.G. Shor Jr., 1975. Two seismic refraction profiles in the Philippine Sea, in Initial Reports of the Deep-Sea Drilling Project, 31, 611.

Hess, H.H., 1948. Major structural features of the western north Pacific, an interpretation of H.O. 5485, bathymetirc chart, Korea to New Guinea, Bull. Geol. Soc. Am., 59, 417-446.

Johnson, S.H., M.D. Cranford, B.T. Brown, J.E. Bowers, and R.E. McAllister, 1977. A free-fall direct recording ocean bottom seismograph, Mar. Geophys. Res., 3, 103-117.

Jordan, T.H., 1978. Proceedings of the second international Kimberlite Conference, eds. F.R. Boyd, and H.O.A. Meyer, AGU, Washington, D.C.

Karig, D.E., 1975. Basin genesis in the Philippine Sea, in Initial Reports to the Deep-Sea Drilling Project, 31, 857-879.

Karig, D.E., 1971a. Structural history of the Mariana island arc system, Bull. Geol. Soc. Am., 82, 323-344.

Karig, D.E., 1971b. Origin and development of marginal basins in the western Pacific, J. Geophys. Res., 76, 2542-2561.

Karig, D.E., R.N. Anderson, and L.D. Bibee, 1978. Characteristics of back-arc spreading in the Mariana Trough, J. Geophys. Res., 83, 1213-1226.

Karig, D.E., J.C. Ingle Jr., A.H. Bouma, H. Ellis, N. Haile, I. Koizumi, I.D. Macgregor, C. Moore, H. Uyiie, T. Watanabe, S.M. White, M. Yasui, H. Ti Ling, 1973. Origin of the West Philippine Basin, Nature, 246, 458-461.

Katasumata, M., and L.R. Sykes, 1969. Seismicity and tectonics of the western Pacific: Izu-Mariana-Caroline and Ryukyu-Taiwan region, J. Geophys. Res., 74, 5923-5948.

Kroenke, L., and R. Scott, 1978a. In the Philippine Sea: old questions answered--and new ones asked, Geotimes, 20-23.

Kroenke, L., and R. Scott, 1978b. Marginal basin and remnant arc evolution, western Philippine Sea: Leg 50 DSDP results (abstract), EOS Trans., AGU, 1179.

LaTraille, S.L., J.F. Gettrust, and M.E. Simpson, 1982. The ROSE seismic data storage and exchange facility, J. Geophys. Res., 87, 8359-8363.

Lawson, A.C., 1932. Insular arcs, foredeeps and geosynclinal seas of the asiatic coast, Bull. Geol. Soc. Am., 43, 353-382.

Lawver, L.A., and J.W. Hawkins, 1978. Diffuse magnetic anomalies in marginal basins: their possible tectonic and petrologic significance, Tectonophysics, 45, 323-339.

Lee, C.S., and T.W.C. Hilde, 1982. Entrapment and backarc spreading origin of the West Philippine Basin, EOS Trans., AGU, 1114.

LePichon, X., J. Francheteau, and J. Bonin, 1973. Plate Tectonics, Elsvier, Amsterdam, 90.

Lewis, B.T.R., and W.E. Snydsman, 1979. Fine structure of the lower oceanic crust on the Cocos Plate, Tectonophysics, 55, 87-105.

Lewis, B.T.R. and W.E. Snydsman, 1977. Evidence for a low velocity layer at the base of the oceanic crust, Nature, 266, 340.

Lewis, S.D., C.L. Mrozowski, and D.E. Hayes, 1982. A new hypothesis for the origin of the West Philippine Basin, EOS Trans., AGU, 1114.

Louden, K.E., 1980. The crustal and lithospheric thicknesses of the
     Philippine Sea as compared to the Pacific, Earth Planetary
     Science Letters, 50, 275-288.

Louden, K.E. 1976. Magnetic anomalies in the West Philippine Basin,
     in The Geophysics of the Pacific Ocean Basin and its Margin,
     eds. G.H. Sutton, M.H. Manghanani, R. Moberly, Geophys. Mon.
     19, AGU, Washington, D.C.

Morris, G.B., 1972. Delay-time-function-method and its application to
     the Lake Superior Refraction Data, J. Geophys. Res., 77.

Morris, G.B., R.W. Raitt and G.G. Shor Jr., 1969. Velocity aniso-
     trophy and delay-time maps of the mantle near Hawaii, J. Geophys.
     Res., 74, 4300-4316.

Mrozowski, C.E., and D.E. Hayes, 1979. The evolution of the Parece
     Vela Basin, eastern Philippine Sea, Lamont-Doherty Geological
     Observatory, contribution no. 2890.

Murauchi, S., N. Den, S. Asano, H. Hotta, T. Yoshii, T. Asanuma,
     K. Hagiwara, K. Ichikawa, T. Sato, W.J. Ludwig, J.I. Ewing,
     N.R. Edgar, and R.E. Houtz, 1968. Crustal structure of the
     Philippine Sea, J. Geophys. Res., 73, 3143-3171.

Packham, G.H., and D.A. Falvey, 1971. An hypothesis for the formation
     of marginal seas in the western Pacific, Tectonophysics, 11,
     79-109.

Parker, R.L., D.W., and D.W. Oldenburg, 1973. A thermal model of
     oceanic ridges, Nature Phys. Sci., 242, 137-139.

Parsons, B., and J.G. Sclater, 1977. An analysis of the variation
     of ocean floor bathymetry and heat flow with age, J. Geophys.
     Res., 82, 803-827.

Raitt, R.W., G.G. Shor Jr., T.J.G. Francis, and G.B. Morris, 1969.
     Anisotrophy of the Pacific upper mantle, J. Geophys. Res., 74,
     3095.

Raitt, R.W., 1963. The crustal rocks, in The Sea, 3, ed. M.N. Hill,
     85-102, John Wiley, New York.

Salisbury, M.H., and N.I. Christensen, 1978. The seismic velocity
     structure of a traverse through the Bay of Islands ophiolite
     complex, Newfoundland, an exposure of oceanic crust and upper
     mantle, J. Geophys. Res., 83, 805-817.

Scheidegger, A.E., and P.L. Willmore, 1957. The use of a least-
     squares method for the interpretation of data from seismic
     surveys, Geophysics, 22, 9.

Scheidegger, K.F., and J.B. Corliss, 1981. Petrogenesis of secondary alteration of upper layer 2 basalts of the Nazca Plate, Geol. Soc. Am., Memoir 154, 77-107.

Sclater, J.G., C. Jauport, and D. Galson, 1980. The heat flow through oceanic and continental crust and the heat loss of the earth, Rev. Geophys. Sp. Phys., 18, 269-311.

Sclater, J.G., D.E. Kang, L.A. Lowver, and K.E. Louden, 1976. Heat flow and crustal thickness of the marginal basins of the south Philippine Sea, J. Geophys. Res., 81, 309-318.

Sclater, J.G., R.D. Jarrard, B. McGowran, and S. Gartner Jr., 1974. Comparison of magnetic and biostratigraphic time scales since the Late Cretaceous, in Initial Reports of the Deep Sea Drilling Project, 22, 381-386.

Sclater, J.G., R.N. Anderson, and M.L. Bell, 1971. Elevation of ridges and evolution of the central eastern Pacific, J. Geophys. Res., 76, 7888-7815.

Sclater, J.G., and J. Francheteau, 1970. The implication of terrestrial heat flow observations on current tectonic and geochemical models of the crust and upper mantle of the earth, Geophys. J. Roy. Astron. Soc., 20, 509-537.

Seekins, L.C., and T.L. Teny, 1977. Lateral variations in the structure of the Philippine Sea Plate, J. Geophys. Res., 82, 317-324.

Sheriff, R.E., 1973. Encyclopedic dictionary of exploration geophysics, Soc. of Exploration Geophysicists, Oklahoma, 200.

Shimamura, H.V., V. Tomoda, and T. Asada, 1975. Seismographic observation at the bottom of Central Basin Fault of the Philippine Sea, Nature, 253, 177-179.

Shor, G.G. Jr., H.W. Menard, and R.W. Raitt, 1971. Structure of the Pacific basin in The Sea, ed. A.E. Maxwell, New York, John Wiley and Sons, Inc., 4, 3-27.

Shor, G.G. Jr., P. Dehlinger, H.K. Kirk, and W.S. French, 1968. Seismic refraction studies off Oregon and northern California, J. Geophys. Res., 81, 3007-3012.

Soga, N., 1967. The elastic constants of garnet under pressure and temperature, J. Geophys. Res., 72, 4227-4234.

Solomon, S.C., and N.H. Sleep, 1974. Some simple models for absolute plate motions, J. Geophys. Res., 79, 2557-2567.

Talwani, M., X. LePichon, and M. Ewing, 1965. Crustal structure
    of the mid-ocean ridges, 2. computed model from gravity and
    seismic refraction data, J. Geophys. Res., 70, 341-352.

Uyeda, S., and D.M. Hussong, 1978. General results of DSDP Leg
    60, the eastern portion of the south Philippine transect along
    18°N (abstract), EOS Trans., AGU, 1179.

Watanabe, T., M.G. Langseth, and R.N. Anderson, 1977. Heat flow in
    back-arc basins of the western Pacific, in Island Arcs, Deep
    Sea Trenches and Back-arc Basins, eds. M. Talwani and W.C.
    Pitman III, Am. Geophys. Union, Maurice Ewing Ser. 1.

Willmore, P.L., and A.M. Bancroft, 1960. The time-term approach to
    refraction seismology, Geophysics J., 3, 419.

Yoshii, T., 1973. Upper mantle structure beneath the north Pacific
    and the marginal seas, J. Phys. Earth, 21, 313.

Zakariadze, G.S., L.V. Dmitriev, A.V. Sobolev, and N.M. Suschevsky,
    1978. Petrology of basalts of holes, 447A, 449, and 450, South
    Philippine Sea transect, in Initial Reports of the Deep Sea
    Drilling Project, 59, 669.

APPENDIX

SYNOPSIS OF SITES CORED IN THE WEST PHILIPPINE
BASIN FROM THE DEEP SEA DRILLING PROJECT

Since the Deep Sea Drilling Project (DSDP) became operational
in the summer of 1968, six drilling sites in the West Philippine
Basin have been attempted (Figure 2). Most of these, Sites 290 -
294(-5), stem from Leg 31 (Guam to Hakodate, June - August 1973)
and Site 447 from Leg 59 (Okinawa to Guam, Feb. - March 1978) aboard
the GLOMAR CHALLENGER. A summary of some of the important coring
results (in Table I of main text) and a brief synopsis from each
site review is given.

Site 290: Primary goal of this site, located in the most eastern
section of the West Philippine Basin and distal edge of the Palau-
Kyushu Ridge, was to determine basement age and the history of the
Palau-Kyushu Ridge. A volcanic ash between 70 - 80 m of the core
was identified, and is thought to be related to the opening of the
Parece Vela Basin. A Paleocene period of volcanic activity, from
late Eocene to early oligocene, is determined from the decrease in
volcanic ash upward, between 90 - 139 m of the core, and from the
earliest age of the volcaniclastics, which are thought to be debris
flow, in part, derived from basement slumping. Accordingly, an
Eocene-Oligocene age for local basement was assigned.

Site 291: Located in the southern region of the West Philippine
Basin, close to the Philippine trench, the objective at Site 291 was
to obtain an extended section of basement for investigations into

the nature of basaltic crust in marginal basins, hence to determine basement age and basin origin as well. The entire sediment section was pelagic down to a fine grained tholeiitic basalt. It is not known if the basalt represents true basement since no volcanic sediments or ash layers directly overlying the basalt were found. Furthermore, the depth to basalt from a second hole (291A) drilled a 120 meters from 291 was 9 meters shallower, indicating the possibility of faulting, an additional complexity to ascertaining the age of the local basement. High torques from both these holes limited penetration to several meters.

Site 292: In the westernmost section of the West Philippine Basin and slightly north of the Philippine Trench lies a region of significantly elevated topography. This region, referred to as the Benham Rise, is about 3 km shallower at its crest than the rest of the basin and is thought to be a result of crustal flexure, related to the cessation of subduction along the east side of Tuzon (Karig, 1973), or a result of volcanism subsequent to the formation of the basin. The major goal at this site was not a tectonic one but designed to obtain a calcareous fossil-rich biostratigraphic reference section for which the rest of the basin, because of its great depth and turbulent bottom currents is deficient in. Results from drilling were extraordinarily favorable in this respect as well as tectonically. Nearly 76 m of basalt basement was drilled. K-Ar analysis of the basalts revealed an age range from 36 to 39.2 m.y., upholding a late Eocene formation. From the vesicle size in the basalt a water depth less than 500 meters is estimated at time of emplacement. Volcanic episodes were found to occur near the

Oligocene-Miocene boundary, late Miocene, and Pleistocene-Recent, with some moderate activity documented during the late Eocene-Oligocene, the time of activity along the Palau-Kyushu Ridge. The rise is interpreted as resulting from midplate production sometime during mid to late Eocene, followed by several kilometers of subsidence to its present state.

Site 293: This drill hole, situated in the complex region where the Central Basin Fault meets the Ryukyu and Luzon arcs, was designed to determine the age of local basement, duration of apron formation, and periods of activity, if any, along the fault. Local basement was assigned a minimum age in the late Eocene from the oldest pelagic sequence above the breccia, since no in situ basaltic material was cored. The presence of the basaltic breccia dated younger than the shallower layers, implies significant faulting, which is estimated to have occurred sometime in the mid-Tertiary, before the apron sediments formed but after some pelagic accumulation. The presence of reworked pelagic and benthonic foraminifera in the turbidites, of late Cretaceous age gives reason to believe that deep basins (marginal?) of the same age existed nearby.

Site 294/5: The primary objective at this site located in the northeast section was to obtain an age of basement and the history of the Oki-Daito Ridge. Two holes 2.4 km apart were drilled here, with results being somewhat similar. The oldest sediments recovered were Eocene in age but containing reworked Paleocene planktonic forminifera. The basalt in the base of the retrieved core is thought to be a result of a later dated basalt flow since reflection profiles showed strong returns deeper at the drilling site. A

conservative minimum Eocene-Paleocene age is assigned for basement. No mention of volcanic episodes on the Oki-Daito Ridge in the site reports are given for this hole.

Site 447: Analysis of Leg 31 results revealed that better control on the age and nature of basement was needed in the eastern part of the West Philippine Basin. On Leg 59 this hole was cored in the eastern section, close to Site 290, but 35 km northwest of it in hopes of avoiding any volcanic debris derived from the Palau-Kyushu Ridge. Though volcanic debris was encountered, drilling was not hampered and nearly 120 m of basalt basement, pillow lava and flows, was cored. The basalt was identified as being tholeiitic, the typical chemistry of mid-ocean ridge basalts. Because of the excellent core recovery of the basalt paleomagnetic measurements were made. Results indicated the region existed at a lower latitude, either 10.5°S or 10.5°N. A date of middle oligocene for basement was assigned, but recognized as possibly older if a hiatus between basement formation and sediment accumulation occurred.